ELECTRON PARAMAGNETIC RESONANCE STUDIES

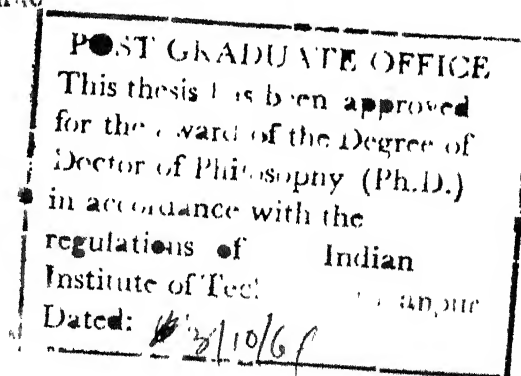OF VO^{2+} AND Mn^{2+} IN SINGLE CRYSTALS

A thesis submitted

In Partial Fulfilment of the Requirements

for the Degree of

DOCTOR OF PHILOSOPHY

by

KOCHARLAKOTA VENKATA SUBBA RAO

to the

DEPARTMENT OF PHYSICS

INDIAN INSTITUTE OF TECHNOLOGY KANPUR
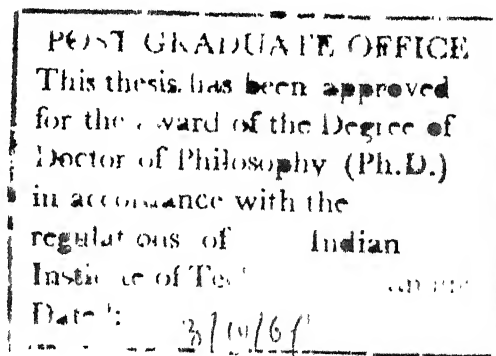
JUNE 1969

Certified that the work presented in this thesis has been done by Mr. K. V. Subba Rao under my supervision. Dr. M. D. Sastry joined me in supervising the work connected with Chapter III, IV, and V.

Putcha Venkateswarlu
Putcha Venkateswarlu
Professor of Physics
Indian Institute of Technology
Kanpur

ACKNOWLEDGEMENTS

The author wishes to thank Professor Putcha Venkateswarlu for his invaluable assistance in this thesis and throughout his graduate career. His inspiring guidance and valuable suggestions are gratefully acknowledged.

The author is thankful to Dr P.K. Kelkar, Director, Indian Institute of Technology, Kanpur for his interest in this work.

The author is extremely grateful to Dr M.D. Sastry whose cooperation and encouragement contributed greatly to the success of this work.

Thanks are due to Dr G.C. Upreti for many helpful discussions.

The continuous encouragement of Professor J. Mahanty throughout the course of this work is gratefully acknowledged.

Thanks are due to M/s. P.A. Narayana, R. Janakiraman, E.V.R. Sastry, A.V. Jagannadham, S.D. Pandey, N.R. Krishna, T.S. Kannan, P.R. Rao, Drs. R.D.N. Rao, D.R. Rao, T.M. Srinivasan, B.V.R. Chowdari and D.R.S. Somayajulu for their interest and encouragement and to Mr. A.A. Khan for typing this thesis.

The author is thankful to Dr. N.A. Narasimham, Spectroscopy Division, Bhabha Atomic Research Centre, Bombay for the spectrochemical analysis of the doped crystals.

Financial support from the Council of Scientific and Industrial Research, India is gratefully acknowledged.

(K.V. Subba Rao)

CONTENTS

PREFACE

In the recent years there has been a considerable amount of experimental research activity in the field of electron paramagnetic resonance (EPR) in solids. Of primary importance among the materials investigated have been the single crystals containing the various ions of the iron group. But relatively very few resonances of the molecular ion VO^{2+} in single crystals have been reported. The importance of VO^{2+} as a paramagnetic ion lies in the fact that it has only a single 3d electron, resulting in a spin of ½ and only two populated Zeeman energy levels at all temperatures. Paramagnetic resonance of this ion with its simple energy level structure can act as a useful experimental tool for verifying any theoretical calculations. The divalent manganese with its $3d^5$ electronic configuration has the ground state $^6S_{5/2}$ which is uneffected by crystalline electric fields in the first order. It has, however, long been known that a zero field splitting of this state does occur. So the paramagnetic resonance data of this ion can provide useful information regarding the splitting of the S- state ions in crystals.

The thesis describes the research work done by the author on the electron paramagnetic resonance of VO^{2+} in ammonium and potassium aluminum alums, VO^{2+} in methyl ammonium gallium (MAG) alum, VO^{2+} in potassium and cesium nitrates, VO^{2+} in ammonium ,sodium and barium nitrates and Mn^{2+} in ammonium aluminum alum. All these systems have been studied in the form of single crystals over a wide temperature range ($300^{\circ}c$ to-$196^{\circ}c$) and interesting results have been obtained on the effect of substitution of paramagnetic ions VO^{2+} and Mn^{2+} on the structure of alums and about the

rotation of VO^{2+} ion in the nitrates. All the spectra discussed in the thesis have been obtained for the first time.

Chapter I gives an introduction to EPR. The theory and the experimental setup used in the present investigations are briefly dis - cussed in chapter II.

Chapter III describes the EPR studies of VO^{2+} ion in ammonium and potassium aluminum alums single crystals. In both crystals it is observed that VO^{2+} ion substitutes for an Al^{3+} ion, and forms a $[VO(H_2O)_5]^{2+}$ complex forming a distorted octahedron with an H_2O vacancy along the V-O bond direction. The octahedron axes are found to coincide with the crystallographic $\langle 100 \rangle$ axes indicating that the presence of VO rotates the octahedron axes so as to coincide with the crystallographic axes. The formation of the vanadyl pentahydrate complex has been confirmed by taking an optical absorption spectrum. By correlating the EPR and optical absorption data the covalency rates of bonding between the vanadium atom and the equitorial ligands and between the vanadium atom and the vanadyl oxygen have been estimated.

Chapter IV describes the EPR studies of VO^{2+} ion in MAG alum. As mentioned above, in this system also, VO^{2+} ion substitutes the trivalent ion Ga^{3+} and forms a $[VO(H_2O)_5]^{2+}$ complex, a distorted octahedron with an H_2O vacancy along VO bond direction. However in this case the octa- hedron cubic axes are found to be displaced from the crystallographic $\langle 100 \rangle$ axes by 9^0 in the $[110]$ plane. The EPR results suggest that the host alum

probably belongs to β-type in which the presence of VO^{2+} twists the octa-hedron cubic axis by about 9^0 from the crystallographic $\langle 100 \rangle$ axis. Optical absorption studies confirm the formation of $[VO(H_2O)_5]^{2+}$. The covalency rates have been estimated as in the earlier case by correlating the EPR and optical absorption data .

Chapter V deals with the EPR studies of VO^{2+} ion in potassium and cesium nitrate single crystals. Room temperature studies reveal that there is a very fast readjustment of VO^{2+} ion, in both crystals, which is manifested in the presence of a single isotropic octet, thereby exhibiting a low viscous" liquid like" nature. At low temperatures an anisotropic spectrum is obtained due to the hindered rotation of VO^{2+} ion. The line-widths at room temperature are found to depend on the m_I quantum number and an attempt is made to fit the linewidth data of the present study in the theoretical expression of Kivelson. It is found that Kivelson's theory can qualitatively explain the observed variation of linewidth with nuclear quantum number m_I but the experimental data could not be fit quantitatively into the theory.

Chapter VI deals with the EPR studies of VO^{2+} in ammonium, sodium and brarium nitrates. As in the potassium and cesium nitrate crystals an isotropic octet is obtained at room temperature in all these crystals. As the temperature is lowered anisotropic spectra are obtained which is again because of the hindered rotation of VO^{2+} ion in these crystals at low temperatures. The temperature, at which the hindered rotation sets in,

changes from crystal to crystal — -20°, -196° and -90°c respectively in NH_4NO_3, Na NO_3 and $Ba(NO_3)_2$ crystals. A comparison of the present EPR results with those of VO^{2+} in KNO_3 and $CsNO_3$ is made and the results are examined in relation to the recently reported low temperature phase transitions in these crystals. A probable phase transition around -110°c in $CsNO_3$ is suggested. This comparison also suggests that VO^{2+} ion probably enters interstitially in $Ba(NO_3)_2$ and $CsNO_3$ and substitutionally in $NaNO_3$ and KNO_3.

Chapter VII deals with the EPR studies of Mn^{2+} ion doped in ammonium aluminum alum single crystals. At low concentrations of Mn^{2+} an isotropic sextet is obtained indicating thereby that the site symmetry at Mn^{2+} ion is cubic. At higher concentration an orthorhombic spectrum, with its z-axis along crystallographic $\langle 110 \rangle$ direction, superimposed on a broad resonance is obtained. This spectrum is due to Mn^{2+} which subs — titutes $(NH_4)^+$ and gets associated with a first neighbour ammonium ion vacancy along $\langle 110 \rangle$ direction. The cubic axes of the octahedron of waters around Mn^{2+} are found to coincide with the crystallographic $\langle 100 \rangle$ axes indicating that the presence of Mn^{2+} probably rotates the octahedron axes so as to coincide with the crystallographic axes.

The different chapters in this thesis are written so as to be suitable for publication as articles. They are self contained and self explanatory. Therefore repetition of certain things has become unavoidable in a few places in the thesis.

CHAPTER I

INTRODUCTION

After the development of techniques in microwave generation and detection, electron paramagnetic resonance has become a powerful tool of research for investigating the low lying energy levels and the effect of crystalline fields on the energy levels of paramagnetic ions in solids. Paramagnetism occurs whenever a system of charges has a resultant angular momentum. This angular momentum is due partly to the orbital motion and partly to the intrinsic spin motion with each of which is associated a magnetic dipole moment. Such paramagnetism of electronic origin is found in ions having partly filled inner electronic shells as in the transition elements.

Electron paramagnetic resonance consists in observing the transitions taking place between the electronic Zeeman levels of a para-magnetic system under the influence of a periodic magnetic field of resonance frequency. The method can be illustrated in a simple way as follows. If a free ion with a resultant angular momentum J is placed in a magnetic field H, then its electronic energy levels are given by $E_M = g \beta H M$, where g is the Lande's g factor, β is the Bohr magneton and M is the component of J along the magnetic field direction. If an alter-nating microwave field of frequency ϑ is applied at right angles to H, magnetic dipole transitions are induced according to the selection rule. $\triangle M = \pm 1$, when the quantum of energy applied $h\vartheta$, becomes equal to the energy level difference between adjacent levels i.e. $E_M - E_{M'} = g \beta H$ where $M' = M \pm 1$. Energy will be absorbed from the microwave field when the spin of the electron is flipped from a direction parallel to the magnetic field to that of antiparallel direction and there is an induced

emission corresponding to the reverse process. Even though both the transitions have the same a priori probability, in a system at thermal equilibrium there will be a net absorption of energy because of its greater population in lower state. This resonance absorption can be detected by the loss of energy from the microwave field which causes a damping of the tuned circuit in which the paramagnetic ion is placed.

The spectrum of paramagnetic ion when placed in a crystal lattice is more complex than that of the simple example described above. If the paramagnetic ion is placed in a crystal, there are strong interactions between it and its surroundings. These interactions are in main, of two types (i) interactions between the magnetic dipoles and (ii) interactions between the paramagnetic ion and the diamagnetic neighbours. The inter-action between the various dipoles is not of any significance here as it contributes only to the line broadening of the spectrum that is observed. This interaction can be reduced effectively to a small value by using crystals diluted with an isomorphous diamagnetic salt. The interaction of paramagnetic ion with the diamagnetic neighbours is the main topic of interest here. These diamagnetic neighbours called "ligands" set up strong internal electric fields at the site of the paramagnetic ion. The effect of this crystalline electric field is to "quench" the orbital motion of the electrons of the paramagnetic ion. This quenching of orbital angular momentum can be conceived quantum mechanically as follows . The crystalline electric fields split the energy levels of the paramagnetic ion into a number of components. The number of such components and the extent of splitting depend critically on the symmetry and strength of the field. In the transition metal compounds

of iron group where there are unfilled 3d electrons, which are responsible for the paramagnetism of these compounds , are directly exposed to the crystalline field. The crystalline field in these compounds is of moderate strength being larger than the spin – orbit coupling but smaller than the Coulomb interaction between the electrons. So for these ions the crystalline field removes the orbital degeneracy of the energy levels either partially or completely, depending on its symmetry, thus quenching the orbital motion either partially or completely. However the electronic spin with its corresponding magnetic moment has no direct interaction with the electrostatic field, and remains free to orient itself in an external magnetic field. Thus the magnetic properties of the salts of the iron group correspond substantially to "spin only" magnetism. However, when the spin-orbit coupling is included , the energy levels will become admixtures of the other orbital states and then the magnetic properties of these levels will deviate from the spin only values. In the rare earth group where the unfilled electronic shell is the inner 4f shell, the interaction of the crystalline field with the magnetic ion is much less. The paramagnetism of these ions is close to that of free ions in a first approximation.

Due to the quenching of orbital angular momentum of the paramagnetic ion in a crystal, the orbital angular momentum of a free ion and that of the ion in a crystal are different in the ground state. As para – magnetic resonance is usually restricted to the ground state of the ion, the g-value obtained here will be different from the free ion g-value. Also the magnitude of the orbital part of the magnetic moment depends on the crystal field. This will be different for different directions of H

and shows an angular variation which follows the symmetry of the crystal field.
The total g-value (spin plus orbit) is thus anisotropic to the extent which
depends on the magnitude of the orbital contribution to the magnetic moment
and on the asymmetry of the crystal field. This anisotropic g-value can be
described by three principal values g_x, g_y and g_z which are measured in three
perpendicular directions and include the maximum and minimum values. This
g-value can be written as $g^2 = (l^2 g_x^2 + m^2 g_y^2 + n^2 g_z^2)$ where (l,m,n) are the
direction cosines of g with respect to the principal axes of g (x,y,z).

In salts where the ground state is an orbital singlet with
a multiplicity more than 2 in the spin ($S = 1$ or more) the degeneracy of the
spin levels is often lifted even in the absence of external magnetic field.
In the presence of these initial splittings the Zeeman energy levels of the
ion are not equally spaced and hence the different transitions ($\triangle M = \pm 1$)
will occur at different frequencies. So the spectrum consists of 2M transitions
and this is called the "fine structure" of the spectrum. For example the
ground state ^4F of V^{2+} splits in a cubic crystalline field into a lower orbital
singlet (A_2) and two higher lying triplets $(T_1$ and $T_2)$. If a small axial field
is also present, then $^4A_2$ splits into two Kramers doublets. Due to this zero
field splitting three fine structure lines are obtained in the paramagnetic
resonance spectrum of V^{2+}.

If the nucleus of the paramagnetic ion has a spin I, then due
to the interaction between the nuclear magnetic moment and electronic magnetic
moment, each of the electronic energy levels splits into $(2I + 1)$ components.
Hence each fine structure line splits into $(2I + 1)$ components. This is called

hyperfine structure. For example, the nuclear spin of vanadium is 7/2 and hence each of the three fine structure transitions splits into eight hyperfine lines giving a 24 line spectrum for V^{2+} in axial fields.

The resolution of the lines of a paramagnetic resonance spectrum is limited by the width of the lines themselves. The two major causes for this linewidth are (i) the spin-lattice interaction i.e., the interaction between the paramagnetic ion and the lattice and (ii) the spin - spin interaction i.e., the interaction between the various paramagnetic ions themselves.

The scope of the application of this resonance method in physics is given below.

1.   The lowest electronic energy levels and therefore the resonance spectrum are extremely sensitive to the environment of the paramagnetic ion in the crystal. The spectrum may thus provide information about the symmetry of the surroundings of the ion and about the nature and strength of the bonding between the ion and the ligands.

2.   The study of paramagnetic ions doped in single crystals having phase transitions can provide useful information about the nature of the phase transitions. Hitherto unknown phase transitions can be detected by EPR.

3.   Information on the nucleus of the paramagnetic ion can be obtained if the resonance spectrum consists of hyperfine structure. For example the nuclear spin and approximate values for the nuclear magnetic dipole and electric quadrupole moments can be found.

4. The existence of further structure called superhyperfine structure will provide useful information on the covalency of the paramagnetic ion in the lattice.

5. Under certain conditions the resonance data may be very useful in obtaining the bulk properties of the crystals containing paramagnetic ions, for example the susceptibility and specific heat. This is especially true at very low temperatures, when such properties depend only on the energy levels within a few cm^{-1} of the ground level i.e., on those levels measured by resonance methods.

6. Since the width of the absorption lines depend on the spin-lattice, the spin-spin and exchange interactions, the resonance spectrum gives information concerning these factors.

* * *

This chapter is based on the following books and review articles.

1. W. Low , Paramagnetic Resonance in solids(Academic Press,New York and London 1960).

2. S. A. Al'tshuler and B. H. Kozyrev, Electron Paramagnetic Resonance (Academic Press,New York and London 1964).

3. B. Bleaney and K. W. H. Stevens, Reports on Progress in Physics 16, 108 (1953).

4. K. D. Bowers and J. Owen, Reports on Progress in Physics 18,304 (1955).

CHAPTER II

THEORY OF ELECTRON PARAMAGNETIC RESONANCE OF
TRANSITION METAL IONS OF IRON GROUP

ABSTRACT

The theory of electron paramagnetic resonance of transition metal ions doped in single crystals is developed. A brief discussion is presented on the crystalline fields, spin-Hamiltonian formalism, fine structure, hyperfine structure, superhyperfine structure and covalency effects. The essential features of the instrument used in these investigations are briefly described.

The transition metal ions of the iron group in their divalent or multivalent ionic states have the electronic configurations of the type (Ar core)^{18} 3d^n (n = 1, ...10) in which the unfilled shell is now the outermost shell. For this reason, the orbital motion of the 3d electrons are strongly perturbed by the crystalline field and energies of the order of 10,000cm^{-1} are associated with the coupling of the orbitals with this field. The crystalline field is completely external to the ion and has a definite symmetry. By knowing this symmetry and by using group theory, it is possible to predict the splitting of the energy levels and transformation properties of the eigenfunctions representing the states. Based on experimental data these crystalline fields are divided into three classes:

(i)   Weak fields, in which the Stark splittings are small compared to the separation between the spin-orbit multiplets. These occur in the case of rare earth ions where the unpaired f electrons are shielded by the outer electrons.

(ii)   Medium fields, in which the Stark splittings are of the same order of magnitude as the intervals between multiplets arising from the same electron configuration. These occur in the case of transition metal ions of the iron group where the unpaired 3d electrons are fully exposed to crystalline electric fields.

(iii)   Strong fields, in which the crystalline potential is of the same order of the energy of the mutual interaction between the electrons. These will occur in the case of 4d and 5d transition metal groups where there is considerable chemical bonding between the paramagnetic ion and the ligands.

From these relative magnitudes of the crystalline fields and the terms in the free ion Hamiltonian, it can be seen that perturbation theory holds good for 3d and 4f transition group ions in the calculation of the energy levels of these ions in crystalline field. The calculation of these energy levels consists in finding out the matrix elements of the crystalline potential between the eigen states of the free ion Hamiltonian of the paramagnetic ion.

Excluding the nuclear interactions, which will be discussed later, the Hamiltonian for the transition metal ions can be written as

$$\mathcal{H} = \sum_{i=1}^{m} (p_i^2/2m - Ze^2/r_i) + \sum_{i>j=1}^{n} e^2/r_{ij} + \mathcal{H}_{cr} + \lambda \bar{L} \cdot \bar{S} + \beta (\bar{L}+2\bar{S}).\bar{H}$$

The terms in the Hamiltonian are in the decreasing order of magnitude. The first three terms are the free ion terms. $\mathcal{H}_{cr}$ is the interaction with the crystal field, $\lambda \bar{L}.\bar{S}$ is the spin-orbit interaction and the last term is the interaction with the external magnetic field. $\bar{L}$ and $\bar{S}$ are the orbital and spin angular momentum operators. $\mathcal{H}'_{cr}$ is treated as a perturbation on the free ion Hamiltonian and can be represented in the form.

$$\mathcal{H}_{cr} = \sum_i - e \, V(x_i, y_i, z_i)$$

where V is the potential of the crystalline field and x_i, y_i and z_i are the coordinates of the i-th electron of the unfilled shell. By assuming that the electrons of the paramagnetic ion and of the ligands do not overlap the potential V satisfies Laplace's equation $\nabla^2 V = 0$. Such a potential V can be expanded in terms of spherical harmonics:

$$V = \sum_{n,m} A_n^m \, r^n \, Y_n^m (\theta, \phi)$$

Symmetry arguments will reduce the terms in this expansion. In the case of d electrons terms for which $n > 4$ will vanish. The reason for this is that the wave function of the electrons can also be expanded in harmonic functions. Matrix elements are of the form $\psi_\ell^i V_n^m \psi_\ell^i$ and are therefore zero for all potentials for which $n > 21$. All terms in V with odd n must vanish. The reason for this lies in the fact that the product $\psi_\ell^i \psi_\ell^i$ is unchanged by inversion symmetry whereas the potential changes its sign. Finally since V is real $A_n^m = (A_n^{-m})^*$. The term with $n = 0$ gives a negligible additive constant which can be set equal to zero. To have further simplifications the symmetry of the crystalline field is to be taken into account. The spherical harmonic has axial symmetry when $m = 0$, tetragonal symmetry when $m = \pm 4$, trigonal symmetry when $m = \pm 3$ and orthorhombic symmetry when $m = \pm 2$. So the potential of the fields of different symmetries will become[1]

$$V_{cubic} = U_4^0 + U_4^4$$

$$V_{tetragonal} = U_2^0 + U_4^0 + U_4^4$$

$$V_{rhombic} = U_2^0 + U_2^2 + U_4^0 + U_4^2 + U_4^4$$

where $U_n^0 = A_n^0 \, r^n \, Y_n^0(\theta, \phi)$ and

$$U_n^m = r^n \, A_n^m \, Y_n^m(\theta, \phi) + A_n^{-m} \, Y_n^{-m}(\theta, \phi)$$

These potentials can be expanded in terms of the coordinates of the electron of the paramagnetic ion. Putting $U_n^m = B_n^m \, V_n^m$ these V_n^m's can be written as

$$V_2^0 = 3z^2 - r^2 \qquad\qquad V_2^2 = x^2 - y^2$$

$$V_4^0 = (35z^4 - 30r^2z^2 + 3r^4) \qquad V_4^2 = (7z^2 - r^2)(x^2 - y^2)$$

$$V_4^4 = (x^4 - 6x^2y^2 + y^4)$$

where $B_2^0 = \tfrac{1}{4}\sqrt{5/\pi}\,A_2^0$

$\qquad\qquad B_2^2 = \tfrac{1}{2}\sqrt{15/2\pi}\,A_2^2$

$\qquad B_4^0 = (3/16\sqrt{\pi})\,A_4^0$

$\qquad\qquad B_4^2 = (3/4)\sqrt{5/2\pi}\,A_4^2$

$\qquad B_4^4 = (3/8)\sqrt{35/2\pi}\,A_4^4$

The crystal field perturbation $-e\sum_i V(\bar{r}_i)$ caused by the presence of the ligands , destroys the spherical symmetry of the environment of a certain ion. Therefore L^2 and L_z no longer commute with the Hamiltonian. After the crystal field perturbation is taken into account they may be actually replaced by other observables depending on the type of local symmetry. S^2 and S_z commute with the crystal field Hamiltonian, which does not depend on spin coordinates. Placing the ion in the crystal results in the representation $D_L \times D_S$ becoming reducible and being reduced in terms of the irreducible representations of the symmetry group, G_c, which leaves $\mathcal{H}_{cryst}$ unchanged. The spin does not appear in $\mathcal{H}_{cryst}$ and only D_L is reduced into irreducible representations Γ_i of G_c. $D_L = \sum_i c_i \Gamma_i$. These crystal field splittings of the free ion energy levels are obtained group theoritically. To have exact information about the order of the levels one has to calculate the matrix elements of the crystal field potential in the form discussed above between the free ion levels. Table II - I gives the 3d electronic configuration, the ground state and the crystalline field splittings of this ground state of the transition metal ions of iron group. Mulliken's

Table II ‑ I^{2+}

Metal ion	3d electronic configuration	Ground state of the free ion.	Octahedral states and energies in Dq units.
VO^{2+}, Ti^{3+}	d^1	^{2}D	$^2T_{2g}(-4)$, ^2E_g (+6)
V^{3+}	d^2	^{3}F	$^3T_{1g}$ (-6), $^3T_{2g}$ (+2), $^3A_{2g}$ (+ 12)
V^{2+}, Cr^{3+}	d^3	^{4}F	$^4A_{2g}$ (- 12), $^4T_{2g}$ (-2), $^4T_{1g}$ (+6)
Cr^{2+}	d^4	^{5}D	^5E_g (-6), $^5T_{2g}$ (+4)
Mn^{2+}, Fe^{3+}, Cr$^+$	d^5	^{6}S	$^6A_{1g}$ (0)
Fe^{2+}	d^6	^{5}D	$^5T_{2g}$ (-4), ^5E_g (+ 6)
Co^{2+}	d^7	^{4}F	$^4T_{1g}$ (-6), $^4T_{2g}$ (+2), $^4A_{2g}$ (+ 12)
Ni^{2+}	d^8	^{3}F	$^3A_{2g}$ (-12), $^3T_{2g}$(-2), $^3T_{1g}$ (+ 6)
Cu^{2+}	d^9	^{2}D	^2E_g (-6), $^2T_{2g}$ (+4)

+ reference 2.

notation is used in designating the crystal field splittings. The EPR absorption takes place in the manifold of this lowest level and is described by spin-Hamiltonian method developed by Pryce[3] and Abragam and Pryce[4].

Spin-Hamiltonian Formulation

Electron paramagnetic resonance is generally observed in the ground state of the paramagnetic ion. This lowest group of electronic states can be characterised by a single quantum number S' eventhough each state is really a complicated mixture of spin and orbital wavefunctions of the free ion. S' is called the "fictitious" or " effective spin" of the system and is defined by equating 2S' + 1 to the number of electronic states in the lowest group. For some ions S' is equal to the free ion spin S, for example VO^{2+}, Ti^{3+} and Cu^{2+}. For some other ions S' is not equal to S, for example Mn^{2+} in cyanides and Co^{2+}. The use of an effective spin means that for temperatures where only the (2S'+1) lowest electronic energy levels are appreciably populated the paramagnetic ion is treated like a magnetic dipole which has (2S' +1) allowed orientations in an applied magnetic field and each energy level is associated with one orientation . But the effective magnetic moment of this dipole (and hence the splittings produced by the applied magnetic field) does not correspond to the spin only value. It is different by a factor g/g_s where g_s is the free electron g value.

The lowest energy levels, the multiplicity of which is given by (2S' + 1), can be described by the use of a "spin-Hamiltonian"

introduced by Pryce[3] and Abragam and Pryce[4]. By taking into account the first and second order perturbations due to the spin-orbit and the Zeeman terms on the crystal field states, Abragam and Pryce[4] have shown that the eigen values will be given by the Hamiltonian

$$\mathcal{H} = \left\{ -\lambda^2 \wedge_{ij} \right\} S_i S_j + 2 \beta \left(\delta_{ij} - \lambda \wedge_{ij} \right) H_i S_j$$

where

$$\wedge_{ij} = \wedge_{ji} = \sum_{n \neq 0} \frac{\langle 0 | L_i | n \rangle \langle n | L_j | 0 \rangle}{E_n - E_o}$$

$|0\rangle$ is the lowest crystal field level among the Zeeman components of which EPR absorption is taking place and $|n\rangle$ is any high lying crystal field level. This Hamiltonian is usually expressed as

$$\mathcal{H} = \bar{S} \cdot \underline{D} \cdot \bar{S} + \beta \bar{H} \cdot \underline{g} \cdot \bar{S}$$

where $\underline{g}$ and $\underline{D}$ are symmetric tensors given by the expressions

$$D_{ij} = (-\lambda^2 \wedge_{ij}) \text{ and } g_{ij} = 2 (\delta_{ij} - \lambda \wedge_{ij}).$$

When the crystalline field is having an axial symmetry, the Hamiltonian in the principal axis system of the g-tensor can be written as

$$\mathcal{H} = \beta g_{\parallel} H_z S_z + \beta g_{\perp} (H_x S_x + H_y S_y) + D \left[S_z^2 - (1/3) S (S + 1) \right].$$

When the crystalline field has an orthorhombic component a term of the type $E (S_x^2 - S_y^2)$ is added to this Hamiltonian, together with the coefficients g_x and g_y to replace $g_\perp$. The constants g_x, g_y, g_z, D and E can be obtained emperically from the EPR spectrum. Apart from the axial and rhombic terms which are quadratic in spin variables, Van Vleck and Penney[5] had shown that a third order effect arising from the coupling of tetragonal field and the spin-orbit interaction would also give a similar spin dependence. The interaction via cubic field gives a term

proportional to $S_1^4 + S_2^4 + S_3^4$. S_1, S_2 and S_3 being components referred to the cubic axes, but because of the higher order coupling involved, the coefficient is small.

The fine structure part of the spin-Hamiltonian of an orthorhombic symmetry can be written as[6]

$$\mathcal{H} = g_z \beta H_z S_z + g_x \beta H_x S_x + g_y \beta H_y S_y$$

$$+ (a/6) \left[S_1^4 + S_2^4 + S_3^4 - (1/5) S(S+1)(3S^2 + 3S-1) \right]$$

$$+ D \left[S_z^2 - (1/3) S(S+1) \right]$$

$$+ F \left[35 S_z^4 - 30 S(S+1) S_z^2 - 6S(S+1) + 3S^2 (S+1)^2 \right]$$

$$+ E (S_x^2 - S_y^2) \qquad\qquad ..... \quad (1)$$

Here "a" is the coefficient of the cubic field terms whose axes are represented by 1,2 and 3. D and F are the coefficients of second and fourth order axial terms and E is the coefficient of orthorhombic terms. The axes of these terms are represented by x,y and z. These fine structure constants are related to B_n^m's by the equations[7]

$$D = 3B_2^0$$
$$3a + 2F = 360 B_4^0$$
$$5a = 120 B_4^4$$
$$E = B_2^2 .$$

The importance of the spin-Hamiltonian lies in the fact that its employment makes it possible to give a description of the resonance properties of an ion in terms of a small number of constants.

Hyperfine structure

If the nucleus of the paramagnetic ion has a nuclear spin I then there exists[4] a magnetic interaction between the nuclear and electronic spins. Since the nucleus has $(2I + 1)$ orientations in the magnetic field arising from each of the $(2S + 1)$ orientations of the electronic moment, each electronic level is subdivided into $(2I + 1)$ components. The selection rule for the transition between these levels is $\triangle m_I = 0$. The physical reason for this selection rule is that the microwave field exerts negligible effect on the nuclear moment so that its orientation does not change in an electronic transition. So each of the fine structure lines splits into $(2I + 1)$ hyperfine components. This hyperfine interaction is written as

$$\mathcal{H}_{I.S} = 2 \; \gamma \beta \beta_n \left[\sum_k \left\{ \frac{(\bar{I}_k \cdot \bar{s}_k) \cdot \bar{I}}{r_k^3} \; \frac{3(\bar{r}_k \cdot \bar{s}_k)(\bar{r}_k \cdot \bar{I})}{r_k^5} \right\} \right. $$

$$\left. + (8 \pi/3) \; \delta(r_k)(\bar{s}_k \cdot \bar{I}) \right]$$

Here β_n and γ refer to the nuclear magneton and nuclear gyromagnetic ratio respectively. The first term in the square brackets describes the dipolar interaction between the nuclear and electronic magnetic moments. The second term denotes the anomalous interaction of S electrons with the nuclear spin[8]. From the results of paramagnetic resonance it is observed[4] that in transition elements this configurational interaction involving unpaired S electrons is of importance and contributes considerably to the hyperfine splitting. In a principal axes system in which the hyperfine interaction tensor A is diagonal, this Hamiltonian can be written as

$$\mathcal{H}_{I.S} = A_x\, I_x\, S_x + A_y\, I_y\, S_y + A_z\, I_z\, S_z$$
$$= \bar{I}.\ \bar{A}.\ \bar{S}$$

In order to take into effect the hyperfine interaction these terms are to be added to the spin-Hamiltonian (1).

The distortion in the crystalline field will also determine the anisotropy in the hyperfine interaction and hence the principal axes of A and the crystalline field tensors will be identical[9]. The principal axes of the g tensor need not coincide with that of the A tensor, eventhough they usually do so in many systems. When these two axes do not coincide additional terms of the form[10]

$$\sum_{i,j}' F_{ij} \left[S_i I_j + I_i\, S_j \right]$$

need to be included. If the z axes coincide and the x, y principal axes do not, the off-diagonal terms then contain only the products $S_x\, I_y$ and $S_y\, I_x$. In this case the observed hyperfine constants A, B_x, B_y, F_{xy} ($F_{xy} = F_{yx}$, since the tensor is symmetric) are related to the diagonal values of the hyperfine tensor

$$A = A_z$$
$$B_x = A_x \cos^2\Theta + A_y \sin^2\Theta$$
$$B_y = A_x \sin^2\Theta + A_y \cos^2\Theta$$
$$F_{xy} = F_{yx} = \tfrac{1}{2}\,(A_y - A_x)\, \sin\Theta \cos\Theta$$

where Θ is the angle between the principal axes of the two tensors. If the principal axes of the g and A tensors coincide, the extrema for all the

hyperfine lines occur at the same angle and if they do not, they occur at different angles for different hyperfine lines. This has been predicted and observed by Borcherts and Kikuchi[10] in VO^{2+} doped in Tutton salt.

Nuclear quadrupole effects

If the nucleus of the paramagnetic ion has an electric quadrupole moment Q and if it is in an electric field gradient $\partial E/\partial z$, there exists an electrostatic interaction between these two. This interaction is given by

$$\mathcal{H}_Q = \left[e^2 \, Q/2I(I-1)\right] \sum_j \left\langle I(I+1)/r_j^3 - 3(\bar{r}_j \cdot \bar{I}_j)^2/r_j^5 \right\rangle$$

This is represented in the operator form as

$$Q' \left[I_z^2 - (1/3) \, I(I+1)\right] + Q'' \, (I_x^2 - I_y^2) \qquad \cdots \quad (2)$$

where $Q' = \frac{3}{4}\left[e \, Q/I(2I-1)\right] V_{zz}$

and $Q'' = \frac{3}{4}\left[e \, Q/I(2I-1)\right] (V_{xx} - V_{yy})$

where V_{xx}, V_{yy} and V_{zz} are the principal values of the electric field gradient tensor. The effect of this quadrupole interaction results in the appearence of transitions in which the nuclear quantum number m_I changes by one or two. The physical reason for the occurrence of such "forbidden transitions" is that the quadrupole interaction tries to align the nucleus along the symmetry axis, whereas the magnetic field established by the electrons tries to align the nucleus nearby, at right angles to the symmetry axis. The selection rules then are broken down since several nuclear states become admixed. The reason for this break down lies in the off-diagonal

terms giving rise to transitions for which $\triangle m_I = \pm 1$ and $\triangle m_I = \pm 2$. Bleaney[11] has derived formulae for these transitions. In order to take into effect the quadrupole interaction the terms given in (2) have to be added to spin-Hamiltonian (1).

Superhyperfine structure

If the electrons of the paramagnetic ion and the ligands overlap with each other there can exist a magnetic interaction between the electronic spin of the ion and the nuclear spin of the ligands. In such a case, each of the hyperfine levels of the paramagnetic ion splits into $(2I_L + 1)$, where I_L is the total nuclear spin of the equivalent ligands. The selection rule for the transition between these levels is $\triangle m_{I_L} = 0$ and so each of the hyperfine lines splits into $(2I_L + 1)$ components. This structure is called "superhyperfine structure" and is first observed by Owen and Stevens[12] in ammonium chloroiridate. Later on, this has been observed by several workers[13,14]. This structure appears in mostly covalent systems and the other effects of this covalency are

(i) an increase in fine structure parameters[15]

(ii) a reduction in the magnitude of hyperfine constant[16]

(iii) a change in the orbital contribution to the observed g-value[17].

In order to take into effect the superhyperfine interaction a term of the type $\sum_N A_{ij}^N \cdot S_i \cdot I_j^N$, where N is the number of surrounding ligands, has to be added to spin-Hamiltonian (1).

After adding the above described terms to spin-Hamiltonian (1)

it will be a general Hamiltonian of orthorhombic symmetry. In the case of axial symmetry

$$g_z = g_{\parallel}$$

$$g_x = g_y = g_{\perp}$$
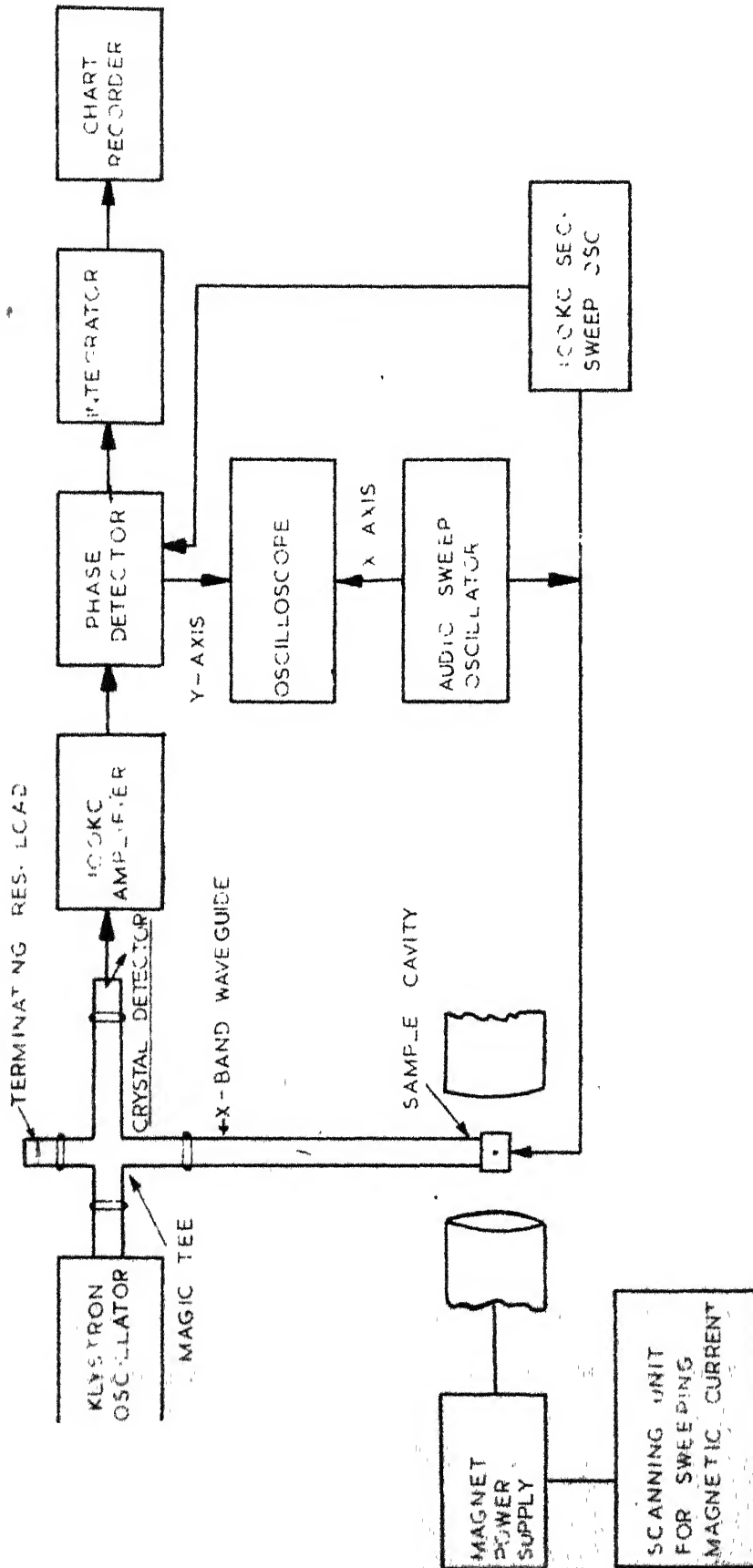
$$A_z = A$$

$$A_x = A_y = B$$

$$E = 0$$

and $\quad Q'' = 0$

Application of the general spin-Hamiltonian for special cases of VO^{2+} and Mn^{2+} is discussed in corresponding chapters of this thesis.

Instrumentation

The equipment used in the present study is a Varian V-4502 X-band EPR spectrometer system, with a Varian V-4540 model variable temperature accessory. A simplified block diagram of the system is given in Figure II – I. The description of the instrument and details of operation can be found elsewhere[18,19]. Essential features are described below.

A klystron oscillator generates a microwave power of 300mW operating at a frequency 9.5 GHz. This microwave power after being attenuated to lmW, is fed to a resonant microwave cavity. The klystron can be locked to the resonant frequency of the cavity within one part in 10^6 by using an automatic frequency control (AFC) locking system. The cavity is connected to one end of a hybrid tee , the other arm of which

CHART RECORDER

INTEGRATOR

100KC SEC. SWEEP OSC

PHASE DETECTOR

OSCILLOSCOPE

x AXIS

Y-AXIS

AUDIO SWEEP OSCILLATOR

100KC AMPLIFIER

TERMINATING RES. LOAD

CRYSTAL DETECTOR

X-BAND WAVE GUIDE

SAMPLE CAVITY

KLYSTRON OSCILLATOR

MAGIC TEE

MAGNET POWER SUPPLY

SCANNING UNIT FOR SWEEPING MAGNETIC CURRENT

contains a dummy load. The hybrid tee essentially acts as a bridge circuit for microwave power, and the bridge can be adjusted for balance in the absence of resonance absorption. When the resonance occurs, power is absorbed from the cavity. This energy change unbalances the microwave bridge and results in energy reaching the crystal detector.

The d.c. magnetic field at the sample position is modulated at 100 KHz using a set of Helmholtz coils mounted on the cavity walls. The EPR signal information reaching the crystal detector appears as an a.c. modulation on the power reflected from the sample cavity. The signal is then amplified and phase detected and is applied to a graphic recorder for display.

The magnet used for this experiment is a Varian 9 inch magnet operated at an air gap of 2.675 inches in the middle. It provides a very homogeneous magnetic field(within 15 milligauss over the sample region for a field intensity of about 3400 gauss) which can be varied from near zero to about 10 Kilogauss over the sample region.

In order to determine the magnetic field accurately diphenyl-picryhydrazil (DPPH) is placed in the cavity at the site of the sample. Since the g-value of DPPH is known to be 2.0036, the exact field at the sample site is determined from the resonance condition. The microwave frequency is measured, by Model 8370AH Beckman Universal EPUT and Timer attached to Model 7571 Beckman 10-110MC converter, to an accuracy of 1 cycle in 10^{6}.

The sensitivity of the spectrometer is $2 \times 10^{11} \Delta H$ where ΔH is the line width in gauss at half maximum absorption.

References

1. S. A. Al'tshuler and B. M. Kozyrev: Electron Paramagnetic Resonance: Academic Press (New York and London) p44 (1964).

2. C. J. Ballhausen: Introduction to Ligand Field Theory: McGraw Hill Company (New York) p74 (1962).

3. M. H. L. Pryce Proc. Phys. Soc. (London), $\underline{A63}$, 25 (1950).

4. A. Abrangam and M. H. L. Pryce, Proc. Roy. Soc. (London), $\underline{A205}$, 135 (195

5. J. H. Van Vleck and W. G. Penney, Phil. Mag. $\underline{17}$, 961 (1934).

6. W. Low: Paramagnetic Resonance in Solids: Academic Press (New York and London) p46 (1960).

7. C. F. Hempstead and K. D. Bowers, Phys. Rev. $\underline{118}$, 131 (1960).

8. E. Fermi, Z. Physik, $\underline{60}$, 320 (1930).

9. G. D. Watkins, Phys. Rev. $\underline{113}$, 79 (1959).

10. R. H. Borcherts and C. Kikuchi, J. Chem. Phys. $\underline{40}$, 2270 (1964).

11. B. Bleaney, Phil. Mag. $\underline{42}$, 441 (1951).

12. J. Owen and K. W. H. Stevens, Nature, $\underline{171}$, 836 (1953).

13. S. Ogwa, J. Phys. Soc. Japan, $\underline{15}$, 1475 (1960).

14. M. D. Sastry and P. Venkateswarlu, Proc. Indian. Acad. Sci. $\underline{66}$, 208 (1967).

15. R. S. Title, Phys. Rev. $\underline{130}$, 170 (1963).

16. R. S. Title Phys. Rev. $\underline{131}$, 623 (1963).

17. W. Low, Phys. Rev. $\underline{101}$, 1827 (1956).

18. Varian Associates, Instruction Manual V-4502 EPR spectrometer systems.

19. The NMR - EPR staff of Varian Associates, NMR and EPR spectroscopy, Pergamon Press (New York) (1960).

CHAPTER III

ELECTRON PARAMAGNETIC RESONANCE STUDIES OF VO^{2+} DOPED IN

$KAl(SO_4)_2 \cdot 12H_2O$ AND $NH_4Al(SO_4)_2 \cdot 12H_2O$ SINGLE CRYSTALS[*]

ABSTRACT

The electron paramagnetic resonance spectra of VO^{2+} ion doped in potassium aluminum and ammonium aluminum alums single crystals are studied. In both crystals it is observed that VO^{2+} ion substitutes for an Al^{3+} ion, and forms a $\left[VO(H_2O)_5\right]^{2+}$ complex, forming a distorted octa - hedron with an H_2O vacancy along the VO bond direction. The octahedron axes are found to coincide with the crystallographic $\langle 1CO \rangle$ axes indicating that the presence of VO rotates the octahedron axes so as to coincide with the crystallographic axes. The formation of the vanadyl pentahydrate complex has been further confirmed by taking an optical absorption spectrum. By correlating the EPR and the optical absorption data the covalency rates of σ -bonding between the vanadium atom and the equitorial ligands and of the π -bonding between the vanadium atom and the vanadyl oxygen have been estimated.

Introduction

Alums containing paramagnetic impurities have been the subject of investigations from several points of view since the early days of electron paramagnetic resonance (EPR). Earlier EPR investigations in potassium chrome alum and ammonium chrome alum[1,2,3] have lead to a new understanding of the structure of alums. This chapter deals with the EPR studies of VO^{2+} ion doped in potassium aluminium(KAl) and ammonium aluminium (NH_4Al) alums single crystals. The recent studies of Sastry and Venkateswarlu[4] and the work described in chapter V show that VO^{2+} entering NH_4Cl,KNO_3 and $CsNO_3$ single crystals, can reorient its bond freely resulting in a random distribution of the V-O bond axis, whereas the EPR studies of VO^{2+} in Tutton salt by Borcherts and Kikuchi[5] show that there is a formation of a distorted octahedron of oxygens about V^{4+}, the distortion being in the V-O bond direction. The recent EPR studies of VO^{2+} in rubidium aluminum (Rb Al) and cesium aluminium (Cs Al) alums by Manoogian and Mackinnon[6] show how the presence of VO^{2+} effects the structure of the host lattices. The present EPR studies of VO^{2+} in potassium aluminum and ammonium aluminum alums have been taken up to get information about the structure of the vanadyl complex in the respective single crystals and also about the effect of VO on the structure of these alums.

Structure of alums

The structure of alums has been determined by Lipson and Beevers[7] and Lipson[8]. The alums belong to the cubic system and possess point symmetry

$T_h = \dfrac{(2)\overline{3}}{m}$. There are four formula units per unit cell. The ions and molecules can be arranged in three slightly different ways within the cubic lattice. These three ways of arrangement have been named as α, β and γ structures. Potassium aluminum and ammonium aluminum alums belong to α-type of alums. In this type of structure half of the waters form regular octahedra around aluminum and each of these waters makes external bonds with one oxygen of the $(SO_4)^{2-}$ group and the potassium water. These two bonds and the one from water to aluminium are almost coplanar. Each of the remaining water molecules links two oxygens of the $(SO_4)^{2-}$ group, one aluminum water and one potassium atom, the arrangement of the bonds being approximately tetrahedral. The structure of α-type of alums and the bonds between the different ions and the water molecules are shown in Figure III-I[7,8]. In α-type of alums the $\langle 111 \rangle$ axes of the octahedron coincide with the $\langle 111 \rangle$ axes of the crystal, but the cubic axes of the octahedron are displaced from the crystal cubic axes by a rotation about the $\langle 111 \rangle$ direction. Lipson obtains a rotation angle of 9.5° for α-type of alums. The octahedron may be said to have a small trigonal distortion along the crystallographic $\langle 111 \rangle$ direction.

Potassium aluminum alum has been found to have a gradual phase transition[9] around $160^{\circ}K$ while ammonium aluminum alum has been found to have a sudden transition[9] around $80^{\circ}K$. The actual mechanism of these phase transformations has not been discussed in the literature.

Theory

A tetravalent vanadium ion with outer electronic configuration

32

FIGURE III-I   (a). Crystal structure of α-type of alums.

(b). Electrostatic bonding details in the α-type of alums.

(a)

(b)

K or NH4

Al

S

} H2O

0
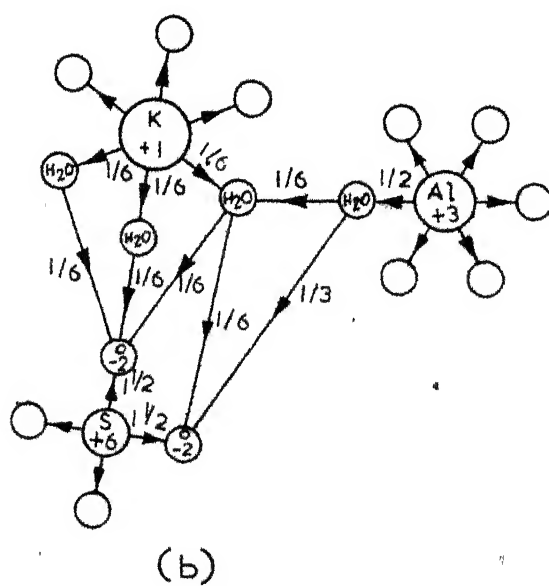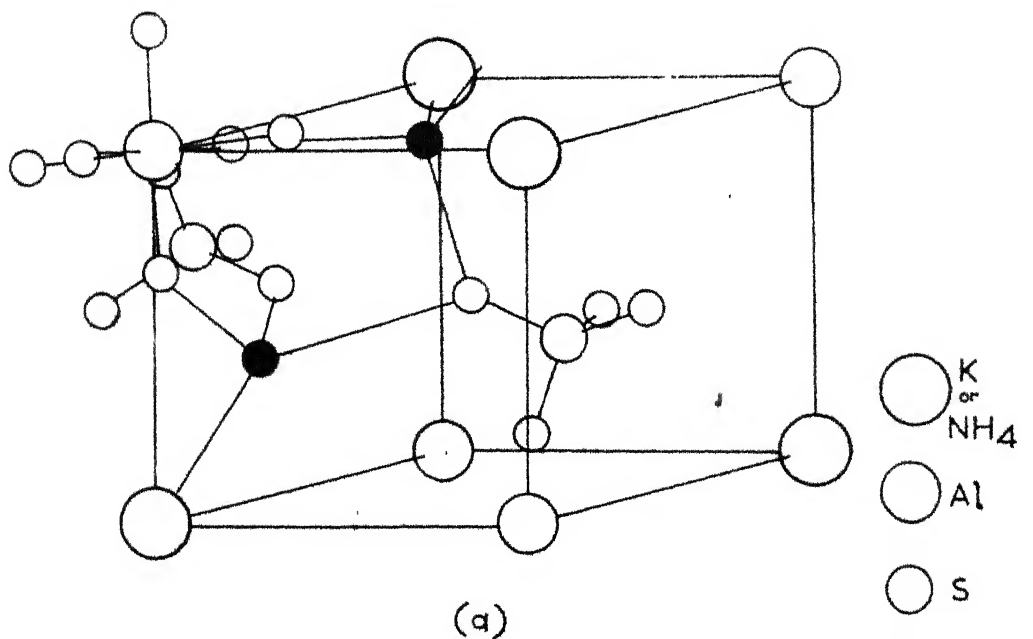
$3d^1$ exists in most stable form as VO^{2+}, the binding with the oxygen being highly covalent. The LCAO-MO description of this molecular ion in the complex $[VO(H_2O)_5]^{2+}$ had shown[10,11] that the unpaired d electron occupies a non-bonding b_2 type of vanadium orbital $(3d_{xy})$ and the lowest state becomes an orbital singlet. The molecular orbital scheme for $[VO(H_2O)_5]^{2+}$ given by Ballhausen and Gray[10] is shown in Figure III-II. Due to the magnetic interaction with the vanadium (I of V^{51} = 7/2) the EPR spectrum shows a characteristic eight line hyperfine structure. The g-factor, the value of which is close to g_e, the free electron g-value, is however anisotropic because of the proximity of e_π^* and b_1^* levels to the b_2 level. The EPR spectrum of VO^{2+} when having a tetragonal site symmetry can be described by a spin-Hamiltonian of the type[12]

$$\mathcal{H} = g_\parallel \beta \, H_z S_z + g_\perp \beta \, (H_x S_x + H_y S_y) + AI_z S_z + B \, (I_x S_x + I_y S_y) \quad \ldots(1)$$
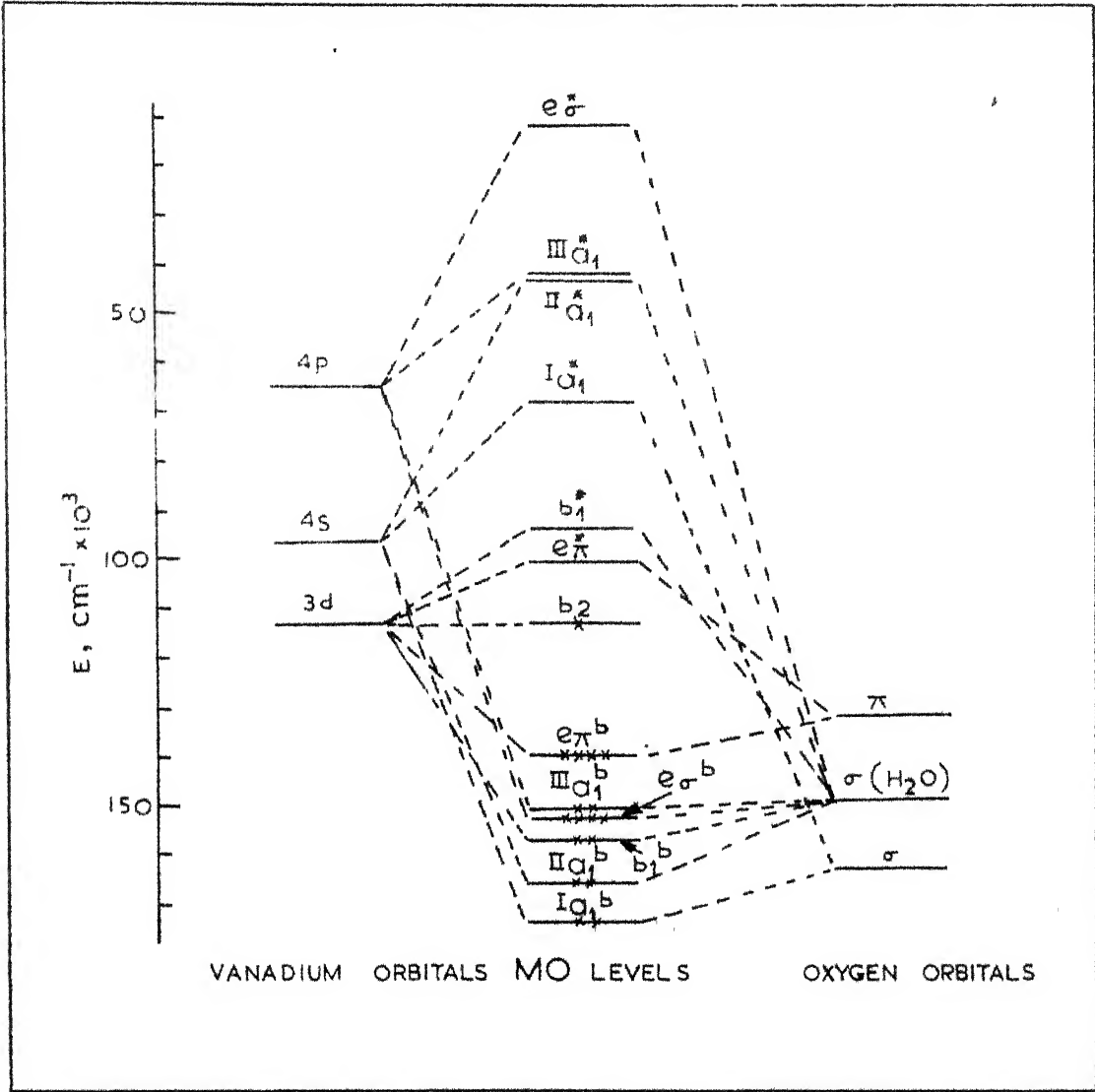
a solution of which gives the magnetic field resonance values by[12]

$$H = H_0 - \frac{Km_I}{g\beta} - \frac{B^2(A^2+K^2)}{4H_0 g^2 \beta^2 K^2} \left[I(I+1) - m_I^2 \right]$$

$$\frac{-(A^2-B^2) \, g_\parallel^2 \, g_\perp^2}{2H_0 g^2 \beta^2 K^2 g^4} \sin^2\theta \cos^2\theta \, m_I^2 \quad \ldots(2)$$

where $g^2 = g_\parallel^2 \cos^2\theta + g_\perp^2 \sin^2\theta$, $H_0 = \frac{h\nu}{g\beta}$ and $K^2 g^2 = A^2 g_\parallel^2 \cos^2\theta + B^2 g_\perp^2 \sin^2\theta$ in which θ is the angle between the z-axis and the direction of the magnetic field.

35

FIGURE III-II. Molecular orbital scheme for $[VO(H_2O)_5]^{2+}$.

VANADIUM ORBITALS MO LEVELS OXYGEN ORBITALS

Experimental procedure

Single crystals of potassium aluminium and ammonium aluminum
alums doped with VO^{2+} are grown by slow evaporation of the saturated
solution of the corresponding alum to which 1 mole % by weight of vanadyl
sulphate is added as an impurity . The instrument used in the present
investigations is briefly described in chapter II. A Cary-14 spectro-
photometer is used to record the optical absorption spectrum.

Results and discussion

The EPR spectra of VO^{2+} doped in potassium aluminum alum and
ammonium aluminum alum single crystals, recorded at $+25^{o}$c are shown
respectively in Figures III-III and III-IV. These spectra consist of
sixteen lines. In ammonium aluminum alum the inner group of eight lines
has approximately double the intensity of the outer group. The angular
variation of the spectrum in the $[100]$ plane of VO^{2+} in the potassium
aluminum alum is shown in Figure III-V which is similar to the one
obtained by Manoogian and MacKinnon[6] for the VO^{2+} in the rubidium
aluminum alum. This angular variation study shows that the EPR lines
occur in three groups of octets. It is to be noted in this figure that
two of the groups are found to be angular dependent, while the third
group does not show any variation in this plane. Further, along a
crystallographic $\langle 100 \rangle$ direction, two of the groups of lines collapse
into a single group to give a minimum separation, while the third group
has a maximum separation. The angular variation in ammonium aluminum alum
is similar to that in the potassium aluminum alum.

FIGURE III-III. The EPR spectrum of VO^{2+} ion doped in potassium alum single crystals at $+25^{o}C$ with the magnetic field making an angle of $1/2^{o}$ with <100> axis. The lines marked "a" are parallel transitions and the lines marked "b" are perpendicular transitions.

DPPH
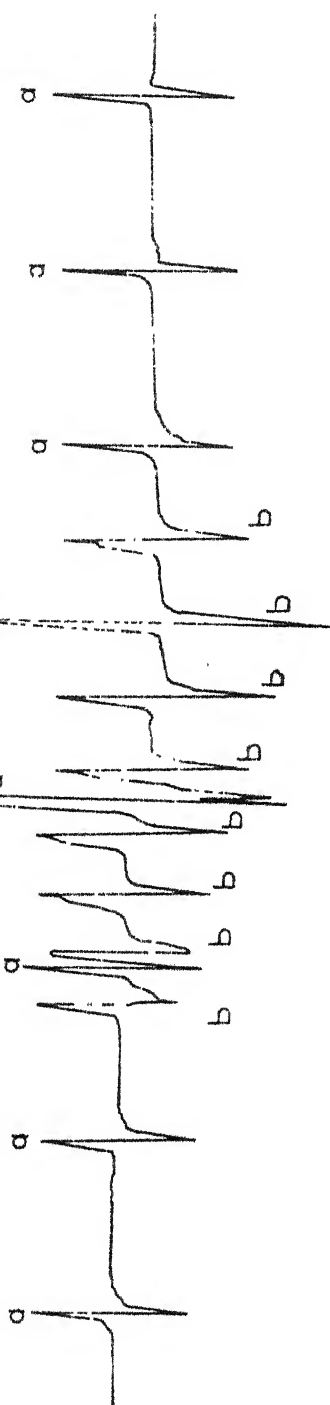
3395G

H

FIGURE III-IV. The EPR spectrum of VO^{2+} ion doped in ammonium alum single crystals at $+25^{o}C$ with $\langle 100 \rangle$ direction parallel to H. Lines marked "a" are parallel transitions. Lines marked "b" are perpendicular transitions.
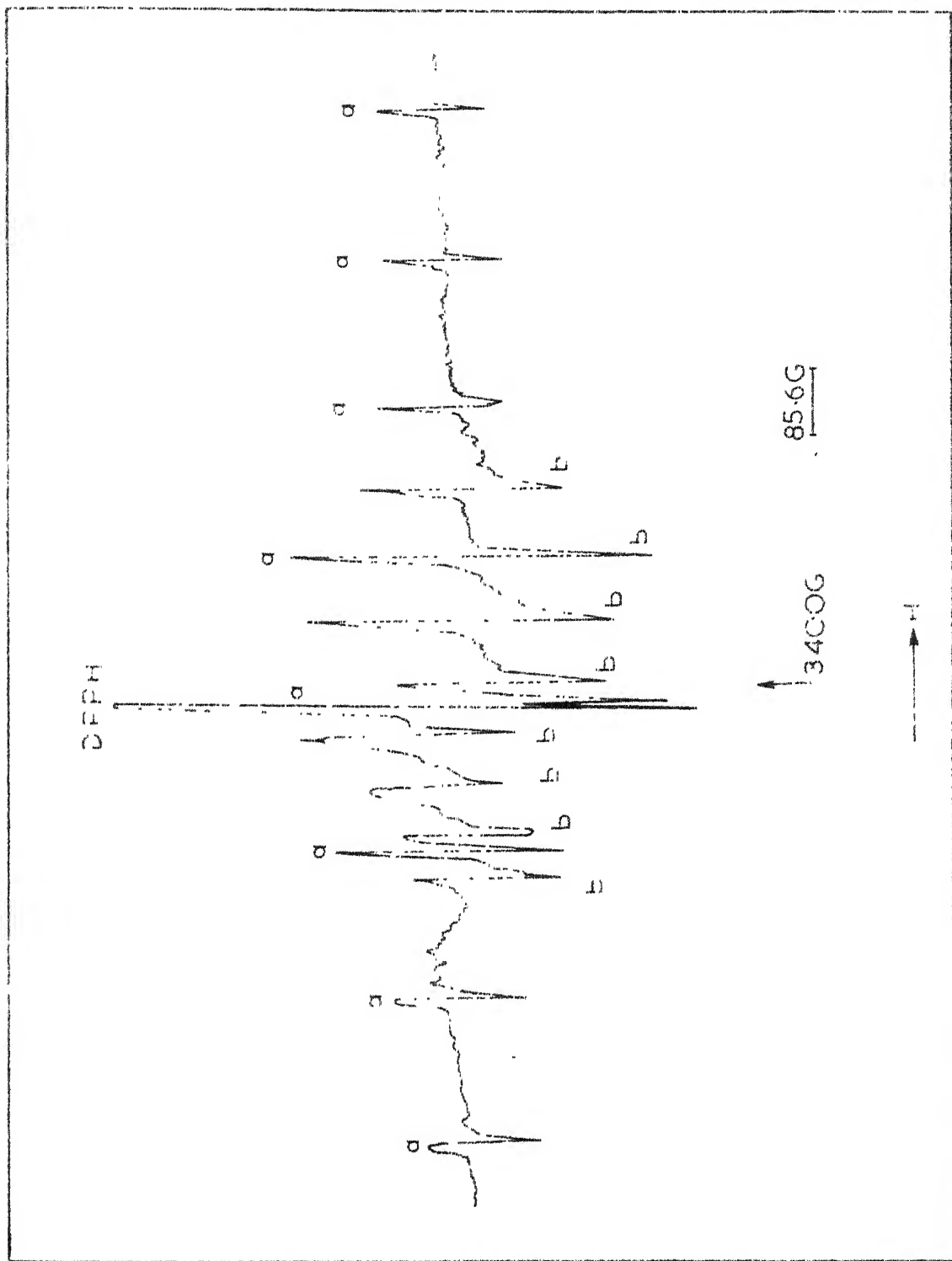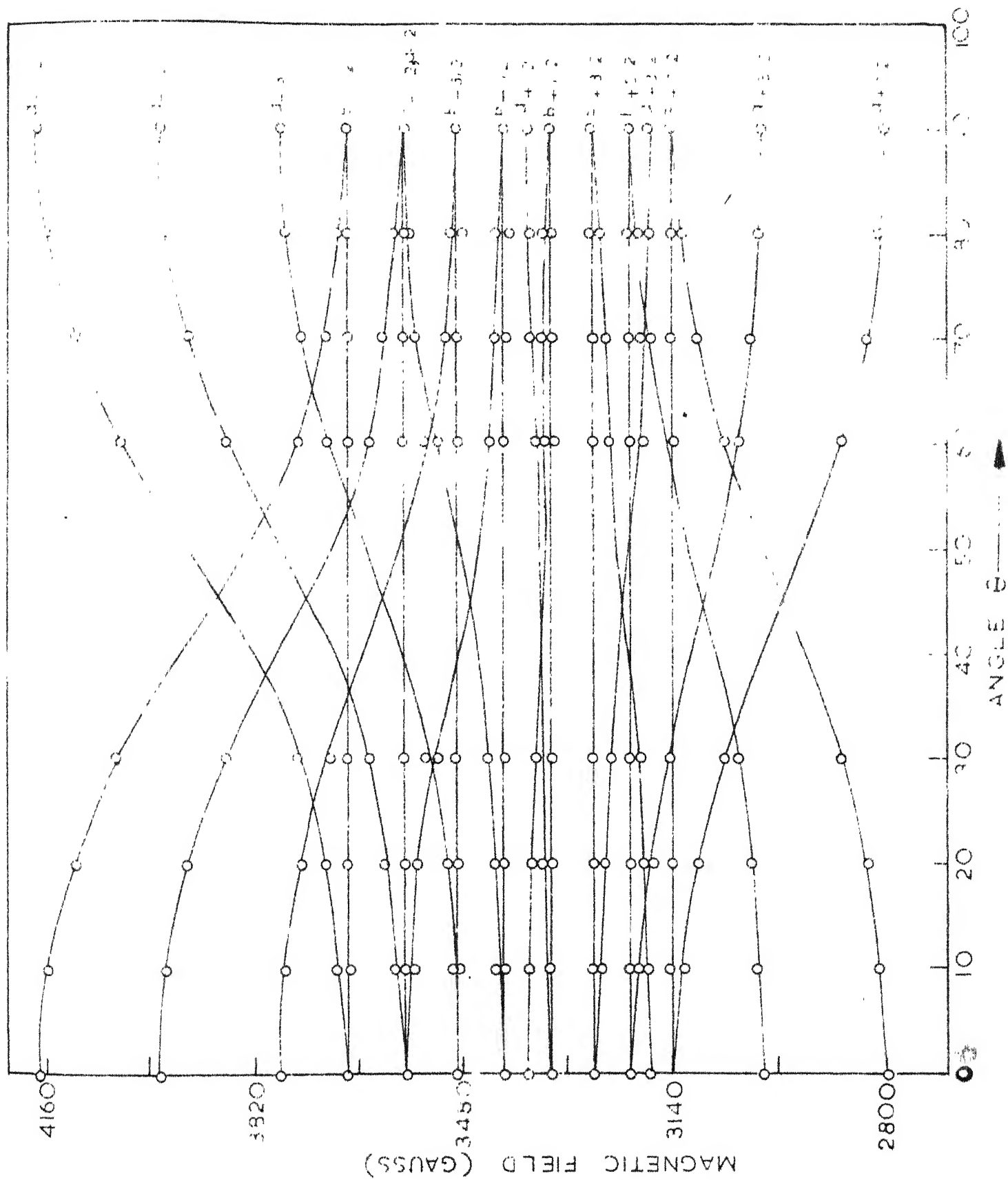
DPPH

85·6G

3400G

H

FIGURE III-V. Angular variation of the EPR spectrum of VO^{2+} ion doped

in the potassium alum single crystal in the $[100]$ plane.

The angular variation suggests that the spectrum is due to a VO^{2+} complex in a tetragonal symmetry having its symmetry axis along the crystallographic $\langle 100 \rangle$ direction. When VO^{2+} enters potassium aluminum alum or ammonium aluminum alum it can go in substitutionally either at K^+(or NH_4^+) site or at Al^{3+} site. If it goes to K^+ site the symmetry axis can not be the $\langle 100 \rangle$ direction, as the K-to-K-water bond is very much away from the $\langle 100 \rangle$ axis (see Fig. III-Ib). However, when VO^{2+} enters the lattice substitutionally at an Al^{3+} site, V^{4+} will be at the Al^{3+} site, associated with O^{2-} along one of the octahedron axes. As $[VO(H_2O)_5]^{2+}$ is found to be highly stable when incorporated substitutionally at Al^{3+} site, it creates an H_2O vacancy along the V-O bond direction thereby forming the stable vanadyl pentahydrate. Further the V-O bond length is shorter[6] than the bond lengths between V^{4+} and the water molecules and this probably causes a strong axial distortion in the V-O bond direction. In an oriented vanadyl pentahydrate complex there will be three possible mutually perpendicular directions for the V-O bond, one direction along each of the octahedron axes. So the twenty four lines which appear when the magnetic field makes an angle with the symmetry axis are probably due to the three vanadyl ions having their V-O bond in the three mutually perpendicular directions[6].

When H is parallel to the $\langle 100 \rangle$ axis one third of the VO^{2+} ions will have their symmetry axes parallel to H while two thirds of them will have their symmetry axes perpendicular to H because of the magnetic equivalence of the two perpendicular directions. Thus in this orientation the perpendicular components $(\theta = 90°)$ will be expected to be twice as

intense as those of the parallel components ($\theta = 0^o$) provided the intensity
of a line corresponding to an ion with $\theta = 0^o$ is same as that of the one
with $\theta = 90^o$. It appears that this expectation is nearly satisfied in the
case of VO^{2+} in ammonium aluminium alum where the perpendicular components
marked "b" in Figure III-IV are in general nearly twice as intense as the
corresponding parallel components marked "a" in the Figure. However there is
no marked diff erence in the intensities of the parallel and perpendicular
components in Figure III-III which represents the spectrum of VO^{2+} in
potassium aluminum alum. It has been observed that the perpendicular lines
in both alums split into two, even when H makes a small deviation from the
$\langle 100 \rangle$ direction of the crystal. It can be seen that all the lines marked
b show a small splitting in Figure III-III which represents the spectrum of
VO^{2+} in potassium aluminum alum with H deviated from the $\langle 100 \rangle$ direction by
about 0.5^o in the $[100]$ plane.

Since the symmetry axis has been found to coincide with the
crystallographic $\langle 100 \rangle$ direction, the substitution of VO^{2+} for Al^{3+} ion
appears to rotate the octahedron in such a way that its cubic axes coincide
with the crystallographic cubic axes. A similar effect was found in VO^{2+}
doped in rubidium aluminum alum[6]. In case the cubic axes of the octahedron
do not coincide with the crystallographic cubic axes then in the $[110]$
plane each of the lines should split into four, and a maximum separation
should be obtained at an angle of 9° from $\langle 100 \rangle$ direction in a $[110]$ plane[6].
As the angular variation in the $[110]$ plane does not show this type of
splitting and separation, it has been concluded that the octahedron cubic
axes coincide with the crystallographic cubic axes.

When the VO^{2+} ion substitutes for an Al^{3+} ion, due to charge imbalance some lattice defects may be created. It was however not possible to observe the effect of these defects in the present experiments.

The EPR spectra are analysed by using equations (2) and the spin-Hamiltonian constants are given in Table III-I. For comparison, the spin-Hamiltonian constants of VO^{2+} ion in other oriented complexes are also included in Table III-I. It can be seen from Table III-I that the spin-Hamiltonian constants obtained in the present study are nearly equal to those reported for $[VO(H_2O)_5]^{2+}$ in Tutton salt[5] and alums[6].

The existence of $[VO(H_2O)_5]^{2+}$ complex has been further confirmed by taking the optical absorption spectrum of VO^{2+} in both alums. The spectra in both alums are essentially similar and consist of two bands, one at $13000 cm^{-1}$ and the other at $15700 cm^{-1}$, which have been attributed by Ballhausen and Gray[10] to the $b_2 \rightarrow e_\pi^*$ and $b_2 \rightarrow b_1^*$ transitions of $[VO(H_2O)_5]^{2+}$. From the second transition the value of Dq turns out to be $\sim 1570 cm^{-1}$.

The EPR and optical absorption data can be correlated by using the expressions[13]

$$g_\perp = g_e \left[1 - \frac{\lambda \gamma^2}{\Delta E(b_2 \rightarrow e_\pi^*)} \right]$$

$$g_\parallel = g_e \left[1 - \frac{4 \lambda \alpha^2}{\Delta E(b_2 \rightarrow b_1^*)} \right]$$

The weaker the covalent character of the bonding, the closer are the

Table III-I

spin-Hamiltonian constants of VO^{2+} in different lattices

	Reference	$g_{\parallel}$	$g_{\perp}$	$Ax10^4$ (cm^{-1})	$Bx10^4$ (cm^{-1})
V^{4+} in TiO_2	16	1.956	1.914[a]	142	37[a]
V^{4+} in GeO_2	17	1.963	1.921[a]	134	37[a]
VO^{2+} in GeO_2 (amorphous)	17	1.929	1.976	175.5	68.2
VO^{2+} in Tutton salt	5	1.933	1.981[a]	182	71.8[a]
VO^{2+} in RbAl alum	6	1.932	1.975	182.2	66.6
VO^{2+} in CsAl alum	6	1.932	1.979	183.4	65.7
VO^{2+} in KAl alum	Present work	1.936± 0.001	1.977± 0.001	177±1	68±1
VO^{2+} in NH_4Al alum	Present work	1.940± 0.001	1.978± 0.001	176±1	67±1

[a] These represent the averages of x and y components.

values of the coefficients of α^2 and γ^2 to unity. The expressions $(1-\alpha^2)$ and $(1-\gamma^2)$ are the covalency rates. The former gives an indication of the influence of the σ-bonding between the vanadium ion and the equitorial ligands, while the latter indicates the influence of the π-bonding between the vanadium ion and the vanadyl oxygen.

By substituting the values of $g_{||}$, $g_{\perp}$, $\triangle E$ $(b_2 \rightarrow e_{\pi}^{*})$ and $\triangle E(b_2 \rightarrow b_1^{*})$ and knowing λ, one can get a reasonably good idea about the measure of the covalency rates $(1-\alpha^2)$ and $(1-\gamma^2)$. However, the magnitude of the spin-orbit coupling constant can not be selected with rigour. Several authors[10,14,15] have chosen the value of λ between $135cm^{-1}$ to $200cm^{-1}$, which yield reasonable results. Kivelson and Lee[15] have however shown from their EPR analysis of V^{4+} in GeO_2, that it seems unlikely that $\lambda < 170cm^{-1}$. In the present calculations, the value of λ has been chosen to be $170cm^{-1}$. Substitution of the values of g_e, and the experimental values $g_{||}$, $g_{\perp}$ and $\triangle E$'s yields $(1-\alpha^2) = 0.28$ and $(1-\gamma^2) = 0.07$ in the ammonium aluminum alum and $(1-\alpha^2) = 0.23$ and $(1-\gamma^2) = 0.03$ in the potassium aluminum alum showing that the covalency rate of the σ-bonding is very much greater than that of the π-bonding in both alums.

The spectra of VO^{2+} in both alums have been studied in the temperature range $+25^{\circ}c$ to $-180^{\circ}c$ to study the effect of the phase transition. There is no essential change in the spectra and the hyperfine constants and g-values also have been found to be essentially constant over the temperature range.

References

1. C. A. Whitmer, R. T. Weidner, J.S. Isiang and P.R. Weiss, Phys. Rev. 74, 1478 (1948).

2. D.M.S. Bagguley and J.H.E. Griffiths, Proc. Roy. Soc.(London) A204, 188 (1951).

3. C.A. Whitmer, R.T. Weidner and P.R. Weiss, Phys. Rev. 73,1468(1948).

4. M. D. Sastry and P. Venkateswarlu, Mol. Phys. 13, 161 (1967).

5. R. H. Borcherts and C. Kikuchi, J. Chem. Phys. 40, 2270 (1964).

6. A. Manoogian and J. A. Mackinnon, Can. J. Phys. 45, 2769(1967).

7. H. Lipson and C.A. Beevers, Proc. Roy. Soc. (London), A148,664(1935).

8. H. Lipson, Proc. Roy. Soc. (London) A151, 347 (1935).

9. D.L. Kraus and G.C. Nutting, J. Chem. Phys. 9, 133 (1941).

10. C.J. Ballhausen and H.B. Gray, Inorg. Chem. 1, 111 (1962).

11. K. De Armond, B.B. Garrett and H.S. Gutowsky , J. Chem. Phys. 42, 1019 (1965).

12. B. Bleaney, Phil. Mag. 42, 447 (1951).

13. J. M. Assour, J. Goldmacher and S.E. Harrison, J. Chem. Phys. 43, 159 (1965).

14. M. Roberts, W.S. Koski and W.S. Caughey, J. Chem. Phys. 34,591(1961).

15. D. Kivelson and S. K. Lee, J. Chem. Phys. 41, 1898(1964).

16. H. J. Gerritsen and H. R. Lewis, Phys. Rev.119, 1010 (1960).

17. I. Siegel, Phys. Rev. 134, A193 (1964).

CHAPTER IV

ELECTRON PARAMAGNETIC RESONANCE STUDIES OF VO^{2+} DOPED IN
METHYL AMMONIUM GALLIUM ALUM SINGLE CRYSTALS[*]

ABSTRACT

The electron paramagnetic resonance of the VO^{2+} ion in methyl ammonium gallium alum single crystals has been studied. It is observed that the VO^{2+} ion substitutes for the Ga^{3+} ion and forms a $[VO(H_2O)_5]^{2+}$ complex , a distorted octahedron with a H_2O vacancy along V-O bond direction. The octahedron cubic axes are found to be displaced from crystallographic $\langle 100 \rangle$ axes by 9° in $[110]$ plane. The EPR results suggest that the host alum probably belongs to β-type, in which the presence of VO^{2+} twists the octahedron cubic axes by about 9° from the crystallographic $\langle 100 \rangle$ axes. Optical absorption studies confirm the formation of $[VO(H_2O)_5]^{2+}$. By correlating the EPR and optical absorption data, the covalency rates of σ-bonding between the vanadium atom and equitorial ligands, and of the π-bonding between vanadium atom and the vanadyl oxygen, have been estimated.

Introduction

Earlier studies on VO^{2+} in NH_4Cl[1] and the work described in chapter V on VO^{2+} in KNO_3 and $CsNO_3$ show that the paramagnetic resonance spectrum of VO^{2+} ion in these crystals is independent of the orientation of the crystal with respect to the magnetic field direction, indicating that there is no preferred orientation of the V-O bond axis in these crystals. On the other hand, the work described in the earlier chapter on VO^{2+} in potassium aluminum (KAl) and ammonium aluminum (NH_4Al) alums, the work of Manoogian and Mackinnon[2] on rubidium aluminum (RbAl) and cesium aluminum (CsAl) alums and that of Borcherts and Kikuchi[3] on Tutton salt, show that it is strongly angular dependent indicating the existence of preferred orientation of V-O bond. Earlier studies[4-7] of transition metal ions in alum single crystals, have given interesting information about the structure of alums. The work of Manoogian and Mackinnon[2] and the work described in chapter III show how the presence of VO^{2+} effects the structure of the host lattices. The present work on methyl ammonium gallium (MAG) alum doped with VO^{2+} has been taken up to get information about the effect of VO on the structure of the alum and also about the structure of the vanadyl complex in the crystal. It was hoped also that a comparison of the results obtained in this alum with those known in other alums might give some indication about its structure (α, β or γ).

Structure of alums

The structure of α-type of alums is described in chapter III. The β alums are described as having perfectly regular groups of water molecules, the axes of the octahedron being directed along the cubic axes of the crystal.

The family to which MAG alum belongs has not been given in literature[8]. The KAl, RbAl, and NH_4Al alums belong to the α-type while CsAl alum belongs to the β-type. Studies of VO^{2+} in RbAl and CsAl alums[2] and the work described in the earlier chapter on VO^{2+} in KAl and NH_4Al alums show that the behaviour of paramagnetic resonance in the α-type alums is different from that in β-type alums. A comparison of the EPR of VO^{2+} in these crystals with that in MAG alum will be made in the latter part of this chapter.

Experimental procedure

Single crystals of MAG alum doped with VO^{2+} ion are grown by slow evaporation of the saturated solution of the alum to which 0.5 mole percent by weight of vanadyl sulphate is added as an impurity . The crystals are found to grow as octahedrons with well defined [111] planes in the usual habit of other alums. The remaining experimental details are same as those given in chapter II.

Results and discussion

The EPR spectrum of VO^{2+} ion doped in MAG alum single crystals, recorded at $+25^{o}c$, along the crystallographic $\langle 100 \rangle$ direction is shown in Figure IV-I. The angular variation of the spectrum is studied in both $[100]$ and $[110]$ planes. When the magnetic field angle is varied in a $[100]$ plane, each of the resonance lines which appeared single in a crystallogrphic $\langle 100 \rangle$ direction splits into two, and when the angle is varied in a $[110]$ plane, the lines split into four, the magnitude of the splitting being different for different lines. A maximum separation for one set of lines is found at an angle of 9° from the crystallographic $\langle 100 \rangle$ direction in $[110]$ plane. The EPR spectrum of VO^{2+} ion in this alum at an angle of 9° from crystallographic $\langle 100 \rangle$ direction in $[110]$ plane, is shown in Figure IV-II.

The results obtained can be well understood if one assumes that VO^{2+} substitutes Ga^{3+} ion in the crystal and forms a $\left[VO(H_2O)_5 \right]^{2+}$ complex, a distorted octahedron with a H_2O vacancy along with VO bond direction as in the case of the RbAl and CsAl alums[2] and NH_4Al and KAl alums (Chapter III). It has been found in these alums that the presence of VO^{2+} rotates the octahedron of water molecules by 8 to 9° from its original position about the $\langle 111 \rangle$ axis.

In the case of the $RbAl^{2}$, KAl and NH_4Al alums (Chapter III) which belong to the $\measuredangle$-type of alums, the V-O bond direction coincides with one of the cubic axes of the crystal, while it makes an angle of

FIGURE IV-I. EPR spectrum of VO^{2+} ion doped in MAG alum with the magnetic field along the crystallographic $\langle 10(\rangle$ direction at $+25^{0}$C. Lines marked "a" are due to the transitions of VO^{2+} ion having the V-O bond at an angle of 9^{0} with the magnetic field and those marked "b" are due to transitions of VO^{2+} ion having its bond at an angle of 90 ± 9^{0} with the magnetic field direction.

DPPH

21·23G

3380G

H →
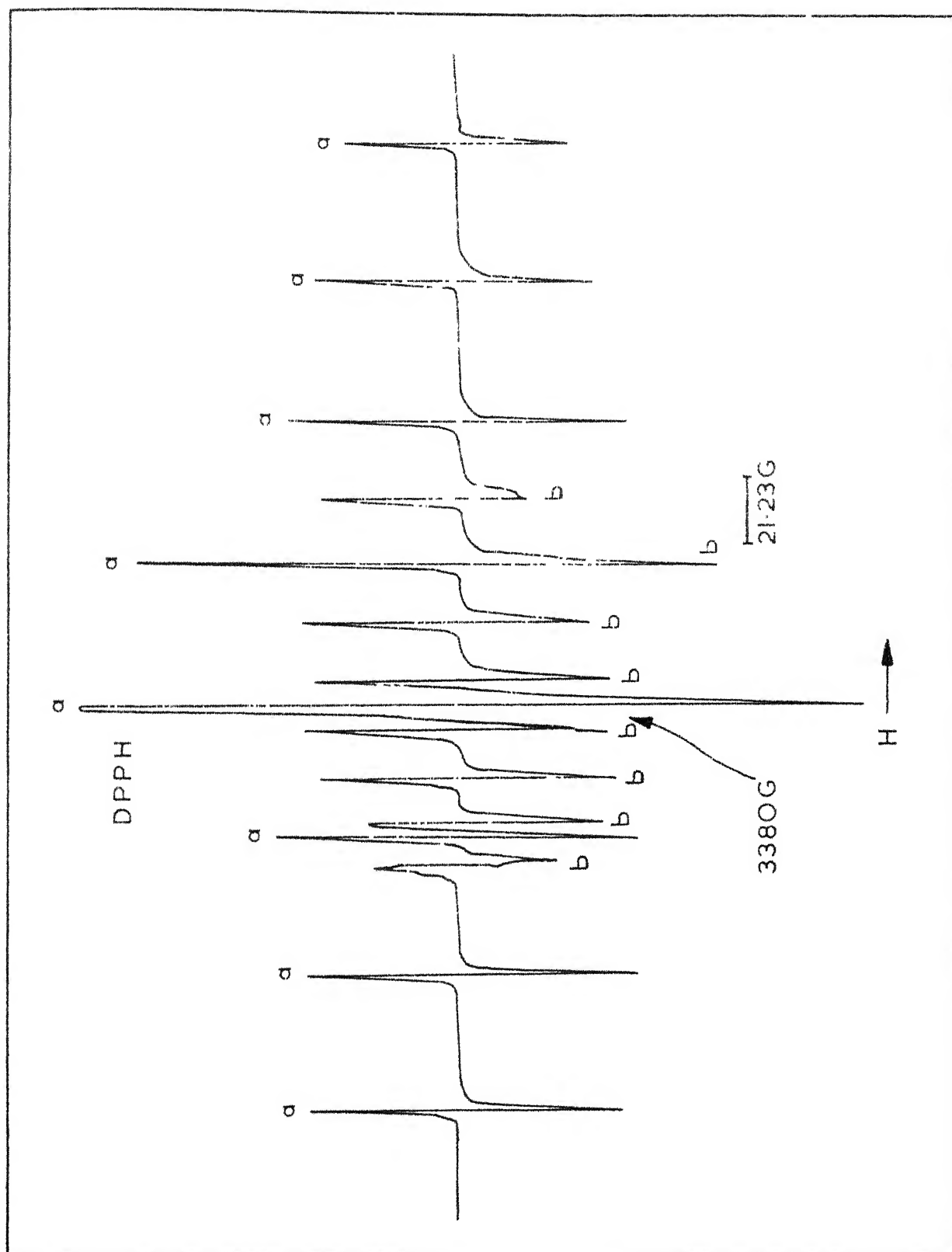
FIGURE IV-II. EPR spectrum of VO^{2+} ion doped in MAG alum with the magnetic
field making angle of 9° from the crystallographic $\langle 100 \rangle$
direction in the $[11.]$ plane at $+25^o C$. Lines marked "a"
are due to the transitions of VO^{2+} ion having the V-O bond
along the direction of the magnetic field, and those marked
"b" are due to transitions of VO^{2+} ion having its bond
perpendicular to magnetic field direction.

DPPH

21·23G

3380G

H
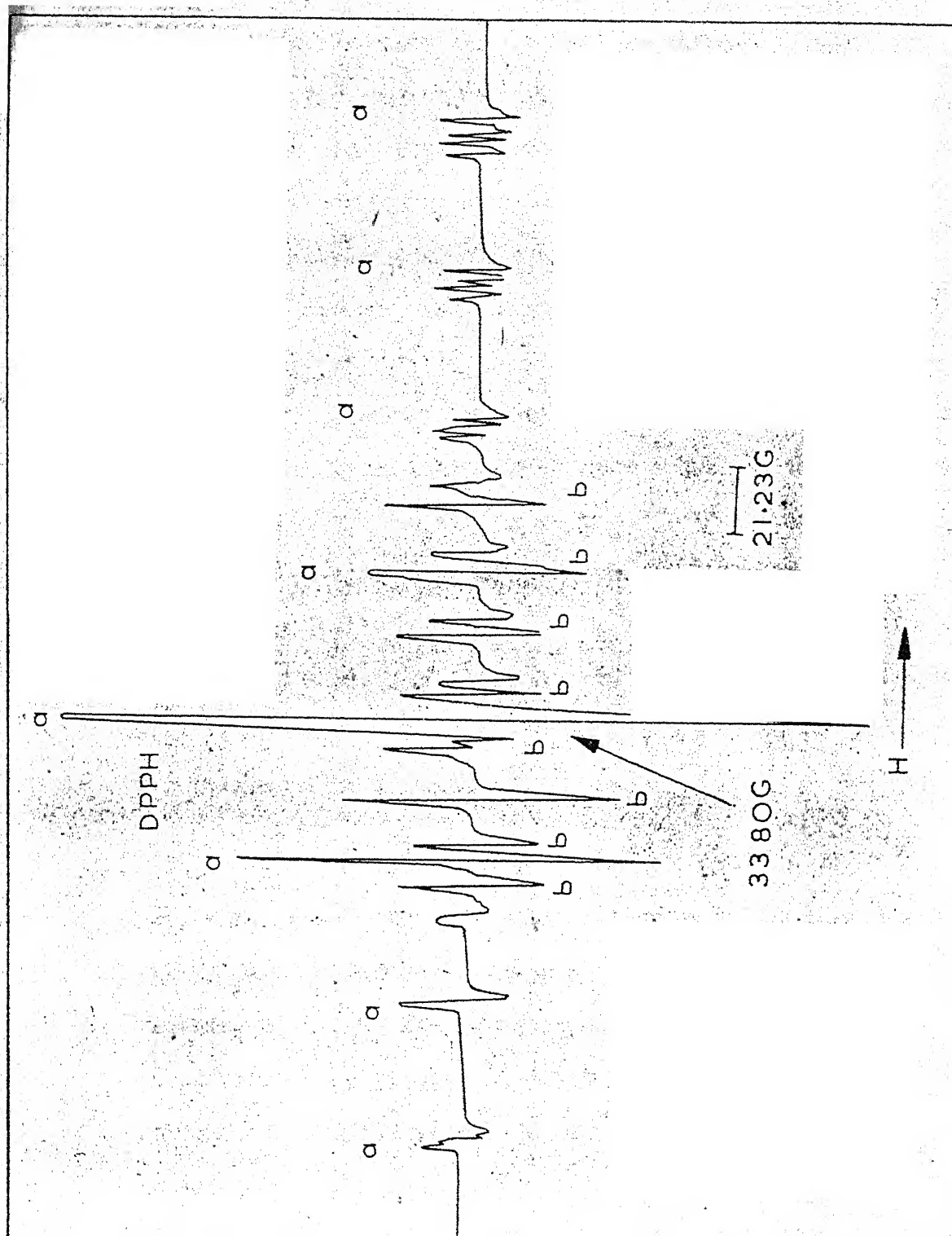
about 8° with the cubic axis in the case of the CsAl alum[2] which belongs
to β-type. The angular variation of the spectrum of VO^{2+} in MAG alum in
the [110] and [100] planes is found to be exactly similar to that in the
CsAl alum[2] suggesting that the MAG alum probably corresponds to the β-type
of alums. Methyl ammonium aluminum (MAA) and methyl ammonium chromium
(MAC) alums belong to the β-type. The indication that the MAG alum belongs
to the β-type as the MAA and MAC alums is consistent with the suggestion
of Lipson and Beevers[9] that the size of the monovalent ion is "solely
responsible" for the behaviour of alums. However the size of the trivalent
ion is also known[10] to play an important role since RbCr and CsCr alums
are both of β- type while RbAl belongs to α-type and CsAl to β-type.
The EPR experiments also show how the alums are effected by the substitution
of VO^{2+} in the place of the trivalent ions. It appears that the sizes
of both trivalent and monovalent ions in the alums are jointly responsible
for the behaviour of alums.

As the maximum spread of the EPR spectrum of VO^{2+} is obtained
when H makes an angle of 9° with $\langle 100 \rangle$ axis in the [110] plane it is
likely that the V-O bond lies in that direction, or nearly about that
direction. If pure MAG alum crystal belongs to the β-type of alums the
cubic axes of the octahedron of waters and those of the crystal coincide,
but the substitution of VO^{2+} at Ga^{3+} site probably twists the octahedron
in such a way that its cubic axes are displaced by about 9° with respect
to those of the crystal making the V-O bond lie nearly in a [110] plane
at an angle of about 9° from the crystallographic $\langle 100 \rangle$ axis. In such a
model there will be four positions of the V-O bond direction that will be

displaced by about 9° from $\langle 100 \rangle$ direction[2,7]. Along a $\langle 100 \rangle$ direction all four positions are equivalent and the spectrum obtained is as shown in Figure IV-I, where the lines marked "a" correspond to 9° while those marked "b" correspond to $90^o \pm 9^o$. When the magnetic field is along a V-O bond direction there are three other V-O bond directions making different angles with the field direction and the lines are expected[2,7] to split into four (Figure IV-II). It is clear from Figure IV-II that all the lines are not uniformly split. The lines with $m_I = -7/2$, $-5/2$, $-3/2$ and $+7/2$ can be clearly seen in the Figure to be split into four but the mutual separation of the components is different in all the lines. This suggests that the splitting is dependent not only on Θ but probably also on the value of m_I. This m_I dependence of splitting comes probably due to the differences in angular dependence of different hyperfine transitions. The angular sensitivity of any line can be clearly seen from the slopes of H (magnetic field resonance values) versus Θ curves for different transitions (see Figure III-V for such curves). By differentiating equation (2) of chapter III one can easily see that the slopes depend upon m_I, through a formula of the type $a_1 + a_2\, m_I + a_3\, m_I^2$, where a's contain A and B. A careful examination of the splittings of the lines clearly shows that they indeed follow this m_I dependence which results in a better resolution of lines of largest m_I.

When H is parallel to a crystallographic $\langle 100 \rangle$ direction, one third of the VO^{2+} ions will have their symmetry axis making an angle of 9° with H while two thirds of them will have their symmetry axis making an angle of 90 ± 9° with H. Thus in this orientation the lines marked "b"

in Figure IV-I will be expected to be twice as intense as those of the lines marked "a" provided the intensity of a line corresponding to an ion with $\theta = 9°$ is the same as that of the one with $\theta = 90 \pm 9°$. However, from Figure IV-I there is no marked difference in the intensities in the lines marked "a" and "b". It may be noted here that such a difference in intensity has been observed in the spectrum of VO^{2+} doped in NH_4Al alum but not in KAl(Chapter III) and RbAl alums[2]. From the g and A values of the spectrum observed in the present experiments along the z-axis (at an angle of $9°$ from the crystallographic $\langle 100 \rangle$ direction in $[1\bar{1}0]$ plane), one would expect a spectrum with values g = 1.938 and A = 190G and another with g = 1.969 and A 78 G for the orientation in which H is parallel to the $\langle 100 \rangle$ direction. It is found that the lines marked "a" yield the constants g = 1.938 and A = 190G and the lines marked "b" yield the constants g = 1.969 and A = 78G as expected, thereby confirming that these are the $9°$ and $90° \pm 9°$ angular parts of the z-spectrum respectively. As a maximum spread of the lines occurs when H is parallel to a particular V-O bond axis, the corresponding spectrum in Figure IV-II for $\theta = 0°$ is analysed by using equations appropriate for tetragonal symmetry[11] and the g-values and the hyperfine constants are given in Table IV-I along with those observed for $[VO(H_2O)_5]^{2+}$ in other alums. It can be seen that the spin-Hamiltonian constants obtained in the present study are nearly equal to those observed for $[VO(H_2O)_5]^{2+}$ in other alums given in Table III-I.

When VO^{2+} ion substitutes for a Ga^{3+} ion, the deficiency of the positive charge is to be compensated by the creation of a negative ion

Table IV-I

Spin-Hamiltonian constants of VO^{2+} in various alums

	Type of alum	Reference	$g_\parallel$	$g_\perp$	$A \times 10^4$ (cm^{-1})	$B \times 10^4$ (cm^{-1})
VO^{2+} in RbAl alum	α	2	1.932	1.975	182.2	66.6
VO^{2+} in CsAl alum	β	2	1.932	1.977	183.4	65.7
VO^{2+} in KAl alum	α	Chapter III	1.936 ± 0.001	1.977 ± 0.001	177 ± 1	68 ± 1
VO^{2+} in NH_4Al alum	α	Chapter III	1.940 ± 0.001	1.978 ± 0.001	176 ± 1	66 ± 1
VO^{2+} in MAG alum	(β)	Present work	1.939 ± 0.001	1.976 ± 0.001	174 ± 1	67 ± 1

vacancy or some other means. The present experiments indicate that the charge compensating site is probably too far from the VO^{2+} ion to have any noticeable effect on the EPR spectrum of the ion.

The existence of $\left[VO(H_2O)_5\right]^{2+}$ complex has been confirmed by taking the optical absorption spectrum of VO^{2+} in this alum. The spectrum consists of two bands one at $12700cm^{-1}$ and the other at $15200cm^{-1}$ which have been attributed, by Ballhausen and Gray[12], to the $b_2 \rightarrow e_\pi^*$ and the $b_2 \rightarrow b_1^*$ transitions of $\left[VO(H_2O)_5\right]^{2+}$. From the second transition the Dq value turns out to be $\sim1520cm^{-1}$.

The optical absorption data can be correlated to the EPR data by using the expressions[13]

$$g_\perp = g_e \left[1 - \frac{\lambda \gamma^2}{\Delta E(b_2 \rightarrow e_\pi^*)} \right]$$

$$g_\parallel = g_e \left[1 - \frac{4\lambda \alpha^2}{\Delta E(b_2 \rightarrow b_1^*)} \right]$$

The expressions $(1-\alpha^2)$ and $(1-\gamma^2)$ are respectively the covalency rates of σ-bonding between the vanadium ion and the equitorial ligands and of the π-bonding between the vanadium ion and the vanadyl oxygen.

By substituting $g_\parallel$, $g_\perp$, $\Delta E(b_2 \rightarrow e_\pi^*)$, $\Delta E(b_2 \rightarrow b_1^*)$ and λ, one can calculate the values of $(1-\alpha^2)$ and $(1-\gamma^2)$. The spin-orbit coupling constant λ has been chosen to be $170cm^{-1}$, due to the reason given in chapter III. The values of $(1-\alpha^2)$ and $(1-\gamma^2)$ have been calculated and

are given in Table IV-II along with those values for KAl and NH_4Al alums. As in KAl and NH_4Al alums (Chapter III), the covalency rates of σ-bonding is found to be very much greater than that of π-bonding in this alum.

MAG alum has been found[14] to have a phase transition at $171^{\circ}K$ below which it is found to be ferroelectric. The spectra of VO^{2+} in MAG alum has been studied in the temperature range 300° to $77^{\circ}K$ with a view to detect the effect of the phase transition on the EPR spectrum. But as in KAl and NH_4Al alums (Chapter III) there is no essential change in the EPR spectra and the hyperfine constant' and the g-value are found to be essentially constant over the temperature range studied.

References

1. M. D. Sastry and P. Venkateswarlu, Mol. Phys. 13, 161 (1967).

2. A. Manoogian and J.A. Mackinnon, Can. J. Phys. 45, 2769 (1967).

3. R. H. Borcherts and C. Kikuchi, J. Chem. Phys. 40, 2270 (1964).

4. C.A. Whitmer, R.T. Weidmer, J.S. Isiang and P. R. Weiss, Phys. Rev. 74, 1478 (1948).

5. D. M. S. Bagguley and J. H. E. Griffiths, Proc. Roy. Soc.(London) A204, 188 (1951).

6. C.A. Whitmer, R. T. Weidmer and P. R. Weiss, Phys. Rev. 73, 1468(1948).

7. B. Bleaney and R.S. Trenam, Proc. Roy. Soc. (London) A223, 1, (1954).

8. R. W. G. Wyckoff : Crystal Structures :Interscience Publishers· (New York),Vol. 3, p875 (1965).

9. H. Lipson and C. H. Beevers, Proc. Roy. Soc. (London) A148, 664(1935).

10. H. P. Klug, J. Amer. Chem. Soc. 62, 2992 (1940).

11. B. Bleaney, Phil. Mag. 42, 447 (1951).

12. C. J. Ballhausen and H. B. Gray, Inorg. Chem. 1, 111 (1962).

13. J. M. Assour, J. Goldmacher and S.E. Harrisson, J. Chem. Phys. 43, 159 (1965).

14. F. Jona and G. Shirane: Ferroelectric Crystals:The Macmillan Company· (New York), (1962).

CHAPTER V

ELECTRON PARAMAGNETIC RESONANCE STUDIES OF VO^{2+}

DOPED IN KNO_3 AND $CsNO_3$ SINGLE CRYSTALS[*]

ABSTRACT

The electron paramagnetic resonance spectra of VO^{2+} ion doped in KNO_3 and $CsNO_3$ single crystals have been investigated over a wide temperature range. Room temperature studies reveal that there is a very fast readjustment of VO^{2+} ion, in both crystals, which is manifested ' in the presence of a single isotorpic octet, thereby exhibiting a low viscous "liquid-like" nature. At low temperatures an anisotropic spectrum is obtained due to the hindered rotation of the VO^{2+} ion. The effect of $CsNO_3$ in hindering the rotation of vanadyl ion is found to be greater than that of KNO_3. The linewidths at room temperature are found to depend upon the m_I quantum number, and an attempt is made to fit the linewidth data of the present study in the theoretical expressions of Kivelson. It is found that Kivelson's theory can qualitatively explain the observed variation of linewidth with nuclear quantum number m_I, but the experimental data could not be fit quantitatively into the theory.
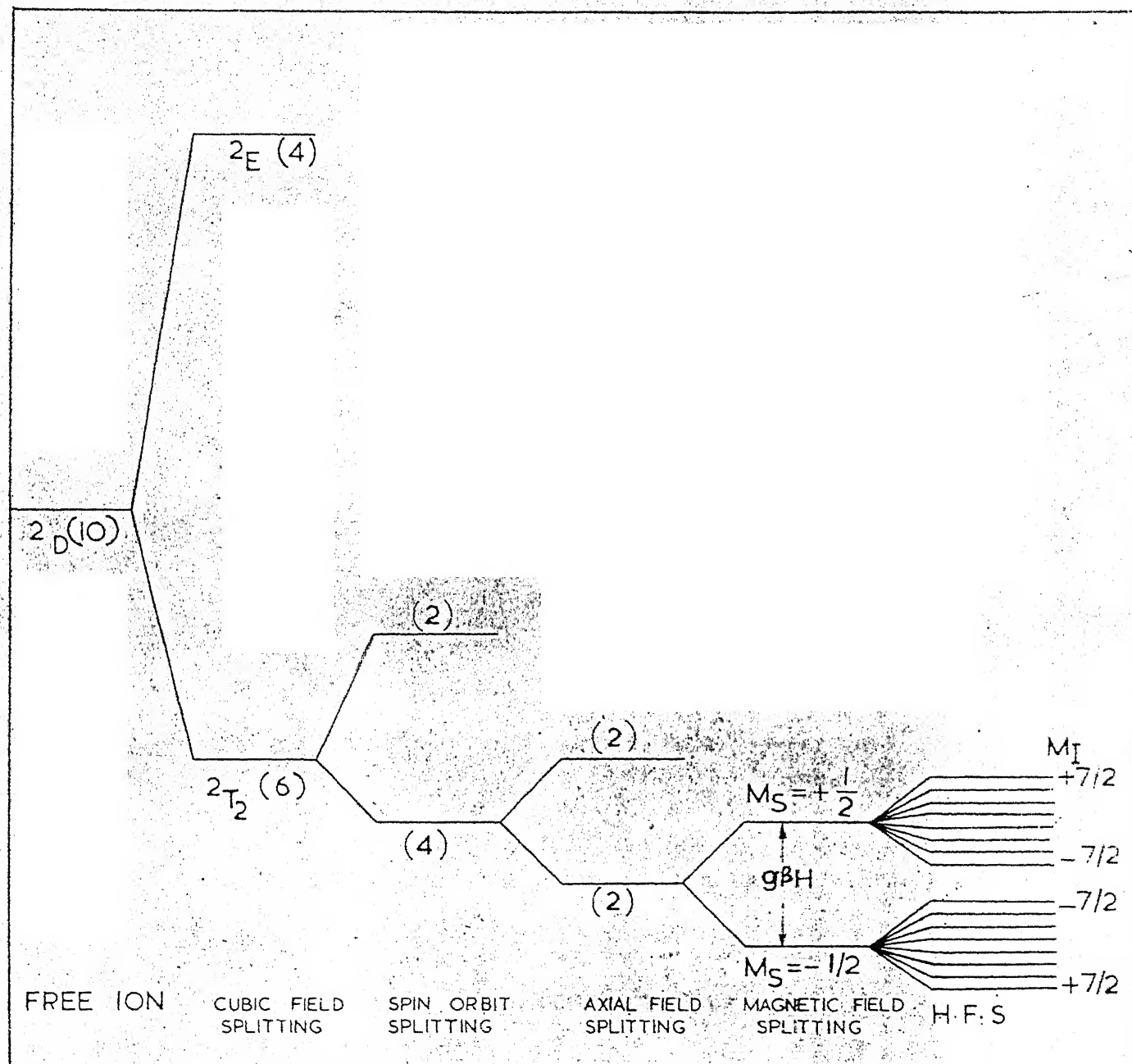
Introduction

The electron paramagnetic resonance (EPR) studies of VO^{2+} in Tutton salts[1] and of V^{4+} in TiO_2[2] and GeO_2[3] indicate that V^{4+} entering the lattice forms a strong covalent bond with one of the oxygens of the lattice and a weak bond with five other oxygens forming a distorted octahedron. In all these cases there is a preferred orientation of V-O because of the bonding of V^{4+} with one of the oxygens of the lattice. On the other hand Sastry and Venkateswarlu[4] have recently reported from their study of the EPR of VO^{2+} in NH_4Cl single crystal that there is no preferred orientation of V-O bond in that crystal. The EPR studies of V-O molecular ion in single crystals can thus be expected to give valuable information about the structure of the V-O complex in such crystals. Further, it was felt that it would be also interesting to examine the applicability of the different paramagnetic relaxation theories developed for liquids to single crystal systems exhibiting liquid-like nature, wherein the V-O bond has no preferred orientation. This chapter deals with the EPR studies of VO^{2+} in KNO_3 and $CsNO_3$ single crystals over a wide temperature range.

Theory

A tetravalent vanadium ion with outer electronic configuration $3d^1$ exists in a most stable form as VO^{2+}. The ground state splitting of this VO^{2+} ion under the crystalline field approximation is shown in Figure V-I. In a crystalline field of symmetry less than cubic(tetragonal or lower), the lowest level will be an orbital singlet and the EPR spectrum

FIGURE V-I. Splitting of ^2D state of VO^{2+} under the action of crystalline fields, spin-orbit coupling, magnetic field and hyperfine interaction. The degeneracy of each level is given in brackets.

$^2E\ (4)$

$^2D\ (10)$

$^2T_2\ (6)$

(2)

(4)

(2)

(2)

$M_S = +\frac{1}{2}$

$M_S = -\frac{1}{2}$

$g\beta H$

M_I

$+7/2$

$-7/2$

$-7/2$

$+7/2$

FREE ION

CUBIC FIELD
SPLITTING

SPIN ORBIT
SPLITTING

AXIAL FIELD
SPLITTING

MAGNETIC FIELD
SPLITTING

H.F.S

consists of a single fine structure line, which further splits into eight lines due to the interaction with the V^{51} nucleus (I= 7/2). The EPR spectrum of VO^{2+} molecular ion· in solutions[5] is usually described by a spin- Hamiltonian of the type

$$\mathcal{H} = g_{||} \ \beta \ H_z \ S_z + g_{\perp} \ \beta \ (H_x \ S_x + H_y \ S_y) + A \ I_z \ S_z + B(I_x \ S_x + I_y \ S_y) \ ..(1)$$

The Hamiltonian (1) can be solved in order to obtain the magnetic field resonance values. The magnetic field values are given by the relation[6]

$$H = H_0 - \frac{Km_I}{g\beta} - \frac{B^2(A^2 + K^2)}{4H_0 g^2 \beta^2 K^2} \left[I(I +1) - m_I^2 \right]$$

$$- \frac{(A^2 - B^2) g_{||}^2 \ g_{\perp}^2 \ \sin^2 \theta \ \cos^2 \theta \ m_I^2}{2H_0 \ g^2 \beta^2 K^2 \ g^4} \qquad ..(2)$$

where $g^2 = g_{||}^2 \ \cos^2 \theta + g_{\perp}^2 \ \sin^2 \theta$, $H_0 = \dfrac{h\gamma}{g\beta}$

and $K^2 \ g^2 = A^2 \ g_{||}^2 \ \cos^2 \theta + B^2 \ g_{\perp}^2 \ \sin^2 \theta$

θ being the angle between the z-axis and the direction of the magnetic field.

Experimental procedure

Single crystals of KNO_3 and $CsNO_3$ doped with VO^{2+} are grown by slow evaporation of saturated solutions of the corresponding nitrates to which 1 mole % by weight of vanadyl nitrate (prepared from a chemical reaction between Ag NO_3 and $VOCl_2$) is added as an impurity. The instrument used in these investigations is briefly described in chapter II. A

General Microwave 454A thermoelectric power meter is used to measure
microwave power.

Results and discussion

Potassium nitrate is known to have[7] aragonite structure D_{2h}^{16} at
room temperature and calcite structure D_{3d}^6 above $+ 128^\circ$c with a probable
ferroelectric metastable phase[8] in between them. Cesium nitrate is also
known to have a phase transition[9] at $+ 161^\circ$c which involves a structural
transformation from trigonal to cubic symmetry.

The EPR spectra of VO^{2+} in KNO_3 and $CsNO_3$ single crystals recorded
at different temperatures are shown respectively in Figures .V -II and
V-III. The spectra recorded at room temperature show isotropic octets
and the linewidths are found to depend upon the nuclear quantum number m_I.
These spectra are referred to , in this chapter, as "spectrum $I(KNO_3)$" and
"spectrum $I(CsNO_3)$" respectively. As the temperature is lowered the
linewidths are found to increase and it becomes difficult to recognize the
lines in the KNO_3 crystal at -150°c and in $CsNO_3$ crystal at -70°c. An
anisotropic spectrum appears to show up in $CsNO_3$ crystal at about -110c,
while a similar spectrum shows up only at about liquid nitrogen temperature
in the case of the KNO_3 crystal. These anisotropic spectra at liquid
nitrogen temperatures are referred to, in this chapter, as"spectrum $II(CsNO_3)$"
and "spectrum $II(KNO_3)$" respectively. These spectra reveal the characteristic
parallel and perpendicular components labelled as "a" and "b" in the Figures,
though they are observed to be angular independent. The spectra I and II
observed here in KNO_3 and $CsNO_3$ are very much similar to those obtained

FIGURE V - II   EPR spectra of VO^{2+} in KNO_3 at $+25^0$c, -15^0c and
-196^0c. Lines marked "a" are parallel transitions
and lines marked "b" are perpendicular transitions.
Some parallel and perpendicular transitions overlap
in the central part of the spectrum at liquid nitrogen
temperature. The spectrum at $+25^0$c is referred to as
spectrum I and the one at -196^0c as spectrum II.
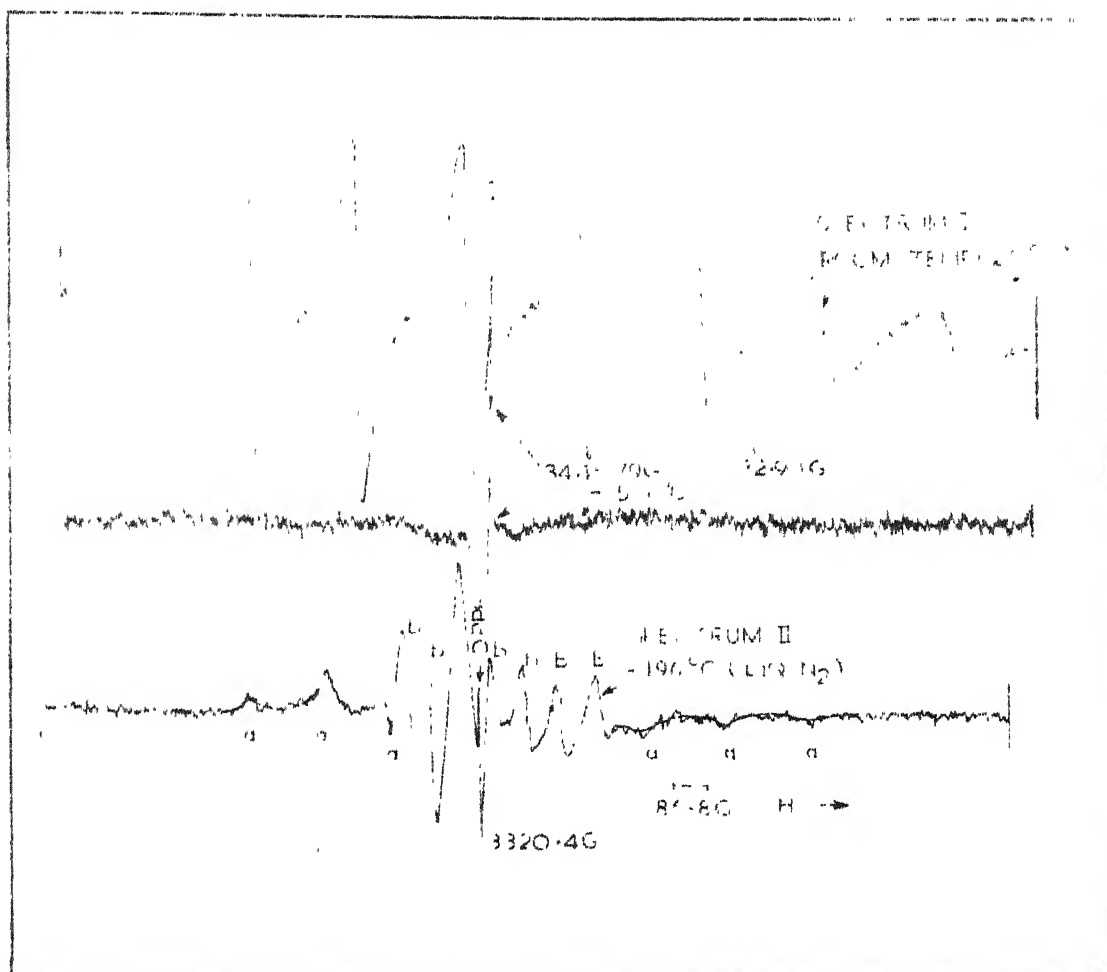
FIGURE V-III.   EPR spectra of VO^{2+} in $CsNO_3$ at $+25^o$c, $-7.^oc$, -110^oc

and -196^oc. Lines marked "a" are parallel transitions

and lines marked "b" are perpendicular transitions. The

existence of the anisotropic spectrum can be seen at

-110^oc (unlike in KNO_3). Some parallel and perpendicular

transitions overlap in the central part of the spectrum

at liquid nitrogen temperature. The spectrum at $+25^o$c

is referred to as spectrum I and the one at -196^oc as

spectrum II.

DPPH

←—3383·8 G

SPECTRUM I
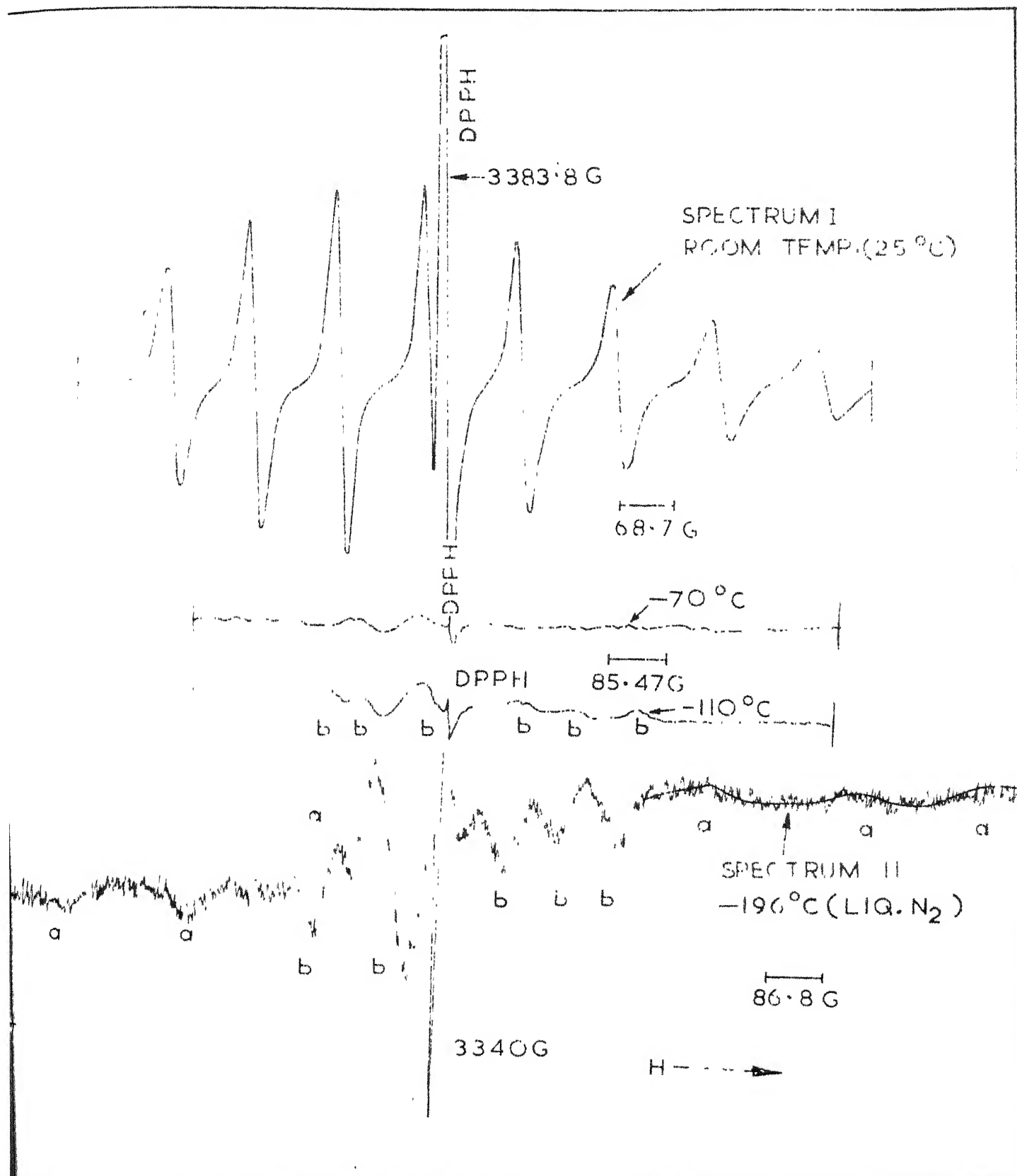ROOM TEMP.(25°C)

68·7 G

DPPH

—70°C

DPPH   85·47G

b b   b   b   b   b   ←—110°C

a   a   a   a

SPECTRUM II
−196°C(LIQ. N$_2$)

a   a   b   b   b

b   b

86·8 G

3340G

H ——→

for VO^{2+} in NH_4Cl single crystal[4]. It can also be seen that the room temperature spectra $I(KNO_3)$ and $I(CsNO_3)$ of the present experiments are similar to the one reported by O'Reilly[5] for vanadyl etioporphirin(VEPI) in benzene solution, while the spectra $II(KNO_3)$ and $II(CsNO_3)$ are similar to those of VEPI dissolved in high viscous oil and of solid asphaltenes containing vanadium porphins[5]. Borcherts and Kikuchi[1] reported for VO^{2+} in polycrystalline Tutton salt a spectrum similar to the anisortopic spectra II obtained here. However the possibility of the formation of Polycrystalline samples at low temperatures in the present study is eliminated as the transformation from spectrum I to II is found to be reversible in $CsNO_3$ as well as in KNO_3.

The above similarity of the features of the spectra obtained here with those of the spectra obtained for VEPI in low and high viscous media suggests that KNO_3 behaves essentially as a liquid for the rotation of the VO^{2+} ion. So all orientations of VO^{2+} ion are possible and there can be readjustment of V-O bond axis from one orientation to another resulting in a random distribution of V-O bond axis. In the case, where the molecule is rotating with a shorter correlation time, the Hamiltonian (1) reduces to an isotropic Hamiltonian with[5,10]

$$g_0 = (1/3)(g_{||} + 2g_{\perp})$$

and
$$A_0 = (1/3)(A + 2B) \qquad \qquad \ldots(3)$$

Therefore the isotropy of spectra $I(KNO_3)$ and $I(CsNO_3)$ at room temperature is probably due to the fast reorientation of the V-O bond axis. Spectrum I is analysed for both crystals and the spin-Hamiltonian constants obtained

are given in Table V-I.

If the correlation time for the rotation of the molecule is sufficiently long, the Hamiltonian (1) remains anisotropic and it must be used with suitable average of the allowed transitions over all orientations. O'Reilly[5] has obtained the eigen values of the Hamiltonian (1) by perturbation theory and calculated the resulting line shape for each value of m_I for $g \beta H \gg A$ and B. The spectrum so obtained is similar to the spectra II(KNO_3) and II($CsNO_3$) shown in Figures V-II and V-III respectively. Due to the similarity of the spectra II with those in highly viscous solutions, it was felt that the anisotropic spectra are due to hindered motion of VO^{2+} ion at liquid nitrogen temperature. Further it is known[11,12,13] that when the substance contains statistically oriented ions the resonance lines are distributed for each m_I value, between two extreme positions which are characteristic of the parallel and perpendicular orientations. The parallel components are expected to be of "absorption type" and the perpendicular components are expected to be of "dispersion type". Spectra II (both in KNO_3 and $CsNO_3$) of the present study contain these parallel and perpendicular components designated as "a" and "b" respectively. It may be mentioned here that the existence and the shape of the spectra II have been ascertained by studying these spectra at different power levels (1 mW, 0.32 mW and 110 μW). The intensity of the spectra is found to decrease with the decrease of microwave power. However the relative intensities of the lines did not change showing clearly that there are no saturation effects that influence the

Table V-I

Spin-Hamiltonian constants for VO^{2+} in KNO_3 and $CsNO_3$ single crystals

Crystal	Spectrum I	Spectrum II
KNO_3	$g_0 = 1.966 \pm 0.001$	$g_{\parallel} = 1.935 \pm 0.004$
	$A_0 = 116.0 \pm 1.0G$	$g_{\perp} = 1.974 \pm 0.003$
		$A = 199 \pm 2G$
		$B = 78 \pm 2G$
$CsNO_3$	$g_0 = 1.964 \pm 0.002$	$g_{\parallel} = 1.919 \pm 0.002$
	$A_0 = 115 \pm 2G$	$g_{\perp} = 1.984 \pm 0.003$
		$A = 218 \pm 1G$
		$B = 67 \pm 1G$

lineshape and intensity. The anisotropic spectra II are analysed using the Hamiltonian (1) and the constants are given in Table V-I.

It was pointed out earlier that the isotropic spectrum in $CsNO_3$ vanished at about $-70^\circ c$, and the anisotropic spectrum has started coming up at $-110^\circ c$ while in KNO_3 the spectrum I vanishes at $-150^\circ c$ and the spectrum II comes up at liquid nitrogen temperature. This shows that the motion of the VO^{2+} ion is hindered at somewhat higher temperatures in $CsNO_3$ than in KNO_3 indicating that $CsNO_3$ is more effective in hindering the motion of the vanadyl ion than KNO_3. In both crystals, as the temperature is increased, the intensity of the lines decreases and the spectrum becomes very weak above $+ 100^\circ c$ making it difficult to detect the effect of the phase transitions mentioned earlier.

The spin-Hamiltonian constants obtained for the spectra I and II in both crystals satisfy the equations (3) thus confirming the basis of the analysis. Though both crystals are having the oxygens in the lattice, the VO^{2+} ion is not found to have any distorted octahedral coordination of oxygens which would have resulted in a preferred orientation of the V-O bond axis as in $TiO_2{}^2$ and $GeO_2{}^3$. This may indicate that the bonding between the nitrogen and the oxygen atoms in the nitrate group is strong enough to overcome the formation of a distorted octahedron with the V^{4+} ion. It is difficult to decide about the position of the VO^{2+} ion in the lattice and also about the associated lattice defects, as the spectra studied are angular independent. It appears that the effect of the crystalline field is not explicitly seen anywhere,

excepting in hindering the motion of the VO^{2+} ion at low temperature.

Study of linewidths

As the present EPR studies clearly indicate that VO^{2+} in KNO_3 and $CsNO_3$ exhibit essentially a liquid like behaviour as far as the paramagnetic resonance and relaxation are concerned, it is felt that it would be interesting to examine the validity of the existing theories of paramagnetic relaxation in liquids for VO^{2+} in KNO_3 and $CsNO_3$ crystals.

McConnell[10] has demonstrated a mechanism whereby the anisotropic nuclear hyperfine interactions can contribute to paramagnetic line broadening in solutions, and this broadening can arise from both spin-lattice relaxation (T_1) and transverse relaxation (T'_2) effects. Later Kivelson[14] has shown that the linewidths will have a symmetrical dependence upon the nuclear spin quantum number m_I, i.e. the linewidths will have a m_I^2 dependence if there is isotropy in g-tensor but not in A-tensor. If the anisotropy in A is negligible (also in g) the linewidths do not depend on m_I. If the anisotropies in both g and A tensors are appreciable, the linewidths are found to have an asymmetrical dependence on m_I, i.e. a linear as well as quadratic one. Rogers and Pake[15] have shown that McConnell-Kivelson's theory can satisfactorily explain the spectra of VO^{2+} in solutions. In the notation used by Rogers and Pake[15], the expression for the linewidths is given by

$$1/_{T_2} = \pi\sqrt{3} \ (a_1 + a_2 \ m_I + a_3 \ m_I^2) \qquad \qquad ...(4)$$

where $\quad a_1 = \tau_c \left[(7/45)(\Delta \gamma B_0)^2 + 63\ b^2/16 \right] + K$

$$a_2 = -\ \tau_c \left[(7/15)\ b\ \Delta \gamma B_0 \right]$$

and $\quad a_3 = \tau_c\ (b^2/10)$ in which $\Delta \gamma = \gamma_{\shortparallel} - \gamma_{\perp} = (\beta/\hbar)\ (g_{\shortparallel} - g_{\perp})$

$\quad b = (2/3)(A - B)$ and $B_0 = \dfrac{h\gamma}{g\beta}$

K is factor which takes into account the contributions from spin-orbit coupling , from interionic interactions and in general from all mechanisms not sensitive to nuclear orientation m_I. The expression for linewidths given above is valid, subject to the following conditions:

I) The spectral lines are to be well separated so that the apparent linewidth will not be effected by the overlap of the tails of the adjacent lines.

II) The Zeeman term is to be the largest term;

III) The anisotropy of the g-factor is to be small so that $|\gamma| \gg |\Delta \gamma|$

IV) The lineshapes are close to Lorentzian.

V) The effect of the interionic interactions and the spin-orbit interaction could be ignored with the understanding that such contributions to the linewidth may be manifested in an additive constant as mentioned above.

The experimental linewidths are determined with the method of Rogers and Pake[15] using the relation.

derivative height $x(\text{width})^2 = $ constant.

This relation is based on the assumption that the population difference between the different m_I levels is small. The width of the line, for which the width is least among the octet of lines, is directly measured and the widths of the other lines are computed by using the above relation. The linewidth of the m_I lines are not the same. Figures V-IV and V-V show plots of linewidth versus m_I at $+30^{\circ}$c in KNO_3 and $CsNO_3$ respectively. These curves fit in very well with equation (4) above, indicating clearly that the m_I dependence of the paramagnetic relaxation in the case of VO^{2+} in KNO_3 and $CsNO_3$ is similar to that of VO^{2+} in solutions and this fact qualitatively confirms that Kivelson's theory can satisfactorily explain the paramagnetic resonance spectrum of VO^{2+} doped in KNO_3 and $CsNO_3$ single crystals. The constants a_1, a_2 and a_3 are calculated from experimental data using the least square method. The constants obtained for KNO_3 are $a_1 = 3.689G$, $a_2 = 0.3622G$, and $a_3 = 0.1832G$, while those for $CsNO_3$ are $a_1 = 2.940G$, $a_2 = 0.3254G$, and $a_3 = 0.1179G$

By taking the values for $\triangle\gamma = (\beta/\hbar)(g_{\shortparallel} - g_{\perp})$ and $b = 2/3(A - B)$ from low temperature data, one should be able to get the value of τ_c if the expressions for a_1, a_2 and a_3 given by the theory hold good quantitatively. Using the low temperature values for $\triangle\gamma$ and b an attempt is made to obtain the values of a_1, a_2 and a_3 in terms of τ_c at low temperature and at room temperature. However, it has been found that there is no agreement between the ratios of a_i (which do not involve τ_c) obtained from room temperature data and those from low temperature data. Here it may be mentioned that Kivelson also did not get an agreement in such a type of analysis by using the data of O'Reilly[5] for VEPI in low and high viscosity solutions.

FIGURE V-IV.   Variation of linewidth versus m_I, the nuclear spin quantum number for VO^{2+} in KNO_3 at the room temperature $(+30^{0}c)$.
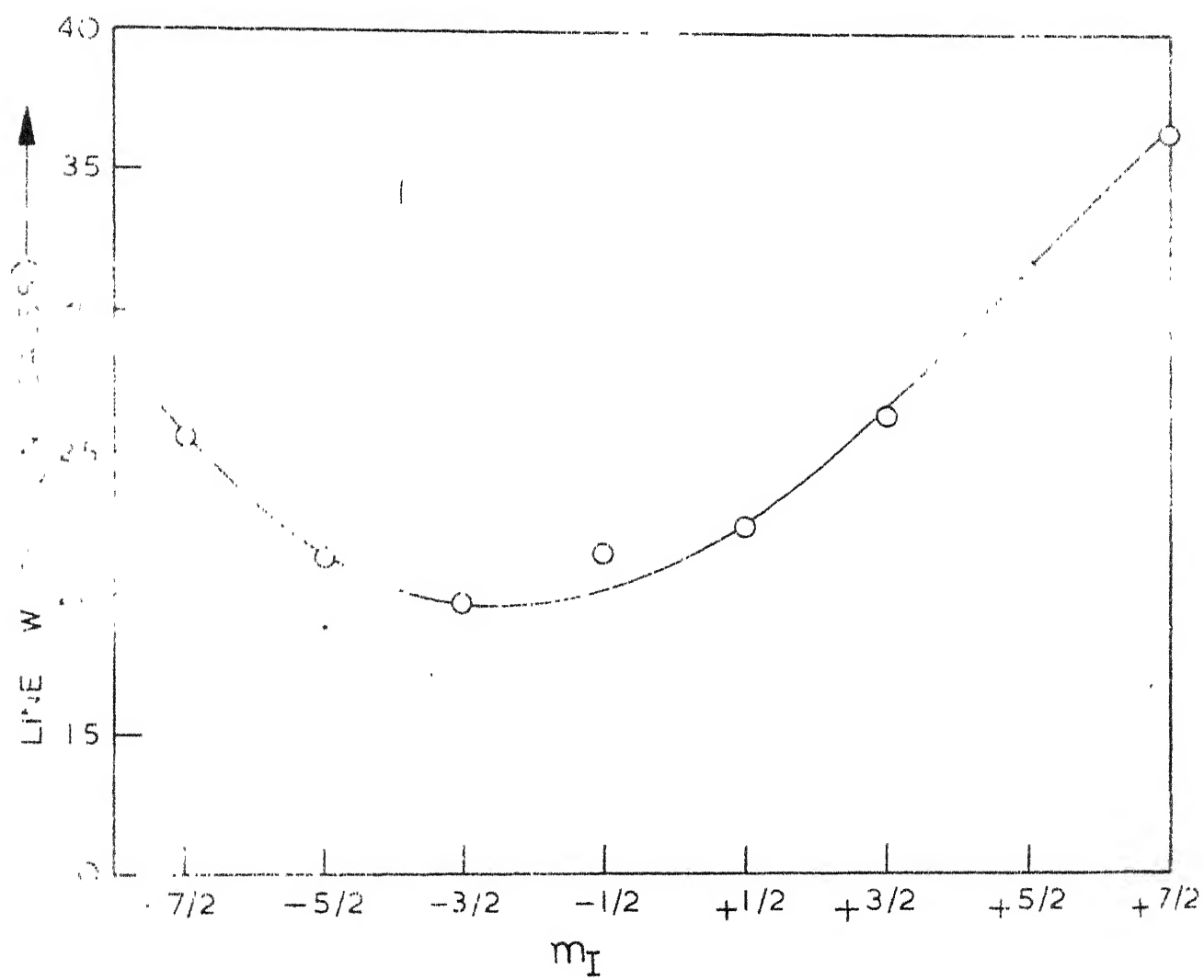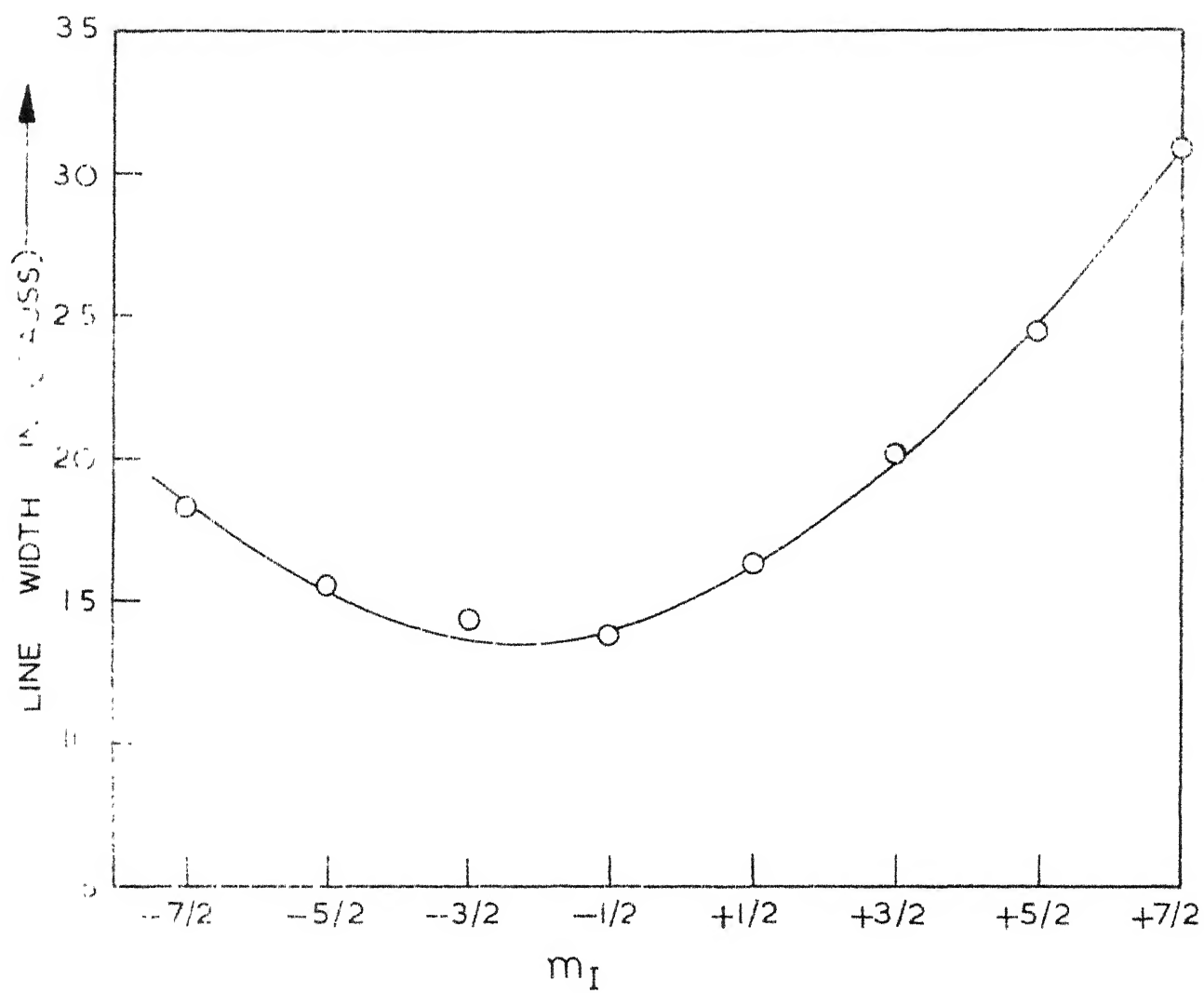
FIGURE V-V .   Variation of linewidth versus m_I, the nuclear spin quantum number for VO^{2+} in $CsNO_2$ at the room temperature $(+30^{\circ}c)$.

The variation of $\Delta \gamma$ and b with temperature may contribute to such a disagreement but, however, this may not be considerable as the low temperature $g_{\parallel}$, $g_{\perp}$, A and $\dot{B}$ and the room temperature g_o and A_o are found to satisfy the equations (3) . However there is a possibility that the temperature dependence of $g_{\parallel}$ and $g_{\perp}$ may be such that $(g_{\parallel} + 2g_{\perp})$ is nearly independent of temperature while $(g_{\parallel} - g_{\perp})$ is dependent on temperature, and similarly for A and B .

As the temperature is lowered the linewidths are found to increase. The increase in the linewidth is probably to a large extent due to the increase of the correlation time.

References

1. R. H. Borcherts and C. Kikuchi, J. Chem. Phys. 40, 2270 (1964).

2. H. J. Gerritsen and H. R. Lewis, Phys. Rev. 119, 1010 (1960).

3. I. Siegel, Phys. Rev. A134, 193 (1964).

4. M. D. Sastry and P. Venkateswarlu, Mol. Phys. 13, 161 (1967).

5. D. E. O'Reilly, J. Chem. Phys. 29, 1188 (1958).

6. B. Bleaney, Phil. Mag. 42, 441 (1951).

7. D. A. Edwards, Z. Krist. 80, 154 (1931).

8. S. Sawada, S. Nomura and S. Fujii, J. Phys. Soc. Japan, 13, 1549 (1958).

9. S. Sato, J. Sci. Research Inst. (Tokyo) 48, 59 (1954).

10. H. M. McConnell, J. Chem. Phys. 25, 1094 (1960).

11. R. Neiman and D. Kivelson, J. Chem. Phys. 35, 156 (1961).

12. G. Hochstrasser, Phys. and Chem. of Glasses 7, 178 (1966).

13. F. K. Kneubuhl, J. Chem. Phys. 33, 1074 (1960).

14. D. Kivelson, J. Chem. Phys. 33, 1094 (1960).

15. R. N. Rogers and G. E. Pake, J. Chem. Phys. 33, 1107 (1960).

CHAPTER VI

ELECTRON PARAMAGNETIC RESONANCE STUDIES OF VO^{2+} DOPED IN NH_4NO_3

$NaNO_3$ AND $Ba(NO_3)_2$ SINGLE CRYSTALS

ABSTRACT

The electron paramagnetic resonance studies of VO^{2+} doped in NH_4NO_3, $NaNO_3$ and $Ba(NO_3)_2$ single crystals have been performed over a wide temperature range. At room temperature an isotropic octet exhibiting m_I dependence of linewidths is obtained in all three crystals. As discussed in the earlier chapter this is thought to be due to a very fast readjustment of VO^{2+} ions which brings the system to an effective liquid with low viscosity. As the temperature is lowered below $-20^{\circ}c$ an anisotropic spectrum is obtained for VO^{2+} in NH_4NO_3 which is presumably due to hindered rotation of VO^{2+} ion. Conductivity measurements on VO^{2+} doped NH_4NO_3 confirmed the earlier studies which reveal an increase in specific volume of the crystal below $-18^{\circ}c$. The hindered motion of vanadyl ion below $-20^{\circ}c$ inspite of volume expansion is attributed to the effect of oxygens of NO_3^- ions on VO^{2+} ion. The anisotropic spectra are observed below $-80^{\circ}c$ and $-196^{\circ}c$ in the case of $Ba(NO_3)_2$ and $NaNO_3$ respectively. A comparison of the present results, with those of VO^{2+} in KNO_3 and $CsNO_3$ discussed in the earlier chapter, is made and the results are examined in relation to the recently reported low temperature phase transitions in these crystals. A probable phase transition around, $-110^{\circ}c$ in $CsNO_3$ is suggested. The m_I dependence of the linewidths for the room temperature spectra is studied using Kivelson's formalism.

Introduction

Among the transition metal oxocations, vanadyl ion VO^{2+} is the simplest and has been the subject of many optical and magnetic studies. Crystallographic, optical and magnetic studies of vanadyl complexes show[1-4] that VO^{2+} always occurs coordinated to other groups both in the solid state and in solutions. A series of electron paramagnetic resonance (EPR) studies in a variety of single crystals has been taken up to study the structure of vanadyl complexes formed in different crystals and also to study the effects of temperature and phase transitions in single crystals on the structure of vanadyl complex. Earlier chapters describe the EPR spectra of VO^{2+} in potassium and ammonium aluminum alums, methyl ammonium gallium (MAG) alum and KNO_3 and $CsNO_3$ single crystals. VO^{2+} is found to substitute trivalent ions in alums forming a stable $[VO(H_2O)_5]^{2+}$ complex. But in KNO_3 and $CsNO_3$ crystals, vanadyl ion is found to undergo a fast readjustment at room temperature, resulting in averaging of g and A tensors, giving rise to an isotropic spectrum with m_I dependence of linewidths. A similar spectrum was reported earlier by Sastry and Venkateswarlu[5] in the case of VO^{2+} in NH_4Cl. The motion of vanadyl ion is found to get hindered in these crystals as the temperature is lowered. The motion of vanadyl ion gets hindered nearly at $-30°c$ in NH_4Cl, at $-196°c$ in KNO_3 and nearly at $-110°c$ in $CsNO_3$. The relatively high temperature ($-30°c$) at which the motion of vanadyl ion gets hindered in NH_4Cl lattice is probably due to volume contraction associated with the order-disorder transition at that temperature[6]. The present chapter deals with the EPR studies of VO^{2+} in ammonium, barium and sodium nitrate single crystals and is a continuation

of the earlier chapter on the EPR work on VO^{2+} in $CsNO_3$ and KNO_3 which will be widely referred to in this chapter.

Ammonium nitrate has phase transitions in the accessible temperature range[7,8] and further the low temperature phase transition involves[8] a volume expansion unlike in NH_4Cl. However, the motion of vanadyl ion is found to get hindered right below $-20^{\circ}c$ inspite of volume expansion at that temperature. This necessitated the repetition of conductivity measurements of Brown and McLaren[8] and our results are found to be in agreement with those reported by them. EPR results of the present study suggest that the oxygens in NH_4NO_3 are probably responsible for hindering the motion of vanadyl ion. The results obtained for $Ba(NO_3)_2$ and $NaNO_3$ are discussed in light of the recently discovered low temperature transitions in these crystals[9,10]. Finally, the EPR ressults in all the VO^{2+} doped nitrate single crystals so far studied are summarized and an attempt is made to determine the position of VO^{2+} in these crystals.

Experimental procedure

Single crystals of NH_4NO_3, $Ba(NO_3)_2$ and $NaNO_3$ doped with VO^{2+} are grown by slow evaporation of the saturated solutions of the corresponding nitrates to which 1 mole % by weight of vanadyl nitrate(prepared from a chemical reaction between $AgNO_3$ and $VOCl_2$) is added as an impurity. The experimental set up used in EPR is briefly described in chapter II.

The single crystals of VO^{2+} doped NH_4NO_3, used in EPR studies have been compressed under high pressure to form pellets and they are used

for electrical conductivity measurements. The compressed powder pellet of 0.2 cms thickness and 1.2 cms in diameter is placed in between two platinum foils and mounted between two brass electrodes. The temperature of the sample is measured by means of a NBS standard chromel-alumel thermocouple. The electrode assembly is placed inside a brass container which is connected to a vacuum pump. For measurements of conductivity as a function of temperrature over the range $+20^{\circ}$c to -80°c the conductivity cell is first cooled to liquid nitrogen temperature and then slowly allowed to warm up. The e.m.f. of the thermocouple is measured by means of a multivolt potentiometer of Leeds and Northrup cat. No. 8696 and the resistance of the sample is measured by means of a d.c. amplifier and electrometer 1230-A to which power is fed from a stabiliser.

Theory

Tetravalent vanadium exists as vanadyl (VO^{2+}) and exhibits paramagnetic resonance absorption due to the single 3d electron present in the molecule. The anisotropic spectrum obtained in the present study can be interpreted in terms of the following spin-Hamiltonian with axial symmetry[11].

$$\mathcal{H} = g_{\shortparallel}\,\beta\,H_z\,S_z + g_{\perp}\,\beta\,(H_x\,S_x + H_y\,S_y) + A\,I_z\,S_z + B(I_x\,S_x + I_y\,S_y) \quad \ldots(1)$$

In the case where the molecule is rotating about with a correlation time (τ_c) much shorter than the reciprocal of the spread of the spectrum in frequency, the equation (1) reduces to an "isotropic" Hamiltonian
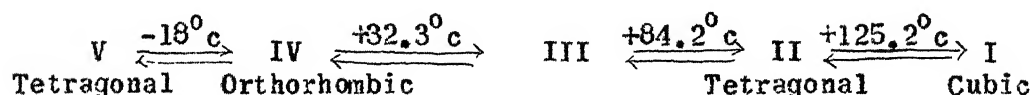
$$\mathcal{H} = g_0\,\beta\,\vec{H}.\,\vec{S} + a\,\vec{I}.\,\vec{S}. \quad \ldots(2)$$

where $g_0 = (1/3)(g_{||} + 2g_{\perp})$ and $a = (1/3)(A + 2B)$.

Results and discussion

(a). Ammonium nitrate

Ammonium nitrate has been found to have the following phase transitions[7,8]

$$V \xrightleftharpoons{-18^0 c} IV \xrightleftharpoons{+32.3^0 c} III \xrightleftharpoons{+84.2^0 c} II \xrightleftharpoons{+125.2^0 c} I$$
Tetragonal   Orthorhombic   Tetragonal   Cubic

The structure of phase III is not clearly given in the literature. However, in dry solid only the transitions $I \rightleftharpoons II \rightleftharpoons IV \rightleftharpoons V$ can take place. The transitions involving phase III require the presence of moisture[8].

(i) EPR studies

The EPR spectra of VO^{2+} in NH_4NO_3 recorded at different temperatures are shown in Figure VI-I . The spectrum recorded at room temperature which will be referred to as spectrum I consists of an isotropic octet showing m_I dependence of linewidth, similar to spectrum I($CsNO_3$ and KNO_3) discussed in the earlier chapter. It is presumably due to a fast readjustment of VO^{2+} molecule ion, resulting in the averaging of anisotropies in g and A tensors. As the temperature is lowered through the phase transition temperature $(V \xrightleftharpoons{-18^0 c} IV)$ the spectrum I started loosing its characteristic features. It can be clearly seen in Figure VI-I that at -20^0c, the lines get broadened and the two high field lines are not seen, probably due to large linewidths at this temperature. These effects are more pronounced at -30^0c. However,

FIGURE VI-I.   EPR spectra of VO^{2+} in NH_4NO_3 at $+25^{o}c$, $-20^{o}c$ and

$-30^{o}c$. The spectrum at $+25^{o}c$ is referred to as

spectrum I. It can be clearly seen that the characteristic

features of spectrum I starts diminishing at $-20^{o}c$ indi-

cating the onset of hindered rotation which becomes more

pronounced at $-30^{o}c$.

DPPH
3362.8G

ROOM TEMP. (25°C)

SPECTRUM I

83.33G

DPPH
3390.0G

85.33G

−20°C

−30°C
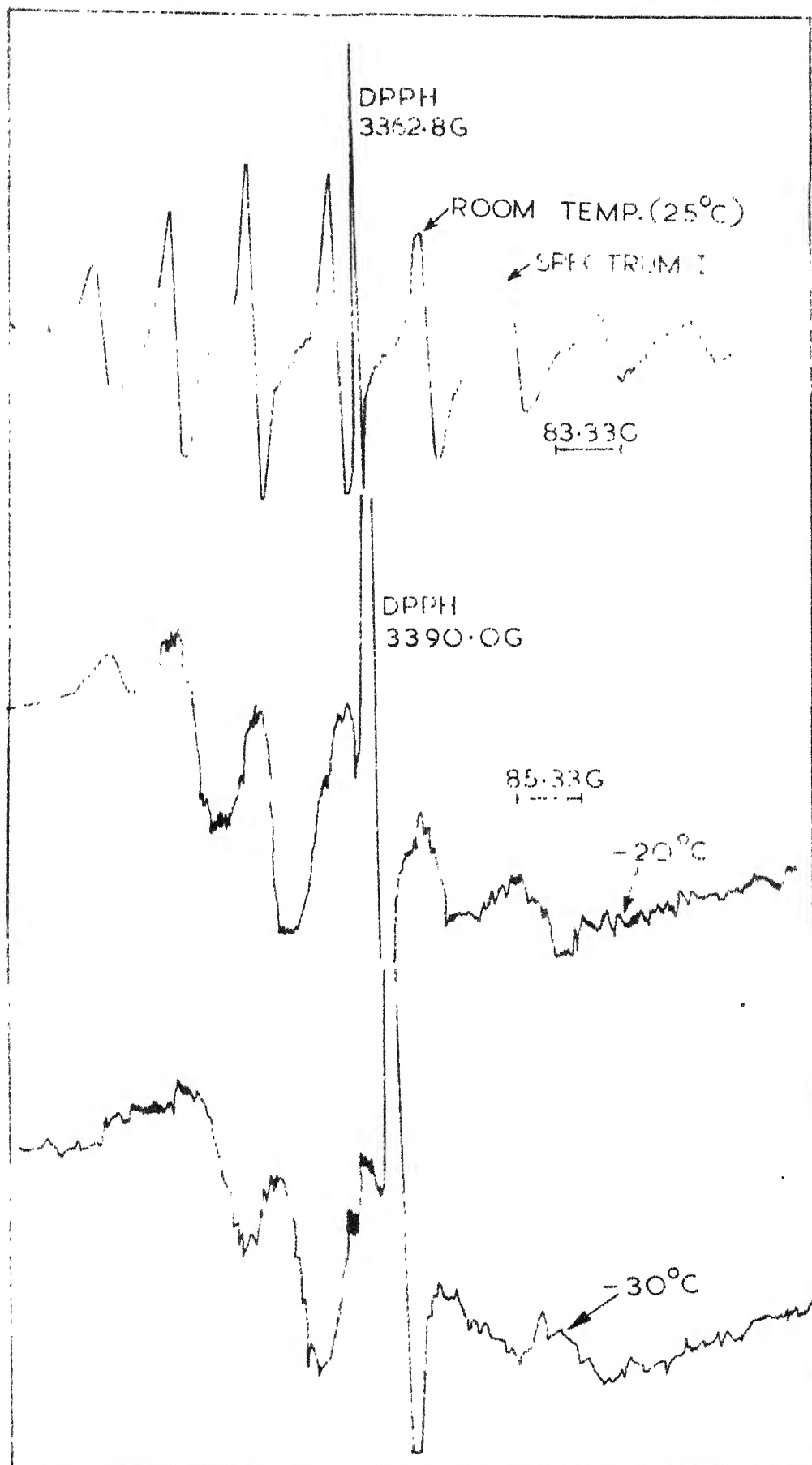
the characteristic features of the anisotropic spectrum are not seen until
-70°c. The spectra observed at -20°c and -30°c probably correspond to
some intermediate phase between the isotropic and anisotropic spectra, wherein
the criterion for complete averaging out of g and A anisotropies is not
satisfied, and at the same time the correlation time τ_c is not long enough
for the parallel and perpendicular components of g and A tensors to be
clearly shown up. It appears that the onset of hindered motion comes in
this temperature range. The appearance of anisotropic spectrum below -70°c
shows the stabilization of hindered motion at that temperature. Figure VI-II
shows a typical anisotropic spectrum recorded at -80°c and will be referred
to as spectrum II. The lines marked "a" are parallel components and those
marked "b" are perpendicular components. This is similar to the spectrum II
discussed in the earlier chapter. The spectrum II (Figure VI-II) shows the
characteristic features of a randomly oriented vanadyl ion, and its nature
is confirmed by studying it at different microwave power levels. No satu-
ration effects are observed. Spectrum I is analysed by using the isotropic
spin-Hamiltonian (2) while spectrum II is analysed by using the spin-
Hamiltonian(1). The constants obtained are given in Table VI-I and they
satisfy the equations

$$a = (1/3)(A + 2B) \text{ and } g_0 = (1/3) (g_{\parallel} + 2g_{\perp})$$

confirming the nature of the spectra. As the temperature is raised above
room temperature, no changes in the spectrum have been observed except for
the over all decrease in intensity. In the orthorhombic phase (IV) the
linewidths are found to increase with the decrease of temperature which is
probably due to the increase of correlation time[12].

FIGURE VI-II.   EPR spectrum of VO^{2+} in NH_4NO_3 at -8° c. Lines marked

"a" are parallel transitions and lines marked "b" are

perpendicular transitions. Some parallel and perpendi-

cular transitions overlap in the central part of the
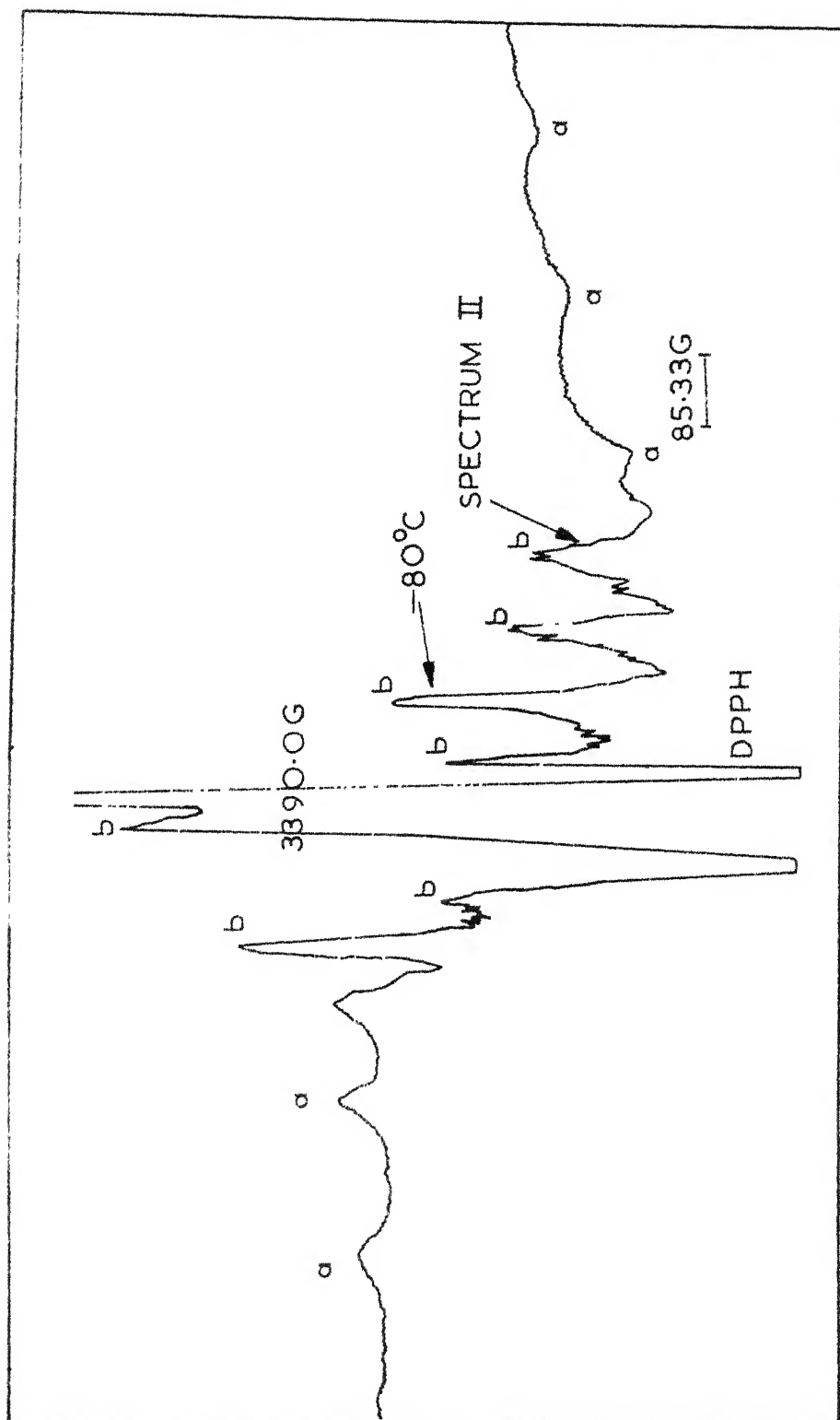
spectrum. This spectrum is referred to as spectrum II.

SPECTRUM II

80°C

3390·0G

DPPH

85·33G

Table VI-I

Spin-Hamiltonian constants of VO^{2+} in different nitrate single crystals.

Crystal	Spectrum I	Spectrum II	Reference
KNO_3	$g_0 = 1.966 \pm 0.001$ $a = 116.0 \pm 1.0G$	$g_{\shortparallel} = 1.935 \pm 0.004$ $g_{\perp} = 1.974 \pm 0.003$ $A = 199 \pm 2G$ $B = 78 \pm 2G$	Chapter V
$CsNO_3$	$g_0 = 1.964 \pm 0.002$ $a = 115 \pm 2G$	$g_{\shortparallel} = 1.919 \pm 0.002$ $g_{\perp} = 1.984 \pm 0.003$ $A = 218 \pm 1G$ $B = 67 \pm 1G$	Chapter V
$NaNO_3$	$g_0 = 1.965 \pm 0.001$ $a = 115 \pm 1G$	$g_{\shortparallel} = 1.947 \pm 0.001$ $g_{\perp} = 1.974 \pm 0.001$ $A = 218 \pm 1G$ $B = 67 \pm 1G$	This chapter
NH_4NO_3	$g_0 = 1.963 \pm 0.001$ $a = 116 \pm 1G$	$g_{\shortparallel} = 1.939 \pm 0.001$ $g_{\perp} = 1.975 \pm 0.001$ $A = 206 \pm 1G$ $B = 72 \pm 1G$	This chapter
$Ba(NO_3)_2$	$g_0 = 1.964 \pm 0.001$ $a = 116 \pm 1G$	$g_{\shortparallel} = 1.919 \pm 0.001$ $g_{\perp} = 1.984 \pm 0.002$ $A = 199 \pm 1G$ $B = 78 \pm 1G$	This chapter

As mentioned earlier, in NH_4Cl the motion of VO^{2+} gets hindered below the λ-point transition(nearly at $-30^\circ c$) which is reported to be associated with anomalous lattice contraction which in turn is responsible for hindering the motion of vanadyl ion. The transition in ammonium nitrate from phase IV to phase V involves a volume expansion. But the present EPR studies show that the motion of vanadyl ion gets hindered in phase V of NH_4NO_3 inspite of the volume expansion and this looks rather paradoxical. Here it may be mentioned that the anisotropic spectra(spectrum II) for VO^{2+} in NaCl, KCl and RbCl are observed[13] only below $-190^\circ c$. These crystals do not exhibit any low temperature phase transitons (nor they contain oxygens with which vanadyl is known to readily from a distorted octahedron), and therefore the hindered motion of VO^{2+} in alkali chlorides, can solely be attributed to temperature effect. This is similar to obtaining anisotropic spectra of $(VO\ F_5)^{3-}$ in frozen solutions[4] of 48% HF at $-196^\circ c$. Therefore, the occurence of anisotropic spectrum at a fairly high temperature($-20^\circ c$) in the present case must be due to the effect of host lattice on the vanadyl ion. Since the volume expansion reported during the phase transition is based on electrical conductivity measurements[8], it is felt necessary to study the conductivity of vanadyl doped ammonium nitrate.

(ii) Conductivity measurements

The electrical conductivity of doped ammonium nitrate powder pellet has been studied in the temperature range $+20^\circ c$ to $-80^\circ c$. The plot of conductivity versus $1000/T^\circ$ K is essentially similar to Figure 5 of Brown and McLaren's paper[8] and is shown in Figure VI-III. This shows

104

FIGURE VI-III. The electrical conductance as a function of temperature in a dried powder pellet of doped ammonium nitrate showing the IV $\rightarrow$ V transition.
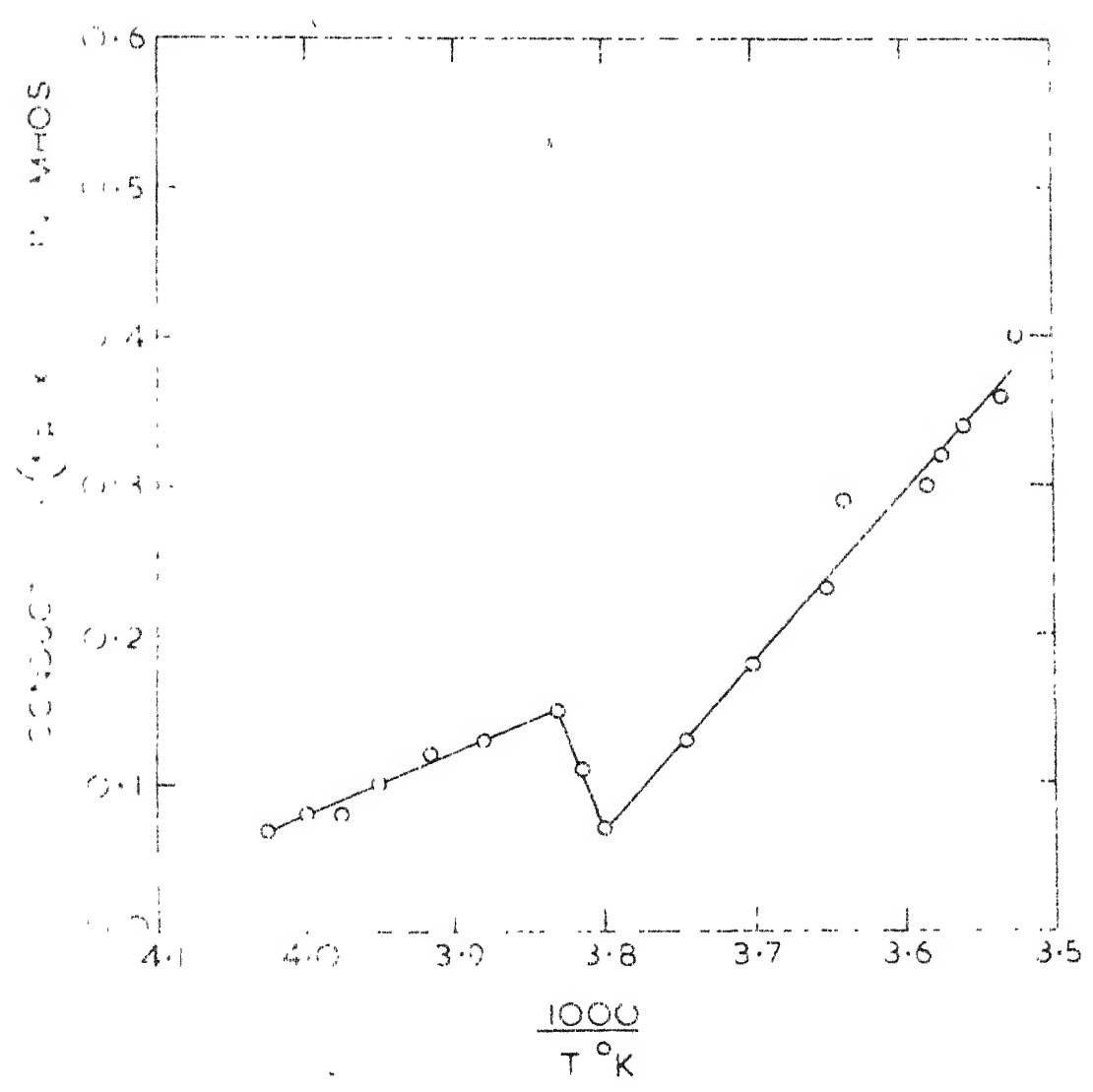
positive ions, namely VO^{2+} and $(NH_4)^+$.

(b) Barium and sodium nitrates

Sodium nitrate is known to have trigonal symmetry[14]. It has a gradual transition[15] in the temperature range $+150^\circ c$ to $+275^\circ c$. This transition has been found to have no phase change except for the initiation of rotation of the nitrate ion about the trigonal axis of the crystal. Barium nitrate is reported to have cubic symmetry[16] at room temperature. Low temperature phase transitions in alkali nitrates have been recently reported by Fermor and Kjekshus[9]. Further Fermer and Kjekshus[10] discovered a gradual transition in $Ba(NO_3)_2$ in the temperature range $-100^\circ c$ to $-55^\circ c$.

The EPR spectrum of VO^{2+} in $NaNO_3$ and $Ba(NO_3)_2$ at room temperature is similar to spectrum I discussed above in the case of NH_4NO_3 showing the characteristic m_I dependence of the linewidths. This shows that the motion of vanadyl ion is not hindered in $NaNO_3$ and $Ba(NO_3)_2$ lattice at room temperature. The anisotropic spectrum(called, spectrum II following the earlier notation) reflecting the hindered motion of the vanadyl ion is observed below $-80^\circ c$ in the case of $Ba(NO_3)_2$. However, it is not seen until $-196^\circ c$ in the case of $NaNO_3$. Spectra I are analysed by using the spin-Hamiltonian (2) and spectra II are analysed by using the spin-Hamiltonian (1). The spin-Hamiltonian constants are given in Table VI-I together with those of other nitrates.

(c) General comments

The EPR studies discussed above clearly show that the vanadyl

ion is free to reorient its bond in $CsNO_3$, KNO_3, NH_4NO_3, $NaNO_3$ and

$Ba(NO_3)_2$ and the motion is found to get hindered as the temperature is

lowered. However, the temperature $(T_{iso \rightarrow aniso})$ at which the nature of

the spectrum changes from isotropic to anisotropic is not same in all these

crystals and this temperature is characteristic of the particular crystal

and therefore is expected to correspond to a physical property of the

crystal. The values of $T_{iso \rightarrow aniso}$ together with phase transition

temperatures and other crystallographic data of nitrate crystals of the

present interest are given in Table VI-II. As discussed in the earlier

section, the temperature $T_{iso \rightarrow aniso}$ is found to coincide with the

λ-transition in NH_4Cl, and the $IV \rightleftarrows V$ phase transition in NH_4NO_3. Appa-

rently the reported[9] phase transitions at $-60^{\circ}c$ and $-30^{\circ}c$ respectively in

KNO_3 and $NaNO_3$ have no effect on the EPR spectra. The hindered motion

of vanadyl ion in these crystals at $-196^{\circ}c$ is purely a temperature effect.

However higher values of $T_{iso \rightarrow aniso}$ in the case of $CsNO_3$ and $Ba(NO_3)_2$

show that these lattices become operative in hindering the motion of

vanadyl ion. In $Ba(NO_3)_2$ as mentioned earlier Fermor and Kjekshus[10]

observed a continuous phase transition in the range $-100^{\circ}c$ to $-50^{\circ}c$,

and the observed $T_{iso \rightarrow aniso}$ ($-80^{\circ}c$) in $Ba(NO_3)_2$ is probably associated

with this phase transformation. The hindered motion should come in either

due to a lattice contraction associated with the phase transition similar

to that in NH_4Cl or due to reasons similar to those stated earlier in

the case of NH_4NO_3. The former seems to be less likely as no lattice

contraction was reported in the low temperature transformations in nitrates

(thermal expansion of c-axis is reported[9] in the case of KNO_3) and the

Table VI-II

Transition temperatures of VO^{2+} in nitrates and crystallographic data of nitrates.

Host lattice	Transition temperature °c $(T_{iso \rightarrow aniso})$	Phase transition temperature repor-ted by Fermor and Kjekshus*(°c)	Lattice constant in Å	r_{x-o} in Å	$(1/r_{x-o}) \times (dr_{x-o}/dT) \times 10^4$
NaNO$_3$	-196	-30	6.3247	2.40	0.32
KNO$_3$	-196	-60	a=0.1709 b=6.4255 c=5.4175	2.83	0.17
CsNO$_3$	-110	-35 -50 to-100	a =10.74 c =7.68	3.05	0.14
NH$_4$NO$_3$	-20	-32	a=7.98 b=9.78	3.02	-
Ba(NO$_3$)$_2$	-80	-50 to-100	8.11	-	-

* references 9 and 10.

nature of this transition is expected to be same in all the nitrates. Therefore the mechanism of hindering the motion of vanadyl ion in $Ba(NO_3)_2$ is probably similar to that in NH_4NO_3. In both cases it is associated with a phase transition of the crystal. $T_{iso \to aniso}$ is nearly $-110^{o}c$ for $CsNO_3$ crystal. Actually the spectrum I in $CsNO_3$ starts losing its characteristics right below $-70^{o}c$ and spectrum II is stabilized at $-110^{o}c$. It is quite probable that this change in the spectrum is also associated with a phase transition in $CsNO_3$ so far not reported clearly . Fermor and Kjekshus[10] also found an indication of the phase transition for $CsNO_3$ in the range -100 to $-50^{o}c$ and the present experiments give a stronger indication for that. The transition is probably of the order-disorder type similar to that in other nitrates and does not involve a considerable lattice contraction.

Following is an attempt to get information about the probable position of vanadyl ion in different nitrate lattices on the basis of $T_{iso \to aniso}$ value which is believed to be influenced by the oxygen environment. Table VI-II includes the host lattices of VO^{2+} ion , the transition temperatures $T_{iso \to aniso}$, the lattice constants[17], the metal-oxygen distances r_{x-o}'s[18] and the rate of variation of these distances with temperature$(1/r_{x-o})$ (dr_{x-o}/dT)[18]. The values of r_{x-o} and$(1/r_{x-o})(dr_{x-o}/dT)$ given in table VI-II for $CsNO_3$ are for cubic phase. These values have not been available for trigonal phase of $CsNO_3$. Spectroscopic data[18] shows a difference of 0.026 $\overset{o}{A}$ in r_{x-o} above and below the transformation point at $+161^{o}c$. Also it is reported[19] that the positions of Cs^+ ions are very little altered during the process of phase transition. Therefore, the

value of r_{X-0} and $(1/r_{X-0})$ (dr_{X-0}/dT) reported for cubic symmetry may be taken to be nearly those for trigonal symmetry.

The lattice constants, metal oxygen distances r_{X-0}'s in the case of KNO_3 and $NaNO_3$ are smaller compared to those of $CsNO_3$. On the other hand$(1/r_{X-0})$ (dr_{X-0}/dT) is larger for $NaNO_3$ and KNO_3 compared to that of $CsNO_3$. Therefore if VO^{2+} ion enters all these crystals in the same manner, either substitutionally or interstitially, one expects that the motion of VO^{2+} should be hindered easily in $NaNO_3$ and KNO_3(i.e. at relatively high temp eratures) than in $CsNO_3$ due to the closeness of oxygens in the former case, which are presumably responsible for hindering the motion of vanadyl ion. However, this is contrary to the observed $T_{iso \to aniso}$ values in these crystals. Therefore the present EPR studies suggest that VO^{2+} ion does not enter all these lattices in the same fashion, and probably it enters substitutionally in $NaNO_3$ and KNO_3 and interstitially in $CsNO_3$. This can account for the higher $T_{iso \to aniso}$ observed in the latter case, due to the smaller distance of separation from the oxygens compared to that in $NaNO_3$ and KNO_3. An extension of the above argument favours the interstitial position of vanadyl ion in NH_4NO_3 and $Ba(NO_3)_2$ lattices also.

Linewidth studies

The linewidths for the isotropic spectrum are found to depend on the nuclear spin quantum number m_I. As discussed in the earlier chapter on VO^{2+} in KNO_3 and $CsNO_3$, and as in the case of NH_4Cl, the linewidths are found to satisfy Kivelson's theory[20] and obey the expression

$$(1/T_2) = \pi \sqrt{3}(a_1 + a_2\, m_I + a_3\, m_I^2).$$

The expressions for a_1, a_2 and a_3 are given in terms of correlation time τ_c, $\Delta g = (g_\parallel - g_\perp)$ and $b = (2/3)$ $(A - B)$ by Rogers and Pake[21]. The linewidths are studied by using the above expression and the constants a_1, a_2 and a_3 are obtained by the method of least squares. These constants a_1, a_2 and a_3 are given in Table VI-III for different nitrates. The constants given in earlier chapter for $CsNO_3$ and KNO_3 are also included for completeness. The agreement between the observed and calculated linewidths is satisfactory but not perfect and a typical example of VO^{2+} in NH_4NO_3 is given in Table VI-IV.

From the spin-Hamiltonian constants obtained from spectrum II, the constants a_1, a_2 and a_3 can be calculated in terms of τ_c. However , there is no agreement between the ratios of a's obtained from room temperature and low temperature data. As pointed out earlier this may be due to the temperature dependence of Δg and b. A better test for the applicability of Kivelson's equations in the present and similar cases can be made if the different principal values of the g and A tensors can be measured at room temperature itself. This can probably be achieved by applying an external electric field to arrest the motion of vanadyl ion at room temperature and thus destroying the isotropy. In competition with this effect the thermal motion disturbs the ordering so that only partial alignment results. Hilbers and McLean[22] could detect the electric field effects in NMR spectrum of nitrobenzene by using the electric fields of strength approximately 34kV/cm . By applying electric fields nearly of this order to the crystal in a direction parallel and perpendicular to the external magnetic field, probably it will be possible to obtain A, $g_\parallel$ and B, $g_\perp$ respectively at room temperature. A comparison of the values of a's

Table VI-III

Constants, a's , obtained from the linewidth
analysis of the EPR spectrum of VO^{2+} in diffe-
rent nitrate single crystals.

Crystal	a_1	a_2	a_3	R. M. S. error	Reference
KNO_3	3.689	0.362	0.1832	0.49	Chapter V
$CsNO_3$	2.940	0.3254	0.1179	0.42	Chapter V
$NaNO_3$	3.344	0.514	0.1501	0.41	This chapter
NH_4NO_3	3.206	0.6132	0.2805	0.60	This chapter
$Ba(NO_3)_2$	1.881	0.420	0.1241	0.32	This chapter

Table VI-IV

Linewidths of VO^{2+} in NH_4NO_3

m_I	Calculated (in gauss)	Experimental (in gauss)
-7/2	24.46	25.23
-5/2	18.64	18.47
-3/2	15.87	16.29
-1/2	16.16	16.51
1/2	19.49	19.94
3/2	25.88	26.11
5/2	35.32	34.53
7/2	47.80	48.85

R. M. S. Error= 0.60

obtained from A, B, $g_\parallel$ and $g_\perp$ of the electric field experiment will unambiguously testify the applicability of Kivelson's theory in the present case.

References

1. M. B. Palma-Vittorelli, M.U. Palma, D. Palumbo and F. Sgarlata, Nuovo Cimento 3, 718 (1956).

2. R. P. Dodge, D. H. Templeton and A. Zalkin, J. Chem. Phys. 35, 55 (1961).

3. K. DeArmond, B. B. Garrett and H. S. Gutowsky, J. Chem. Phys. 42, 1019 (1965).

4. P. T. Manoharan, and M. T. Rogers, J. Chem. Phys. 49, 3912 (1968).

5. M. D. Sastry and P. Venkateswarlu, Mol. Phys. 13, 161 (1967).

6. H.A. Levy and S.W. Peterson, Phys. Rev. 83, 1270 (1951).

7. S. B. Hendricks, E. Posmajak and F. C. Krack, J. Am. Chem. Soc. 54, 2766 (1932).

8. R. N. Brown and A.C. McLaren, Proc. Roy. Soc.(London) A266, 329(1962).

9. J. H. Fermor and A. Kjekshus, Acta. Chem. Scandinavia, 22, 836, 1628 and 2054 (1968).

10. J. H. Fermor and A. Khekshus, (Private communication).

11. D. E. O'Reilly, J. Chem. Phys. 29, 1188 (1958).

12. K.V.S. Rao and M.D. Sastry , Chem. Phys. Letters, 2, 20 (1968).

13. A. V. Jagannadham and P. Venkateswarlu, Proc. Indian Acad. Sci. (1969)(To be published).

14. R. W. G. Wyckoff, Phys. Rev. 16, 149 (1920).

15. F. C. Krack, E. Posmajak and S. B. Hendricks, J. Amer. Chem. Soc. 53, 3339 (1931).

16. S. Nishikawa and K. Hudunuki, Proc. Math. Phys. Soc.(Tokyo) 9, 197 (1917).

17.   R. W. G. Wyckoff "Crystal Structures". Vol. $\underline{2}$, Interscience

Publishes (New York) Chapter VII.

18.   B. Chaver, E. Rhodes and A. R. Ubbelhode, Proc. Roy. Soc. (London)

$\underline{A276}$, 437, 453 (1963).

19.   C. Finbak and O. Hassel, J. Chem. Phys. $\underline{5}$, 466 (1937).

20.   D. Kivelson, J. Chem. Phys. $\underline{33}$, 1094 (1960).

21.   R. N. Rogers and G.E. Pake, J. Chem. Phys. $\underline{33}$, 1107 (1960).

22.   C. H. Hilbers and C. MacLean, Chem. Phys. Letters $\underline{2}$, 445 (1968).

CHAPTER VII

ELECTRON PARAMAGNETIC RESONANCE STUDIES OF Mn^{2+} DOPED

IN AMMONIUM ALUMINIUM ALUM SINGLE CRYSTALS

ABSTRACT

The electron paramagnetic resonance spectra of Mn^{2+} doped in ammonium aluminum alum have been investigated with different concentrations of Mn^{2+} ion over a wide temperature range. At low concentrations of Mn^{2+} ion an isotropic sextet is obtained indicating thereby that the site symmetry at Mn^{2+} ion is cubic. As the concentration of Mn^{2+} ion entering the lattice increases, an orthorhombic spectrum with its z-axis along crystallographic $\langle 110 \rangle$ direction, superimposed on a broad line is obtained. At higher concentrations of Mn^{2+} impurity, some of the Mn^{2+} ions form clusters the presence of which is indicated by a broad resonance. The orthorhombic spectrum observed is due to Mn^{2+} ions substituting probably the NH_4^+ ion and getting associated with a first neighbour NH_4^+ vacancy along a $\langle 110 \rangle$ direction. However, the cubic component of the crystal field is found to be predominant in the spin-Hamiltonian, which is presumably due to the water octahedron about the Mn^{2+} ion. The axes of the octahedron surrounding the Mn^{2+} ions are found to coincide with the crystallographic axes indicating that the presence of Mn^{2+} rotates the octahedron of waters so that the axes of the octahedron coincide with crystallographic axes.

Introduction

Electron paramagnetic resonance (EPR) studies of trivalent metal ions in alums[1,2,3,4] have been the subject of investigation from the early days of EPR. These trivalent ions have been found to substitute the trivalent ions in alums. The recent report[5] of EPR of the divalent ion VO^{2+} in alums and the work described in chapters III and IV have given interesting results on the doping of divalent ion on the structure of alum lattice. This ion has also been found to substitute the trivalent ion in the lattice presumably due to the possible formation of a stable $\left[VO(H_2O)_5\right]^{2+}$ complex. This chapter reports the first observation of the EPR studies of divalent metal ion, Mn^{2+}, substituting a monovalent site NH_4^+ in ammonium aluminum (NH_4Al) alum.

Crystallography of alums

The structure of alums has been determined by Lipson and Beevers[6] and Lipson[7]. These alums have been differentiated[6,7] as of three types, α, β and γ, depending on the size of the monovalent ion. NH_4Al alum with its NH_4^+ ion of intermediate size belongs to α-type of alums. The neutron diffraction studies[8] of the α-alum, $K\,Cr\,(SO_4)_2 \cdot 12H_2O$ have shown that one axis of the octahedral grouping is tilted by about 50° away from the perpendicular to the plane of the other two axes. No such information is available for NH_4Al alum. Recently the structure of α, β and γ-types has been reexamined by Cromer, Kay and Larson[9,10] and Larson and Cromer[11]. A discussion of the structure of α and β-alums with special reference to EPR studies is given by Manoogian and Mackinnon[5] and in chapters III and IV. γ-alums are found to form when the monovalent cation is small[6,7].

The only known example of this type of alum is $NaAl(SO_4)_2.12H_2O$. In these alums both the monovalent and trivalent cations are surrounded by water octahedra[9], as in other alums. Whereas the cubic axes of the octahedron surrounding the trivalent ion coincide exactly with the cubic axes of the unit cell in β-alums, and within a few degrees in α-alums, the octahedron about the trivalent ion in γ-alums is rotated by 39.4^o about the three fold axis of the unit cell[10]. The six water molecules approach the monovalent ion much more closely in γ-alums than in α-alums. The water octahedron surrounding the monovalent ion in γ-alums is distorted along the three fold axis of the unit cells[10]. However the directions of the cubic axes of the water octahedron surrounding the monovalent ion relative to the cubic axes of the unit cell in β and γ-alums are not discussed clearly in literature.

Experimental procedure

The single crystals of ammonium aluminum alum doped with different concentrations of Mn^{2+} ion are grown by slow evaporation of saturated solution of ammonium aluminum alum to which $MnSO_4$ is added as an impurity. The experimental details are briefly discussed in chapter II.

Theory

Divalent manganese has $3d^5$ electronic configuration and ^6S ground state . Such a spherically symmetric state can not be effected directly by crystalline electric fields. It has however long been known that a zero field splitting of this state does occur. Crystalline fields of cubic symmetry split the ^6S state into a doublet and a quartet. When a magnetic
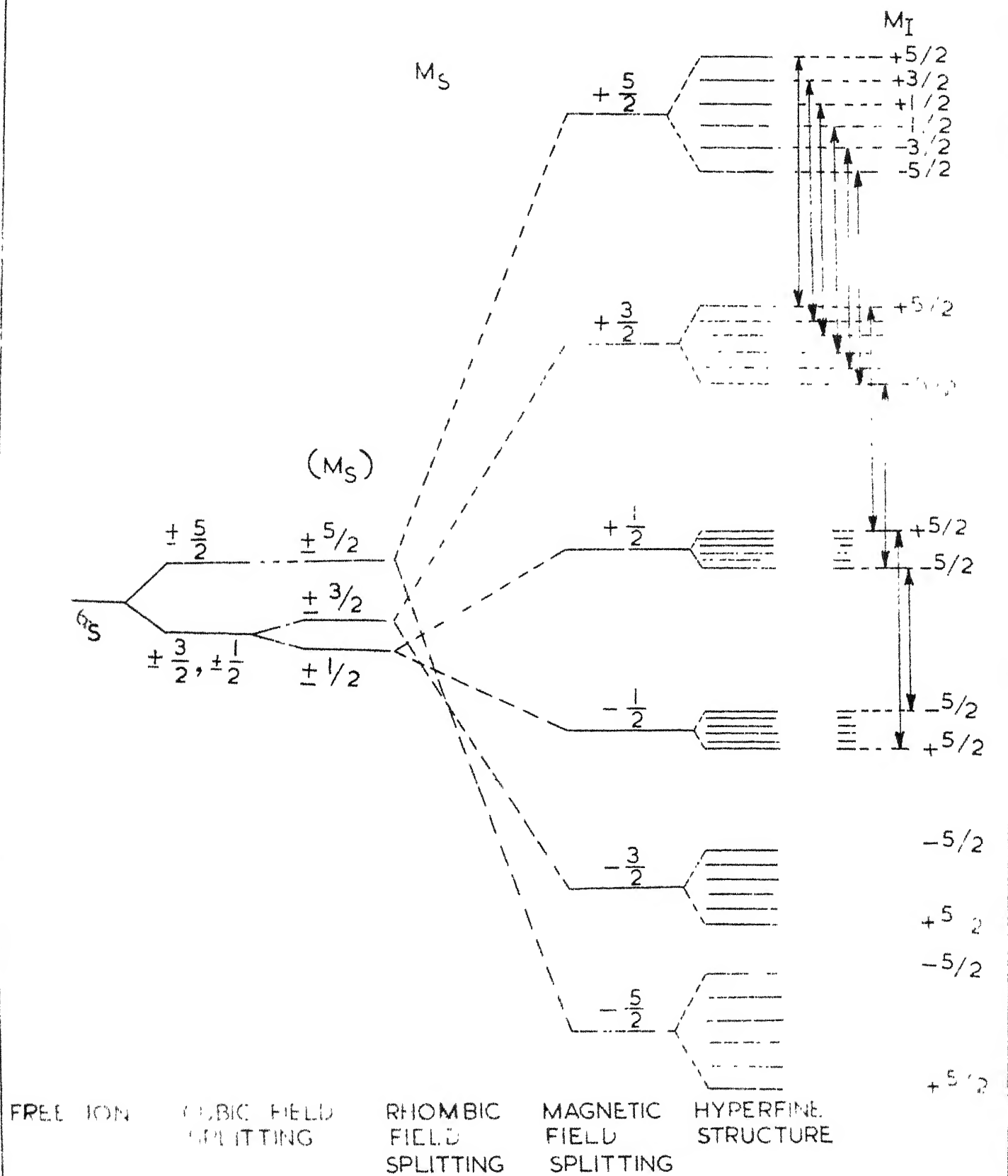
field is applied this degeneracy is removed resulting in the sextet M_S levels. There will be five fine structure transitions ($\Delta M_S = \pm 1$) between these six levels. When the strength of the cubic crystalline field is small, then zero field splitting between the doublet and quartet is small so that the five transitions occur at the same frequency. Since the nuclear spin of Mn^{55} is 5/2 , each electronic level splits into six components. This gives a six line spectrum for Mn^{2+} in cubic fields. This spectrum can be described by a spin-Hamiltonian containing only the Zeeman and hyper-fine interaction terms[12] and can be analysed by using the magnetic field resonance values given by Bleaney[12].

When the crystalline field at the $Mn^{2'}$ ion is of symmetry lower than cubic, like axial or orthorhombic, the ^6S state splits into three Kramers doublets. This splitting of ^6S state in the presence of cubic and lower symmetry crystalline fields and magnetic field is shown in Figure VII-I. In the presence of lower symmetry crystalline fields the five fine structure transitions in EPR occur at different frequencies. This results in a 30 line spectrum for Mn^{2+} ion in tetragonal or orthorhombic symmetries. Such a spectrum can be described by a spin-Hamiltonian of the appropriate symmetry[13-15] and can be analysed by using the resonance values of magnetic field given by Watkins[13].

Results and discussion

The EPR experiments are conducted on NH_4Al alum single crystals having three different concentrations of Mn^{2+} impurity. For convenience they are referred to as crystals -1,2 and 3. Crystals-1 are grown from

123

FIGURE VII-I.   Splitting of ^{6}S state of Mn^{2+} under the action of crystalline fields, magnetic field and hyperfine interaction.

M_I

$+5/2$
$+3/2$
$+1/2$
$-1/2$
$-3/2$
$-5/2$

M_S

$+\frac{5}{2}$

$+\frac{3}{2}$

$+5/2$

(M_S)

$\pm\frac{5}{2}$ $\pm^5/2$

$+\frac{1}{2}$

$+5/2$

^6S

$\pm\frac{3}{2}$ $\pm^3/2$

$-5/2$

$\pm\frac{3}{2},\pm\frac{1}{2}$ $\pm^1/2$

$-\frac{1}{2}$

$-5/2$

$+5/2$

$-\frac{3}{2}$

$-5/2$

$+5 2$

$-5/2$

$-\frac{5}{2}$

$+5 2$

FREE ION   CUBIC FIELD   RHOMBIC   MAGNETIC   HYPERFINE.
           SPLITTING   FIELD   FIELD   STRUCTURE
                         SPLITTING SPLITTING

solutions containing 1 mole percent of $MnSO_4$ by weight. Crystals-2 are grown from solutions containing 5 mole percent of $MnSO_4$ by weight, and crystals-3 are grown from solutions containing nearly 50 mole percent of $MnSO_4$ by weight. Spectroscopic analysis of these crystals has shown that the content of manganese in crystals 1,2 and 3 is 0.001, 0.5 and 0.01 mole % respectively showing thereby that only a small fraction of the impurity added to the solution goes into the alum crystal. The crystals have well developed [111] faces and are clear and transparent. The EPR of Mn^{2+} is in general weak in these crystals which is presumably because only a small amount of manganese could go into the crystals.

A single isotropic sextet has been detected in crystal-1 and is shown in Figure VII-II. When Mn^{2+} enters NH_4Al alum it can go in substitutionally either at NH_4^+ site or at Al^{3+} site. When it substitutes either of the sites it is expected that it would be subjected to an octahedral crystal field superimposed by a slight trigonal component, if any, due to the distortion of the octahedron surrounding the site it occupies[9]. The charge imbalance created by the substitution of Mn^{2+} at the NH_4^+ site or at the Al^{3+} site is to be compensated. This is achieved normally by the creation of lattice defects like vacancies or extra ions. If this defect is nearer to the magnetic ion then the latter is subjected to a crystal field of lower symmetry depending on the position of the defect. If the defect is remote from the magnetic ion then the ion does not feel its presence and essentially the symmetry of the local crystalline field is reflected in the EPR spectrum of such ions. Therefore the single sextet that is observed at room temperature in crystal-1 is probably due to Mn^{2+}

FIGURE VII-II.   EPR spectrum of crystal-1 with 0.001 mole percent concentration of Mn^{2+} ion in NH_4Al alum single crystal recorded at $+25^0c$.

DPPH
3243·89 G

H →

86 96G
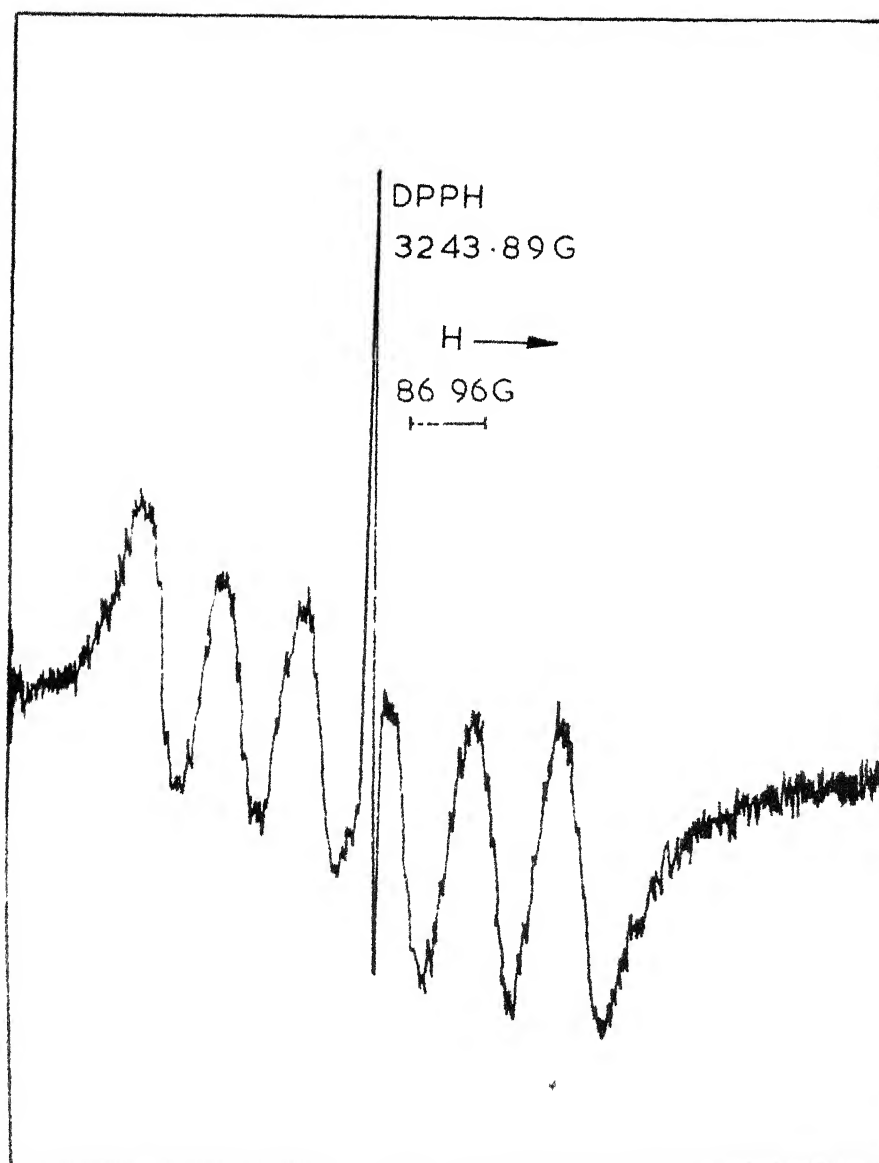
ions which go substitutionally to either NH_4^+ or Al^{3+} ion, with the charge compensating site being quite remote from the Mn^{2+} ion. This spectrum is described by the spin-Hamiltonian [12]

$$\mathcal{H} = g_{\shortparallel} \beta \ H_z \ S_z + g_{\perp} \beta \ (H_x \ S_x + H_y \ S_y) + A \ I_z \ S_z + B(I_x \ S_x + I_y \ S_y)$$

the solution of which gives the resonance field values[12] in the case of Mn^{2+} (I = 5/2)

$$H = H_0 - A \ m_I - (B^2/2H_0) \left[(35/4) - m_I^2 \right]$$

The spectrum is analysed by using the above equations and the spin-Hamiltonian constants are

$$A = 92 \pm 1G \text{ and } g = 2.002 \pm 0.001$$

It may be noted that the spectrum observed is cubic and does not reveal the presence of any trigonal distortion at the Mn^{2+} site.

A broad line superimposed on the hyperfine sextet is obtained in crystal-2. The width of this line is about 175 gauss and the g value is 2.003. This type of broad resonance has been observed in alkali halides doped with Mn^{2+} and may be due to precipitated Mn^{2+} ions[13,14,15].

In crystal-3 a thirty line spectrum superimposed on the broad resonance is obtained. However the general intensity of this spectrum is very low. The angular variation of the spectrum showed that it consists of thirty lines at all angles and has a maximum spread along the crystallographic <110> direction. Figure VII-III shows the spectrum at $+25^{\circ}$c, when the magnetic field is along crystallographic <110> direction.

FIGURE VII-III.   EPR spectrum of crystal -3 with 0./1 mole percent

concentration of Mn^{2+} ion in NH_4Al alum single crystal

recorded at $+25^{o}c$ when the magnetic field is along the

crystallographic $\langle 110 \rangle$ direction. The lines marked "a"

are the hyperfine lines of the fine structure transi-

tion $+5/2 \leftrightarrow +3/2$, those marked "b" are of $+3/2 \leftrightarrow +1/2$,

those marked "c" are of $+1/2 \leftrightarrow -1/2$, those marked "d"

are of $-1/2 \leftrightarrow -3/2$ and those marked "e" are of

$-3/2 \leftrightarrow -5/2$. Some of the hyperfine lines are overlapped

by the DPPH signal. The unaccounted lines in the figure

may correspond to some of the angular parts of the spectrum.
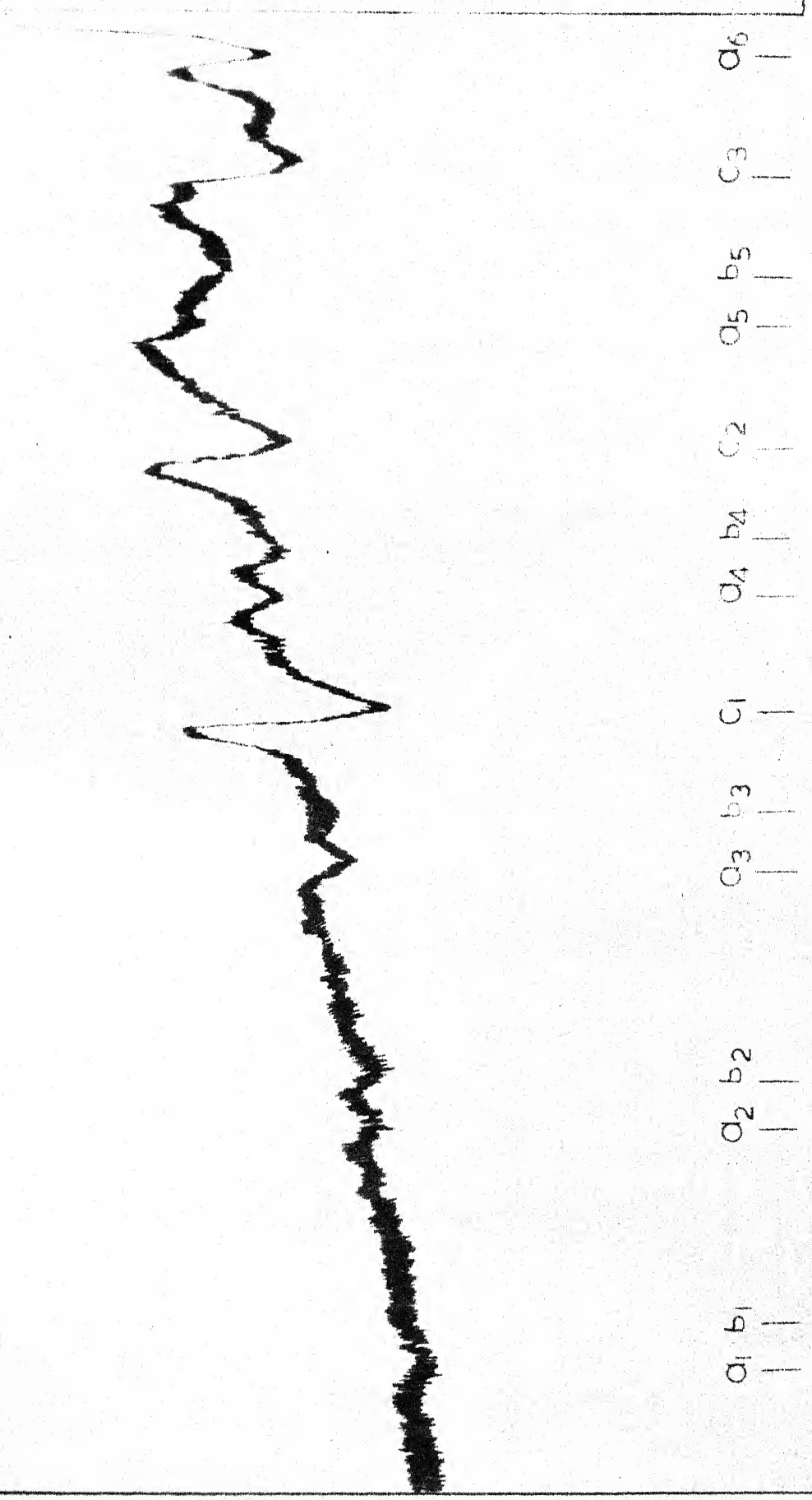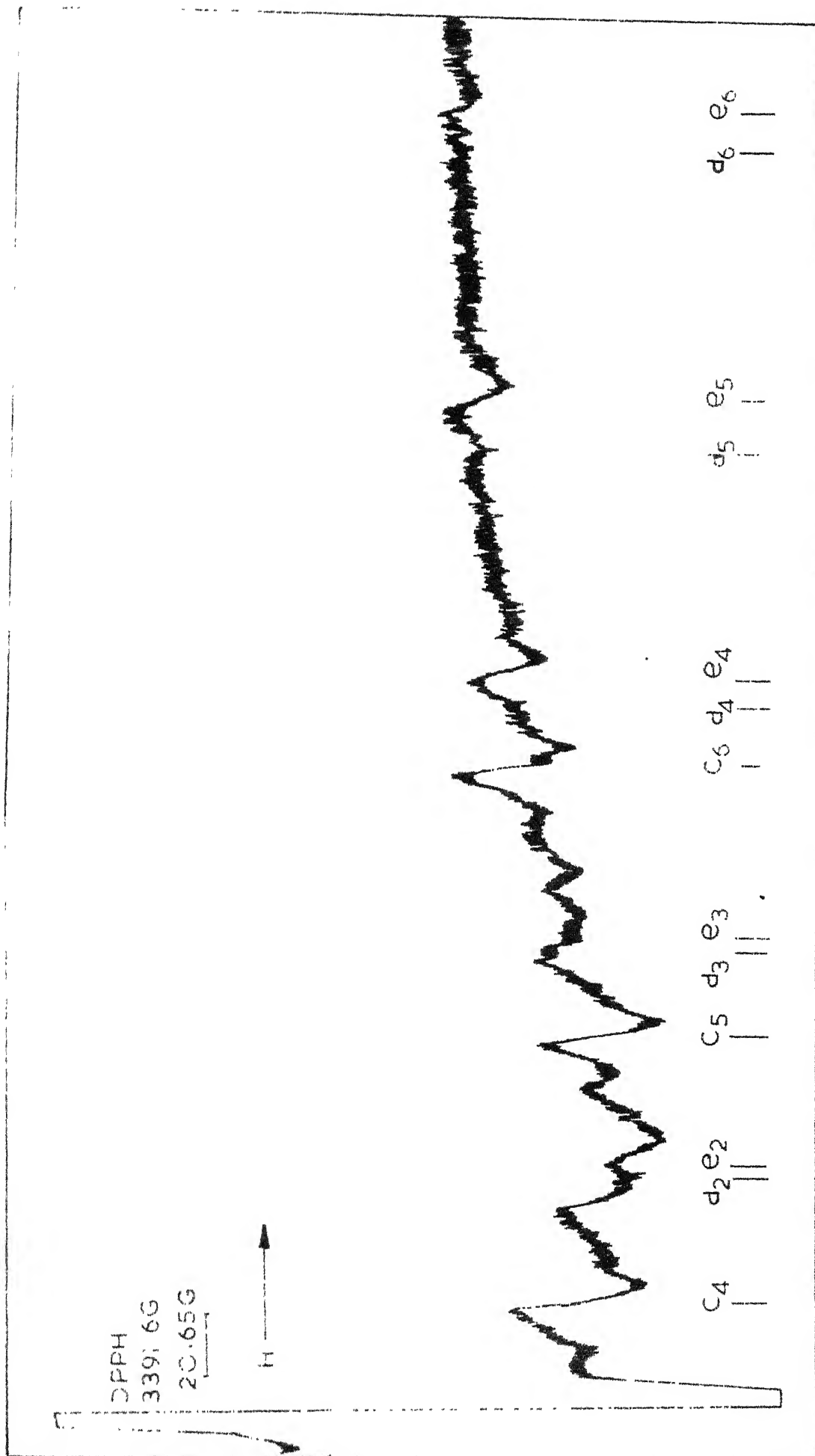
DPPH
339; 6G
20.65G

H

c_4 d_2 e_2 c_5 d_3 e_3 c_5 d_4 e_4 d_5 e_5 d_6 e_6

The 30-line spectrum obtained is found to be predominantly cubic ,
superimposed with a small distortion along a crystallographic $\langle 110 \rangle$
direction. This distortion, which probably arises by the presence of a
lattice defect associated with Mn^{2+} ion, is indicated by the maximum
spread of the spectrum when H is parallel to the $\langle 110 \rangle$ direction of the
crystal. The lattice defect and the observed spectrum can be understood
if one assumes that the spectrum is due to Mn^{2+} which substitutes NH_4^+
and gets associated with a first neighbour ammonium ion vacancy along $\langle 110 \rangle$
direction, the presence of a vacancy being necessary for charge compensation.
It may be noted that it would be difficult to visualize the required
lattice defect in the $\langle 110 \rangle$ direction if Mn^{2+} is assumed to substitute Al^{3+}
in the crystal. Thus it appears likely that Mn^{2+} responsible for the
orthorhombic spectrum goes in at the NH_4^+ site and not at the Al^{3+} site.
When the magnetic field H is along one $\langle 110 \rangle$ direction i.e. along the
z-axis of one ion, there are four z-axes which make about 60° and one
which makes 90° with H. However these angular parts are not clearly seen
in the spectrum shown in Figure VII-III, probably because of their low
intensity and probably also because of the predominant cubic nature of
the spectrum. There are a few weak lines unaccounted for in the middle
of the spectrum shown in Figure VII-III and these may correspond to some
of the angular parts. This spectrum is described by a spin-Hamiltonian
of the type[13,14,15] given in the next page.

$$\mathcal{H} = g_z \beta H_z S_z + g_x \beta H_x S_x + g_y \beta H_y S_y$$

$$+ (a/6) \left[S_1^4 + S_2^4 + S_3^4 - (1/5) S(S+1)(3S^2 + 3S - 1) \right]$$

$$+ D \left[S_z^2 - (1/3) S(S+1) \right]$$

$$+ E(S_x^2 - S_y^2)$$

$$+ A_z I_z S_z + A_x I_x S_x + A_y I_y S_y$$

The solution of this Hamiltonian gives the following magnetic field
resonance values for the allowed($\Delta M = \pm 1$, $\Delta m_I = 0$) transitions of Mn^{2+}

$$H = H_0 - K m_I - (B^2/2H_0) \left[I(I+1) - m_I^2 + m_I(2M-1) \right] f_{M \rightleftarrows M-1}(D,E,a)$$

Here $K^2 = A_x^2 n_x^2 + A_y^2 n_y^2 + A_z^2 n_z^2$, $H_0 = (h\nu/g\beta)$

where H is the magnetic field at which the transition is observed, ν is
the microwave frequency and

$$f_{\pm 5/2 \rightleftarrows \pm 3/2}(D,E,a) = \mp 2D(3n_z^2 - 1) \mp 6E(n_x^2 - n_y^2)$$
$$+ (1/H_0) \left[D^2(1-n_z^2)(1-33n_z^2) \right.$$
$$+ E^2 \left\{ 6n_z^2 + 33(n_x^2 - n_y^2) - 32 \right\}$$
$$+ 2DE(n_x^2 - n_y^2)(1 + 33n_z^2) \left. \right]$$
$$\mp 2 p a.$$

$$f_{\pm 3/2 \rightleftarrows \pm 1/2}(D, E, a) = \mp D(3n_z^2 - 1) \mp 3E(n_x^2 - n_y^2)$$
$$+ (1/4H_0)\left[D^2(1 - n_z^2)(21n_z^2 - 5)\right.$$
$$+ E^2\left\{16 - 36n_z^2 - 21(n_x^2 - n_y^2)^2\right\}$$
$$\left. - 2DE(n_x^2 - n_y^2)(21n_z^2 + 5)\right]$$
$$\pm (5/2)\, p\, a$$

$$f_{+\frac{1}{2} \rightleftarrows -\frac{1}{2}}(D, E, a) = (2/H_0)\left[D^2(1 - n_z^2)(9n_z^2 - 1)\right.$$
$$+ E^2\left\{8 - 12n_z^2 - 9(n_x^2 - n_y^2)^2\right\}$$
$$\left. - 2DE(n_x^2 - n_y^2)(9n_z^2 - 1)\right]$$

where M and m_I are the electronic and nuclear magnetic quantum numbers and $p = 1 - 5(n_1^2 n_2^2 + n_2^2 n_3^2 + n_3^2 n_1^2)$; n_x, n_y and n_z are the direction cosines of the external magnetic field with respect to x, y and z axes while n_1, n_2 and n_3 are the same with respect to cubic coordinate axes 1, 2 and 3. The spectrum has been analysed by fitting it to the above equations and the spin-Hamiltonian constants are

$$g_z = 2.003 \pm 0.001 \qquad A_z = -91 \pm 1G$$

$$a = 116 \pm 1G \qquad D = 71 \pm 1G \text{ and } E = 10 \pm 1G.$$

The existence of a single 30-line spectrum shows that there is a unique orientation of the water octahedron about Mn^{2+}, with respect to crystallographic cubic axes. The cubic axes of the water octahedron about Mn^{2+} probably coincide with the crystallographic cubic axes. This would mean that if the axes of the octahedron of waters at the monovalent site in the NH_4Al alum do not coincide with the cubic axes of the crystal, the substitution of Mn^{2+} at the NH_4^+ site makes them coincide by a suitable distortion of the octahedron. Such distortions by the substitution of VO^{2+} at the Al^{3+} sites in alums have been reported in chapters III and IV.

The transitions shown in Figure VII-III are assigned from the consideration of the variation of hyperfine multiplets[16] assuming that A is negative . In the spectrum shown in Figure VII-III the intensity of all the hyperfine lines in a fine structure transition is not equal though theoretically all the hyperfine lines are expected to have the same intensity. This type of intensity anomaly has been observed in Mn^{2+}: $NaCl$[14] and Cr^{3+}: MgO[17]. The reason for this is not quite clear.

A possible formation of manganese ammonium sulphate in crystals-3 is tested by comparing the spin-Hamiltonian constants obtained in the present study with those reported by Bleaney and Ingram[16] for manganese ammonium sulphate. The general features of the spectrum and the spin-Hamiltonian constants of the present study differ from that of manganese ammonium sulphate reported by Bleaney and Ingram. This further suggests that manganese ion goes substitutionally at NH_4^+ site rather than Al^{3+} site.

As the temperature is raised from $-180^{\circ}c$, i.e. from the lower end of our temperature range, to $+100^{\circ}c$ the intensity of orthorhombic spectrum increases, while that of the broad line decreases. The dissolution of precipitated Mn^{2+} ions with increasing sample temperature may be responsible for the observed increase in intensity of the orthorhombic spectrum with the increase of temperature. It is expected that there might be some variation of the crystal field parameters with temperature as observed earlier in Cr^{3+} in alums[18]. However because of the low intensity of the spectrum obtained , particularly with the small crystals used in the variable temperature cavity, it was difficult to carry out a systematic study of the variation of crystal field parameters with temperature. Above $+100^{\circ}c$ the crystal melts.

References

1. C. A. Whitmer, R. T. Weidner and P. R. Weiss, Phys. Rev. 73, 1468 (1948).

2. C. A. Whitmer, R. T. Weidner, J. S. Isiang and P. R. Weiss, Phys. Rev. 74, 1478 (1948).

3. D. M. S. Bagguley and J. H. E. Griffiths, Proc. Roy. Soc. (London), A204, 188 (1951).

4. B. Bleaney and R. S. Trenam, Proc. Roy. Soc. (London), A223, 1 (1954).

5. A. Manoogian and J. A. Mackinnon, Can. J. Phys. 45, 2769 (1967).

6. H. Lipson and C. H. Beevers, Proc. Roy. Soc. (London), A148, 664 (1935).

7. H. Lipson, Proc. Roy. Soc. (London), A151, 347 (1935).

8. G. E. Bacon and W.E. Gardner, Proc. Roy. Soc. (London), A246, 78 (1958).

9. D. T. Cromer, M. I. Kay and A. C. Larson, Acta.Cryst. 21, 383 (1966).

10. D. T. Cromer, M. I. Kay and A. C. Larson, Acta. Cryst. 22, 182 (1967).

11. A. C. Larson and D. T. Cromer, Acta. Cryst. 22, 182, 793 and 801 (1967).

12. B. Bleaney, Phil. Mag. 42, 447 (1951).

13. G. D. Watkins, Phys. Rev. 113, 79 (1959).

14. K. Morigaki, M. Fujimoto and J. Itoh, J. Phys. Soc. Japan, 13, 1174 (1958).

15. K. N. Shrivastava and P. Venkateswarlu, Proc. Indian Acad. Sci. 63A, 284 (1966).

16. B. Bleaney and D. J. E. Ingram, Proc. Roy. Soc. (London), A205, 336 (1951).

17. J. Wertz and P. Auzins, Phys. Rev. 106, 484 (1952).

18. C. F. Davis and M. W. P. Standberg, Phys. Rev. 105, 447 (1957).

VITAE

K. V. Subba Rao was born on 21st November, 1944 at Lakshmipuram, Andhra Pradesh. He had his undergraduate education at W. G. B. College, Bhimavaram, and obtained Bachelor of Science degree from Andhra University in 1963. He obtained his Master of Science degree in Nuclear Physics from Andhra University in 1965. He joined the graduate programme of the Department of Physics, Indian Institute of Technology, Kanpur in 1966. He holds a Junior Research Fellowship of the Council of Scientific and Industrial Research, India.